**Universidade do Minho**
Escola de Engenharia

João Carlos Leão de Sousa Neto

# Modelling and optimization of a controller for a fuel cell with application in electric vehicles

Outubro de 2022

**Modelling and optimization of a controller for a fuel cell with application in eletric vehicles**
João Leão Neto
UMinho | 2022

**Universidade do Minho**
Escola de Engenharia

João Carlos Leão de Sousa Neto

# Modelling and optimization of a controller for a fuel cell with application in electric vehicles

Dissertação de Mestrado em Engenharia de Sistemas

Trabalho efetuado sob a orientação da
**Professora Doutora Ana Maria Alves Coutinho Rocha**
**Professor Doutor Luís Miguel Silva Dias**

Outubro de 2022

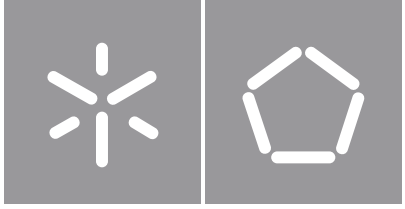

**Universidade do Minho**
Escola de Engenharia

João Carlos Leão de Sousa Neto

# Modelling and optimization of a controller for a fuel cell with application in electric vehicles

Dissertação de Mestrado em Engenharia de Sistemas

Trabalho efetuado sob a orientação de
**Professora Doutora Ana Maria Alves Coutinho Rocha**
**Professor Doutor Luís Miguel Silva Dias**

Outobro de 2022

## ACKNOWLEDGMENTS

I would like to thank to Continental Engineering Services for the opportunity to develop the presented work, mainly Francisco Mendes - System Engineer team leader and Gonçalo Torres - my supervisor, for their guidance, patient, and availability to solve any issue or to talk about any necessary topic. Your expertise and feedback allowed me to successfully complete my dissertation.

I would also like to thank my orientators for the availability to solve issues related with the development of this master dissertation, your help was essential to deliver the presented work.

Finally, I must express my gratitude to my parents, my brother, and friends for providing me with endless support and encouragement. This accomplishment would not be possible without them.

## STATEMENT OF INTEGRITY

I hereby declare having conducted this academic work with integrity. I confirm that I have not used plagiarism or any form of undue use of information or falsification of results along the process leading to its elaboration.

I further declare that I have fully acknowledged the Code of Ethical Conduct of the University of Minho.

**Modelling and optimization of a controller for a fuel cell with application in electric vehicles**

## ABSTRACT

Nowadays, the transportation sector is reaching a decisive point. The electric vehicles are supporting the reduction of $CO_2$ emissions, but advanced technologies must emerge to have a boost in the transition to fully emission-free vehicles. Fuel cells are considered the next big evolution due to their efficiency and low environmental impact, achieving high power density which is a key feature of the automotive industry that always tries to save up space and weight for other necessary components.

This dissertation intends to study all the working principle of the fuel cell and the required components to make it work in the case of vehicle applications. For this, the starting point is to collect information and test data from a low-volume production vehicle that has an FC System. These data will be analyzed to develop a simulation model that can replicate the behavior of the FC System. Thus, the Simulink Design Optimization was used to estimate the model parameter values that meet the design requirements and increase the model accuracy, using two nonlinear least square optimization methods (Trust Region Reflective and Levenberg Marquardt). The method that presented the best results allowed to study and develop a model that incorporates all the control of the FC System. This second model, the Fuel Cell Control Unit model, involved two versions: one based on a classical control algorithm (based on equations) and another with an Artificial Neural Network control algorithm.

Several tests were performed on the FC System model and the controller model, evaluating their output and determining the error between the model response and the corresponding data of the production vehicle. In addition, the tests took into account the comparison between the two versions of the fuel cell control unit with the selection of the version that showed the lowest RMSE value.

The results achieved for the FC System and for the controller are satisfactory, presenting similar behavior. By comparing the obtained results to the verified on the available data of the production fuel cell electric vehicle, they reflect the fuel cell stack voltage and resistance, under the same working conditions.

**Keywords:** Controller, FCCU, FC System, Fuel cell, Simulink

**Modelação e otimização de um controlador para uma célula de combustível com aplicação em veículos elétricos**

## RESUMO

Atualmente, o setor de transportes está a chegar a um ponto decisivo. Os veículos elétricos estão a apoiar a redução das emissões de $CO_2$, mas tecnologias mais avançadas devem surgir para impulsionar a transição para veículos totalmente livres de emissões de gases poluentes. As células de combustível a hidrogénio são consideradas a próxima grande evolução devido à sua eficiência e baixo impacto ambiental, alcançando alta densidade de potência, que é uma característica fundamental da indústria automóvel, que tenta sempre reduzir espaço e peso para outros componentes necessários.

Nesta dissertação é estudado todo o princípio de funcionamento da célula de combustível a hidrogénio e os componentes necessários para o seu funcionamento no caso de aplicações em veículos. Para isso, o ponto de partida é coletar informações e dados de teste de um veículo de baixo volume de produção que possui um sistema de célula de combustível a hidrogénio. Estes dados são analisados para desenvolver um modelo de simulação que possa replicar o comportamento do sistema de célula de combustível a hidrogénio. Assim, foi utilizado o *Simulink Design Optimization* para estimar os valores dos parâmetros do modelo atendendo aos requisitos de projeto e que aumentem a precisão do modelo, utilizando dois métodos de otimização por mínimos quadrados (*Trust Region Reflective* e *Levenberg Marquardt*). O método que apresentou melhores resultados, permitiu estudar e desenvolver um segundo modelo que inclui todo o controlo da célula de combustível e os seus componentes. Este segundo modelo, possui duas versões, com um algoritmo de controlo clássico (baseado em equações) e com um algoritmo de controlo que recorre a uma rede neural artificial. Foram realizados vários testes ao modelo do sistema da célula de combustível e ao seu controlador, avaliando os seus outputs e o erro entre a resposta do modelo e os respetivos dados do veículo de produção. Além disso, os testes levaram em consideração a comparação entre as duas versões da unidade de controlo de célula de combustível, selecionando a versão que apresentou o menor valor de RMSE. Os resultados obtidos para o sistema de célula de combustível a hidrogénio e para o controlador são satisfatórios, apresentando comportamento semelhante. Comparando os resultados obtidos com os verificados nos dados disponíveis do veículo em estudo, eles refletem a tensão e a resistência da célula de combustível, sob as mesmas condições de funcionamento.

**Palavras-chave:** Controlador, FCCU, Sistema de célula de hidrogénio, célula de hidrogénio, Simulink

## TABLE OF CONTENTS

# FIGURE INDEX

# TABLE INDEX

## LIST OF ABBREVIATIONS AND ACRONYMS

| | |
|---|---|
| AFC | Alkaline Fuel Cell |
| AC | Alternate Current |
| ANN | Artificial Neural Network |
| ANNC | Artificial Neural Network Controller |
| CES | Continental Engineering Services |
| DC | Direct Current |
| DMFC | Direct Methanol Fuel Cell |
| EV | Electric Vehicles |
| ECU | Engine Control Unit |
| FC | Fuel Cell |
| FCCU | Fuel Cell Control Unit |
| ICE | Internal Combustion Engines |
| IEA | International Energy Agency |
| LM | Levenberg Marquardt |
| ML | Machine Learning |
| MCU | Micro Control Unit |
| MPC | Model Predictive Control |
| MCFC | Molten Carbonate Fuel Cell |
| NEDC | New European Driving Cycle |
| ODE | Ordinary Differential Equations |
| TRR | Trust Region Reflective |
| PAFC | Phosphoric Acid Fuel Cell |
| PID | Proportional Integrative Derivative |

| | |
|---|---|
| PEMFC | Proton Exchange Membrane Fuel Cell |
| RMSE | Root Mean Square Error |
| SOFC | Solid Oxide Fuel Cell |
| SVM | Support Vector Machine |
| WLTP | Worldwide Harmonised Light-Duty Vehicles Test Procedure |

# 1 INTRODUCTION

The dissertation is the final curricular unit of the master's degree in Systems Engineering, from Universidade do Minho, whose purpose is to promote initiative, decision making, creative and critical thinking. The dissertation consists of a research and development work lasting six months with a private entity that supports the present project.

## 1.1 Background

The continuous growth of the world population has led to a rapid increase in the use of energy that comes from hydrocarbon sources (fossil fuels), which are reaching their exploitation limit (Alanne, 2019). After the industrial revolution, it was noticed an increase in the energy consumption and this led to a direct increase of the Greenhouse gases, mainly carbon dioxide ($CO_2$) (Martinez, 2005). Greenhouse gases play an important role in regulating the planet Earth temperature. Without these gases, all the infrared radiation, which comes from the sun, would be reflected directly into the universe, leading to a drastic decrease in the average temperature of the Earth (Hertzberg et al., 2017). Due to the increase in $CO_2$ concentration, a lot of radiation is reflected and maintained within the atmosphere, increasing the temperature of the planet, causing drastic climate changes (Hertzberg et al., 2017). The demand for using renewable and clean energy sources has increased in the last years as a way to combat the consumption of fossil fuels, to respond the demand for energy consumption (Radcliffe, 2018).

The International Energy Agency (IEA) has reported a long-term goal of 50% reduction in the global average emissions by the year 2030 (Scott & Gössling, 2021). In the last year, 2021, the consumption of oil derived fuels has increased to almost pre-Covid-19 levels, as stated in the IEA report (Ibrahim et al., 2021), with 60% of the oil production being consumed by the transport sector. Within that, automobile brands were forced to develop new powertrains, to meet with the new emissions regulations. Some strategies have been adopted developing engine downsizing technologies and hybrid vehicles in the last decade, but $CO_2$ emissions are not reducing as expected (Namar et al., 2021). The reduction of pollutant gases emitted by vehicles has not decreased the overall $CO_2$ emissions and automotive developers are taking new approaches to develop cars that do not rely only on fossil fuels (Wang et al., 2022).

In the last decade, almost all automobile brand have introduced several models of Electric Vehicles (EV) on the market and this has highlighted even more peaks in electrical energy consumption, increasing the

demand for fossil fuels in order to meet the extra power grid load, since it is not ready to respond to such a high demand for EVs (Hartmann & Özdemir E., 2011).

This type of vehicles presents disadvantages from an end-user point of view, relatively to conventional Internal Combustion Engines (ICE) vehicles, such as long charging time, low range, high acquisition cost and also low energy density of the batteries representing in some cases more than 28% of the total weight of the vehicle (Gelmanova et al., 2018).

Vehicles that rely on $H_2$ use a Fuel Cell (FC) to convert chemical energy into electrical energy, which in turn is consumed by electric motors to move the vehicle according to the drivers input. This type of vehicles is complemented with a small battery pack which helps supplying energy to the engine in case of an unexpected power request from the driver (Yoshida & Kojima, 2015).

This new technology also has advantages from a cost perspective view in relation to EV due to the difference in battery size, reducing the consumption of chemical compounds such as lithium, cobalt, and nickel, as well the cost of battery replacement for the end-user. In the last decade, several studies have been carried out to understand the impact that FC vehicles and EV will have in the future, reducing $CO_2$ emissions. A studied conducted by Thomas (2009), forecasts the impact on $CO_2$ emissions by vehicle powertrain architecture, comparing ICE, EV, FC and hybrid technologies, concluding that the use of EV and FC are the key to massively reduce Greenhouse Gases in the present century. Furthermore, Pollet et al. (2019) developed a studied that focuses on the cost and reliability of FC, concluding that the cost and reliability will match the conventional ICE vehicle in this decade. However, the main disadvantage of FC vehicles are the fuelling stations. Charging EV, even nowadays, is not properly easy due to the low number of chargers and problems in their operation. The $H_2$ fuel stations are complex and costly to implement, and these are the main reasons that justify the low number of refuelling stations (with a target of 3000 by the year 2030) (Staffell et al., 2019).

The use of $H_2$, as a fuel source, is of significant importance because it addresses the problem of greenhouse gas emissions without the disadvantages of EVs, making it the fundamental chemical compound to achieve the goals of European Union till 2050 in the context of decarbonization of the energy and transport sectors (European Commission, 2012).

## 1.2 Motivation

The interest in this technology as a response to the future clean mobility by automotive manufactures has also the interest from Tier 1 technology suppliers such as Continental Engineering Services (CES), to develop powertrain models that can simulate real operating conditions of all components in a system level modelling acting as a base model to test new solutions and specific working conditions.

System level modelling allows to explore the global behaviour of a large physical system without being completely specified and does not require a detailed knowledge of each part of the system. This type of holistic simulation allows to simulate technology concepts and study early development phases of the project.

In this perspective, CES, together with the author of this dissertation, are interested in exploring this technology and developing a model that simulates the real operation of an automotive fuel cell and studies its control logic, serving as a base model for future developments of advanced control strategies and predictive models of degradation of components and reliability of the fuel cell.

## 1.3 Goals and objectives

The main objective of this work is to develop a model in Simulink, an add-on present in MATLAB software, that represents the real working behaviour of a fuel cell system (FC System). An initial theoretical model and data from a vehicle with a fuel cell are the initial point to develop this work. The data obtained, by a governmental entity, through tests on a dynamometer, will be used to reflect the behaviour of the FC System to a Simulink model.

The work comprises the following tasks to achieve the objective:

I. Study and understand the theoretical fuel cell operation
II. Study and understand the fuel cell system for vehicles applications
III. Study and understand fuel cell control strategies
IV. Analyse test data from a fuel cell vehicle
V. Problem formulation and necessary requirements
VI. Model construction and evaluation
VII. Control algorithm and logic construction and evaluation
VIII. Test control strategies and evaluate their application and results

After all of the tasks being completed, the final model should be ready to be used, by the private entity that supports this project, to develop advanced control strategies and evaluate their performance as needed.

## 1.4 Outline

This work comprises six chapters. To understand the working principle of an FC, a brief literature review will be done in Chapter 2, explaining the various types of FC and which ones are applied to vehicles, system architecture and all necessary components. In addition, a review on the modelling strategies that can be implemented to the FC and controller will be performed.

In Chapter 3 the model of the FC is described. To model the FC stack, MATLAB and Simulink will be used to develop a model that is based on the available data. These data were obtained by a governmental entity that carry over multiple tests to a production FC vehicle on a dynamometer. The expected result is to simulate the real working operation of the FC System, mainly obtained similar voltage and resistance signals. To develop that model, a base example model will be used and with the test data and specification data from the production vehicle, the model will be modified and optimized to match the same FC working principle present in the vehicle.

After the development of the model, which contains all the components related to the fuel cell, it is possible to model a control strategy for the FC, described in Chapter 4. Two control strategies will be implemented, to control all the main components, based on real sensors according to specific inputs.

In Chapter 5, the conclusions of this work will be presented, as well as proposals for improvements and future work.

## 1.5 Continental Engineering Services

The present dissertation was developed on a research and development partnership between Universidade do Minho and Continental Engineering Services with the aim to achieve the defined goals.

Continental Engineering Services, CES, – a subsidiary of the Continental – was founded in 2006 to provide engineering services to industries. It started its activity in two German cities (Frankfurt and Nuremberg), and currently has more than 20 locations worldwide.

The work carried out at CES focuses on automotive electronics, driveline and chassis technology, as well as electric mobility and autonomous driving. In addition, they are also working on adapting automotive technologies to a wide spectrum of industrial applications. The work at CES ranges from consulting concept studies to carrying out prototypes and small series, having control of the entire product development process.

CES presents itself as the best partner in engineering solutions within the automotive sector as well as for all industries. In Portugal, it is headquartered in Porto, launched in 2019 and currently has more than 200 employees.


Figure 1 - CES logo.

# 2 LITERATURE REVIEW

In this chapter a literature review at the state of the art will be carried over, investigating critical topics that are essential to understand the behaviour of the fuel cell and the controller that controls all the necessary components. Also, a review on methods that are crucial to develop the project were taken into account that will be used to develop the model on MATLAB.

## 2.1 Fuel Cell

In 1838, Sir William Grove, who was a British physicist discovered the first fuel cell. It was made of sheet iron, copper, porcelain plates and a solution of sulphate of copper and dilute acid, that with a proper assembly, it would generate a small voltage with the reaction between two gases (Grove, 1839). Many years later, in 1930s, Thomas Bacon developed, with success, the first stationary fuel cell capable of 5kW using hydrogen and oxygen as fuel (Cohn, 1965). The race to space and the moon in the mid of 20th century paid much attention to fuel cells because they made it possible to produce electrical energy, when it was needed, based on chemical energy, according to the physical conditions of the universe. It was in the project Gemini from NASA that fuel cells were implemented to solve a real problem and made possible for a human being to go to the space and moon several times (Cohn, 1965). In the 1990s, fuel cells were being applied to vehicles, such as batteries, but were never successful because their limitations in range and system size. On the other hand, low fuel prices have encouraged people to buy ICE vehicles.

A fuel cell consists of two electrodes, called anode and cathode, which are wrapped around, and an electrolyte as presented in Figure 2. On the anode side, fuel ($H_2$, methanol, natural gas, etc) is supplied in the form of gas and a chemical reaction occurs that detaches electrons from the chemical molecule, resulting in a proton. The electrons travel through a conductor and will eventually feed an electrical circuit, giving part of their energy, and returning to the cathode side. At the cathode, air is being supplied from the atmosphere and the $O_2$ molecules will react with the electrons and hydrogen protons, resulting in the formation of $H_2O$. This is the basic dynamics of the fuel cell and will be discussed in depth in the next sections, focusing on the types of fuel cells, how they are composed, and how to control the variety of parameters and components (EG & G Services et al., 2000).

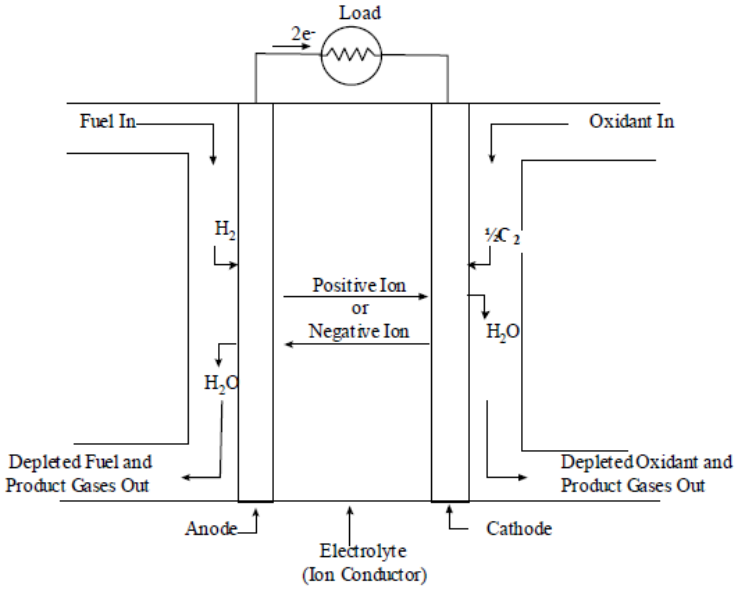


Figure 2 - Schematic of an Individual Fuel Cell (EG & G Services et al., 2000)

## 2.2 Fuel Cell Types

Fuel cells can have multiple applications according to the fuel type present on the anode side, resulting in multiple arrangements of components and materials for their operation. The six main groups of fuel cells according to their electrolyte type are the following: Proton Exchange Membrane Fuel Cell (PEMFC), Solid Oxide Fuel Cell (SOFC), Alkaline Fuel Cell (AFC), Phosphoric Acid Fuel Cell (PAFC), Direct Methanol Fuel Cell (DMFC) and Molten Carbonate Fuel Cell (MCFC).

Each type of electrolyte will determine the chemical reactions that take place on the anode and cathode sides, oxidation, and reduction reactions respectively. Therefore, the electrolyte also defines the fuel type, operating temperature and conditions required to operate the fuel cell, such as start-up and fuel pre-processing processes.

Low temperature FC, such as PEMFC, PAFC, DMFC and AFC require the fuel that enters on the anode must be pure $H_2$ for the oxidation reaction to take place. On the other side, high temperature FC like MCFC and SOFC can be fed with other fuels containing CO or $CH_4$ and due to the high operating temperature, part of these fuels is converted to $H_2$ internally. Table 1 provides a simple overview of the main specifications by FC type and also the main disadvantages and advantages of each one on Table 2 (Codina, 2017).

Table 1 - Comparison of different types of fuel cells

| | PEMFC | SOFC | AFC | PAFC | MCFC | DMFC |
|---|---|---|---|---|---|---|
| Electrolyte material | Polymer | Zirconium dioxide and Yttrium oxide | Potassium hydroxide | Phosphoric Acid | Potassium lithium carbonate | Polymer |
| Electrode material | Carbon | Calcium titanate | Nickel | Carbon | Nickel | Carbon |
| Operating temperature (°C) | 50-100 | 500-1050 | 50-150 | 200 | 650 | 50-100 |
| Oxidation reaction (Anode) | $H_2 \rightarrow 2H^+ + 2e^-$ | $H_2 + O^{2-} \rightarrow H_2O + 2e^-$ | $2H_2 + 4OH^- \rightarrow 4H_2O + 4e^-$ | $H_2 \rightarrow 2H^+ + 2e^-$ | $H_2 + CO_3^{2-} \rightarrow H_2O + CO_2 + 2e^-$ | $CH_3OH + H_2O \rightarrow 6H^+ + 6e^- + CO_2$ |
| Reduction reaction (Cathode) | $\frac{1}{2}O_2 + 2H^+ + 2e^- \rightarrow H_2O$ | $\frac{1}{2}O^2 + 2e^- \rightarrow O^{2-}$ | $O_2 + 2H_2O + 4e^- \rightarrow 4OH^-$ | $\frac{1}{2}O_2 + 2H^+ + 2e^- \rightarrow H_2O$ | $\frac{1}{2}O_2 + CO_2 + 2e^- \rightarrow CO_3^{2-}$ | $\frac{3}{2}O_2 + 6H^+ + 6e^- \rightarrow 3H_2O$ |
| Ion charge carrier | $H^+$ | $0^{2-}$ | $OH^-$ | $H^+$ | $CO_3^{2-}$ | $H^+$ |
| Fuel | $H_2$ | $H_2$, $CH_4$ and $CO$ | $H_2$ | $H_2$ | $H_2$, $CH_4$ and $CO$ | $Methanol$ |
| External reforming of fuel | Yes | No | Yes | Yes | No | Yes |
| Power capacity output (kW) | 1-250 | 5-5000 | 1-100 | 100-1000 | 100-2000 | < 1 |
| Use | Electricity and Heat generation | Electricity, Heat and steam generation | Electricity generation | Electricity and Heat generation | Electricity, Heat and steam generation | Electricity generation |
| Efficiency (%) | < 40 | 60 - 85 | 50 - 60 | 45 - 85 | 40 - 85 | 20 - 25 |

NASA in the Gemini project used an AFC (Figure 3) for its space operation due to its low temperature behaviour, high efficiency, and considerable power output for the requirements of the lunar module. It was possible to control the power output based on $H_2$ and $O_2$ inputs and produce potable water for the astronauts (Cohn, 1965).

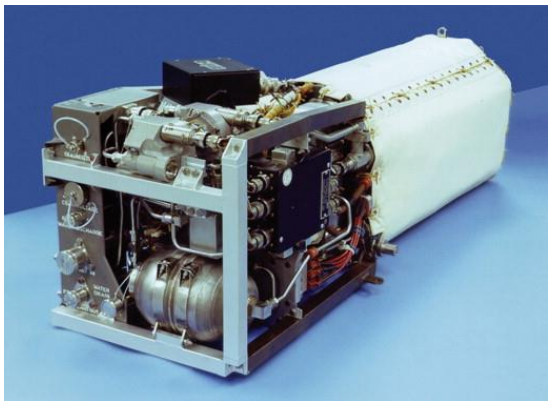

Figure 3 - NASA PC17 C Alkaline Fuel Cell (Cohn, 1965).

In mid-1960s this development was very expensive, so it led to the exploration of other types of FC and other applications as well. For the automobiles, PEMFC are the main focus due to their high-power output,

reliability, low temperature, fast start-up, good efficiency and absence of pollutant gas emissions (Costamagna, 2001).

The first application of an FC to an automobile was made in 1993 during the New Generation of Vehicles program, an partnership between California Environmental Legislations and the United States of America with the support of three main automobile manufactures, began to explore the application of a PEMFC in the transportation sector, developing the first prototypes of FC powered vehicles and also the composite materials needed to manufacture the FC (Costamagna, 2001).

Table 2 - Fuel cells advantages and disadvantages

| Type | Advantages | Disadvantages |
|---|---|---|
| PEMFC | - Quick system start-up and shutdown<br>- Portable applications<br>- Electrolyte is very resistive to gas crossover<br>- High power density | - Expensive catalyst (platinum)<br>- Difficulties in thermal management |
| SOFC | - Fuel flexibility<br>- Nonprecious metal catalyst<br>- Solid electrolytes allow various shapes of cells<br>- High quality heat waste for cogeneration | - High temperature causes material problems such as thermal expansion<br>- Sealing issues<br>- Limited range of material selection<br>- Relatively expansive components and fabrication |
| AFC | - High efficiency<br>- Low manufacturing and operation costs<br>- Mature technology | - Electrolyte is a corrosive liquid<br>- Complex system configuration |
| PAFC | - Mature technology<br>- Cogeneration of heat<br>- Excellent reliability and long-term running<br>- Relatively inexpensive electrolyte | - Slow reduction in the cathode side<br>- Electrolyte is a corrosive liquid<br>- Complex system configuration |
| MCFC | - Fuel flexibility<br>- Non-precious metal catalyst<br>- High quality waste heat for cogeneration<br>- High efficiency | - Corrosive and mobile electrolyte<br>- High temperature results in degradation and reliability issues<br>- High contact resistance and cathode resistance limit power density |
| DMFC | - Simple structure<br>- Good for low power/long operation hours | - Poor cell efficiency<br>- Poor power density |

Other types of FC, such as MCFC and SOFC are being used in the energy system due to the very high-power output and the ability to use multiple fuels, taking advantage of their high operating temperature and reforming the fuel to convert it to $H_2$. The steam generation can also be used to generate power using steam and gas turbines in power plants to maximize the FC efficiency (Choudhury et al., 2013).

In the next sections, only PEMFC will be evaluated because of its applicability to automotive vehicles and, all of the production vehicles, to date, use this type of FC.

## 2.3 Fuel Cell System

The fuel cell system is composed by multiple elements, which have specific functions to achieve maximum efficiency of the system. PEMFCs used in automobiles can be separated into two systems:

- Internal system that handles the chemical reactions inside the fuel cell stack,
- External system that supplies the fuel and air to the fuel cell stack.

The internal system handles the electrochemical, thermodynamics and kinetics of the reactions occurring inside the fuel cell stack. For the internal system to work, the external system must supply the main energy sources, being $H_2$ and air for this specific type of FC, in addition to maintaining an optimal operating temperature.

### 2.3.1 Internal Fuel Cell System

An electrochemical device, such as a fuel cell, allows the generation of electric energy from a chemical reaction as long as $H_2$ and air is supplied. The collisions between $H_2$ and $O_2$ molecules result in a reaction where $H_2$ is oxidized, producing water and heat, as verified in Equation (1) (Kabza, 2016).

$$H_2 + \frac{1}{2}O_2 \rightarrow H_2O \tag{1}$$

In an atomic scale, the hydrogen – hydrogen bonds and oxygen – oxygen bonds are broken and hydrogen – oxygen bonds are formed resulting in energy release in the form of heat. For these bonds to break and form, the transfer of electrons between molecules must take place. Capturing these electrons, while they are being transferred between the molecules, results in a continuous electric current through a conductor. To capture the electrons, it is necessary to spatially separate the reactants $H_2$ and $O_2$ so that the transfer of electrons, necessary to complete the bounding and formulate water, occurs over an extended length scale, and can be harnessed as an electrical current (Kabza, 2016).

Separating the reactants, the overall reaction is divided into two electrochemical reactions called $H_2$ oxidation (Equation (2) and $O_2$ reduction (Equation (3)) (Kabza, 2016).

$$\mathrm{H_2} \rightarrow 2\mathrm{H^+} + 2\mathrm{e^-} \tag{2}$$

$$\frac{1}{2}O_2 + 2H^+ + 2e^- \rightarrow H_20 \tag{3}$$

By spatially separating these reactions, the electrons are forced to flow through an external circuit (resulting in an electrical current) and do work in electronic circuits before they can complete the reaction. This separation is achieved using an electrolyte, which is a material that allows ions (negative or positive charged atoms) to flow through, but not electrons, called proton exchange membrane (Kabza, 2016).

Electrons flow through the electrodes, which are made of a conductor material that will eventually lead the electrons to an electric load. Figure 4 presents the structure of a PEMFC that exemplifies the working concept of a spatially separate chemical reaction. On the anode side the oxidation reaction takes place, the electron is collected by the anode plate, and the proton passes through the electrolyte membrane. On the cathode side the reduction reaction takes place formulating water combining the proton, electron and $O_2$ (Kabza, 2016).

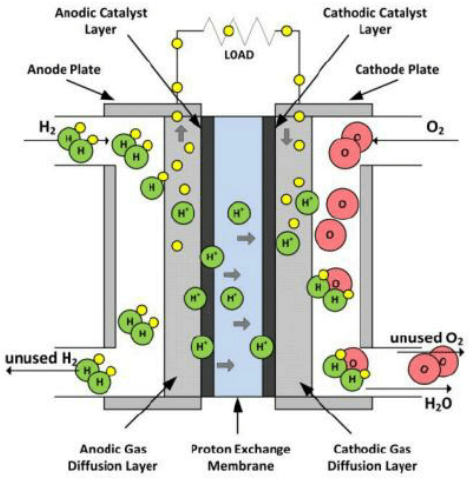


Figure 4 - Proton exchange membrane fuel cell essential components (Vishnyakov, 2006).

In order for these reactions to take place at the anode and cathode, a special arrangement of a catalytic layer combined with a gas diffusion layer is responsible for the electron collection and oxidation and reduction reactions.

The reaction between these elements is categorized as an exothermic reaction, where the enthalpy change is negative, resulting in the release of heat. Therefore, Equation (1) verifies the following condition: $\Delta_r H < 0$, where the reaction enthalpy of hydrogen oxidation ($\Delta_r H$) is equal to the enthalpy of water formation ($\Delta_f H_2 O$) (Kabza, 2016).

The energy content of any fuel is described by its heating value that specifies the amount of heat released during the consumption of that fuel. In this case, water can be formed either in the gaseous or liquid state, corresponding to the higher heating value (HHV) and lower heating value (LHV), respectively

Equations (4) and (5) corresponding to the enthalpy of the reaction, since water is the only by product in this case (Kabza, 2016).

$$H_2 + \frac{1}{2}O_2 \rightarrow H_2O_{(g)} \quad -\Delta_f H_2O = HHV = 285.83\ kJmol^{-1} \tag{4}$$

$$H_2 + \frac{1}{2}O_2 \rightarrow H_2O_{(l)} \quad -\Delta_f H_2O = LHV = 241.82\ kJmol^{-1} \tag{5}$$

These values are obtained under standard thermodynamic conditions (temperature of 25°C and pressure of 100kPa) and are specified in thermodynamic tables (such as JANAF thermochemical tables) that present entropy, enthalpy, Gibbs free energy, specific heat and other factors over a range of temperatures for all species present in the reaction (O'hayre et al., 2016).

The enthalpy represents the energy that the reaction will produce, but it is also important to evaluate the net energy of the reaction, which is the exploitable energy potential to produce electrical energy. This net energy is reflected in the change of Gibbs free energy, denoted as G, which combines enthalpy and entropy (a measure of disorder in a system) of the reaction. Furthermore, the Gibbs free energy can be useful to determine the spontaneity of a reaction. In this case, if $\Delta G = 0$ then no electrical work can be extracted from the reaction (Kabza, 2016). On the other hand, if $\Delta G > 0$ then external work must occur for the reaction occur, which is the case of an energetically unfavourable reaction. Finally, if $\Delta G < 0$ then the reaction occurs spontaneously, being an energetically favourable reaction, possible to extract further energy from it (Kabza, 2016).

Gibbs free energy can be described by the Equation (6), where $H$ is the enthalpy, $S$ is the entropy and $T$ is the temperature. The entropy of water formation can be found in thermodynamic tables for each physical state and temperature (Kabza, 2016).

$$\Delta G = \Delta H - \Delta S * T \tag{6}$$

Therefore, the Gibbs free energy for each physical state are the following:

$$\Delta G_f H_2O_{(g)} = -228.57\ kJmol^{-1}\ \ or\ \ \Delta G_f H_2O_{(l)} = -237.13\ kJmol^{-1}$$

These values represent the energy that can be converted into electrical work. The electromotive force of any electrochemical device is defined by the following Equation (7):

$$E^0 = -\frac{\Delta G}{n*F} \quad (7)$$

Where $n$ is the number of exchanged electrons in the chemical reaction, being in this case two, and $F$ the Faraday constant, resulting in the following electromotive force:

$$E_g^0 = 1.184\,V \; or \; E_l^0 = 1.229\,V$$

These values are the theoretical maximum voltages that can be obtained from the electrochemical reaction of $H_2$ and $O_2$. Besides that, it makes sense to evaluate two other voltage points from an efficiency point of view. If all the chemical energy of hydrogen (heating value) were converted into electrical energy (impossible to happen due to thermodynamic laws) the cell voltage would be as follows:

$$E_{LHV}^0 = \frac{LHV}{2*F} = 1.253\,V \;\; or \;\; E_{HHV}^0 = \frac{HHV}{2*F} = 1.481\,V$$

At this point it is important to evaluate the cell voltage considering the pressure of reactants on each side of the fuel cell. The Nernst equation considers not also the temperature, but also the pressure of $H_2$ and $O_2$ representing a correction to the initial electromotive force equation. The Nernst equation is described in Equation (8) where $E^0$ is the electromotive force value, $R$ is the universal gas constant, $n$ is the number of exchanged electrons, $F$ is the Faraday constant and $p_{H_2}$, $p_{O_2}$, $p_{H_2O}$ correspond to the partial pressure of hydrogen, oxygen and water, respectively (Kabza, 2016).

$$E = E^0 + \frac{R*T}{2F} * \ln\left(\frac{p_{H_2} * p_{O_2}^{1/2}}{p_{H_2O}}\right) \quad (8)$$

This equation reflects how the electrochemical cell voltage varies as a function of reactant concentrations (due to pressure) and temperature making it the fundamental centrepiece of fuel cell thermodynamics. To evaluate the impact of pressures in the fuel cell voltage, a simple example can be elaborate considering the following situations:

1. The fuel cell operates below 100°C so that liquid water is produced, room temperature is 25°C, hydrogen pressure is 3atm, air pressure is 5atm (21% of the air is oxygen) and the resultant water is evacuated at 1atm. The following voltage would be verified at the electrodes:

$$E = 1.229 + \frac{8.314 * 298.15}{2 * 96485} * \ln\left(\frac{3 * \ (5 * 0.21)^{\frac{1}{2}}}{1}\right) = 1.2434\ V$$

2. The fuel cell operates below 100°C so that liquid water is produced, room temperature is 25°C, hydrogen pressure is 1atm, air pressure is 1atm (21% of the air is oxygen) and the resultant water is evacuated at 1atm. The following voltage would be verified at the electrodes:

$$E = 1.229 + \frac{8.314 * 298.15}{2 * 96485} * \ln\left(\frac{1 * \ (1 * 0.21)^{\frac{1}{2}}}{1}\right) = 1.2189\ V$$

Pressurizing the hydrogen and air is beneficial for increasing the fuel cell voltage, but not so much for all the extra work of pressurizing the fuel cell stack (only 25.45mV increase), on the case of an open circuit, meaning that is useless to pressurize the fuel cell stack when there is no current flow. From a thermodynamic perspective it is not worth the extra complexity for such a low increase. But fuel cells must produce electricity to drive a load, and for that three major performance problems occurs, and it significantly decreases the cell voltage when the electrical circuit is close (O'hayre et al., 2016).

As soon as electrons and protons begin to move, multiple voltage losses are verified at different current demands (O'hayre et al., 2016). This voltage losses are nonlinear functions of the load/current and are the following:

1. Activation polarization losses – These are caused by electrochemical reaction kinetics. In the electrodes, where the reduction and oxidation reactions occur, hydrogen and oxygen molecules break their chemical connections and form ions, these are considered to be in their activated state. To convert a molecule into an ion, in an electrochemical reaction, there is certain delay, and this impacts the rate at which electrons can flow, resulting in a decrease of voltage. These losses, verified at low currents, can be determined by the Tafel

equation, where $\alpha$ is the electrons transfer coefficient, $i$ the current and $i_0$ is the exchange current density determined by the electrode's material and design:

$$V_{act} = \frac{R*T}{\alpha*F} * \ln\left(\frac{i}{i_0}\right) \quad (9)$$

2. Ohmic polarization losses – On the other hand, ohmic losses represent all losses related to the movement of the charges (electrons and ions) across the internal fuel cell system. The flow of electrons through the electrode materials and contact pads represents an electrical resistance. In short, the membrane that allows the flow of protons varies its resistance as a function of humidity and material characteristics. The total resistance ($\Omega$) increases proportionally to the current, as verified by Equation (10):

$$V_{ohm} = i * \Omega \quad (10)$$

3. Concentration polarization losses – In the anodic catalytic layer a concentration gradient is formed on its surface when the reactants reach the electrodes. When the reaction starts, the reactants are consumed, resulting in a reduction of the concentration surrounding the electrodes. There is a loss of voltage due to the inability to maintain the initial concentration, meaning that the reactant is being consumed faster than it can reach the surface, a phenomenon verified at high current densities. Equation (11) describes this loss through the parameter $i_L$ which indicates the current density at which the concentration of reactants is lower than the necessary.

$$V_{conc} = \frac{R * T}{n * F} * \ln\left(\frac{i_L}{i_L - i}\right) \quad (11)$$

These losses are often reflected in a polarization curve or current-voltage curve graph, as shown in Figure 5, describing the impact of these losses to the ideal voltage (determined according to the Gibbs free energy). Its magnitude of impact can vary according to the characteristics of material, design of the fuel cell and operating conditions. This curve can be determined with the Butler Volmer equation or through testing the fuel cell (O'hayre et al., 2016).

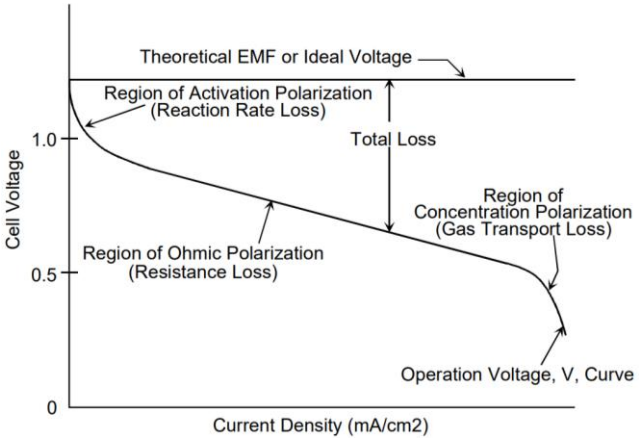


Figure 5 - Fuel Cell polarization curve (EG & G Services et al., 2000).

In addition, fuel cells have two limiting conditions when operating at transient loads. One of them is related to the capability of evacuating the product, water, from the catalytic layer. The gas diffusion layer has two main functions: to proportionally distribute the reactants through the catalytic layer and to remove water from the fuel cell. If the liquid water accumulates in the catalytic layer, it will eventually block the reactant supply and cause the fuel cell performance to deteriorate, because the concentration at the electrodes is significantly lower, and therefore the gas diffusion layer must be designed to remove all the water as quickly as possible to maximize the fuel cell performance at transient loads (O'hayre et al., 2016).

The other limiting factor is the lack of reactants, which means that at transient loads it may occur that the reactants may not reach the gas diffusion layer in time and the catalytic runs out of reactants (because of the high consumption rate), reducing the fuel cell performance and affecting its life duration. To solve this problem one solution is to maintain a minimum level of reactants inside the fuel cell (O'hayre et al., 2016).

A common parameter for determining the excess of reactant within the anode and cathode is the lambda factor that represents the stoichiometry number to maximize fuel cell efficiency. This value reflects the rate at which a reactant is provided to a fuel cell to the rate at which it is consumed (for anode and cathode) (O'hayre et al., 2016).

$$\lambda = \frac{\dot{n}_{provided}}{\dot{n}_{consumed}} > 1 \tag{12}$$

Equation (12) represents how this parameter is determined according to the molar flow ($\dot{n}$) provided and consumed. Maintaining this value above one guarantees the excess of reactant on both sides of the fuel cell. To determine the flow provided, the sensors can be used to read the inlet flow to both sides of the

fuel cell or alternatively based on the *Faradays* law of molar flows ($\dot{n}$) that determines the consumed flow of reactants based on the current:

$$\dot{n}_{H_{2_{consumed}}} = \frac{I}{2F} \tag{13}$$

$$\dot{n}_{air_{consumed}} = \frac{I}{4F * x_{O_2}} \tag{14}$$

For the cathode side, it is necessary to specify the amount of oxygen content in air ($x_{O_2}$). The numbers 2 and 4 in these equations mean the number of electrons exchanged per mole of hydrogen and oxygen, respectively. Considering the molar masses ($M$) of the reactants, the molar flow can be converted into mass flow:

$$\dot{m}_{H_{2_{consumed}}} = \dot{n}_{H_{2_{consumed}}} * M_{H_2}$$

$$\dot{m}_{air_{consumed}} = \dot{n}_{air_{consumed}} * M_{air}$$

Appling the same principles it can be calculated the amount of water produced:

$$\dot{n}_{H_2O_{produced}} = \frac{I}{2F}$$

$$\dot{m}_{H_2O_{produced}} = \dot{n}_{H_2O_{produced}} * M_{H_2O}$$

These parameters help understanding the actual operation of the fuel cell, but as with any energy conversion device, efficiency is of great importance. In determining the efficiency, two central concepts are taken in account: the ideal efficiency and the real efficiency. Efficiency ($\mathcal{E}$) describes the amount of useful energy that can be extracted from the process relative to the total energy used in a specific process:

$$\mathcal{E} = \frac{useful\ energy}{total\ energy}$$

On the case of fuel cells, ideal efficiency is related to the thermodynamic efficiency and is the ratio between enthalpy (or heating value) - $\Delta H$ - and Gibbs free enthalpy ($\Delta G$):

$$\mathcal{E}_{thermo_{LHV}} = \frac{\Delta G_f H_2O_{(g)}}{LHV} = \frac{-228.37}{-241.82} = 94.5\%$$

$$\mathcal{E}_{thermo_{HHV}} = \frac{\Delta G_f H_2O_{(l)}}{HHV} = \frac{-237.13}{-285.83} = 82.9\%$$

These values reflect the theoretical maximum efficiency possible for a fuel cell, according to the physical state of the produced water (O'hayre et al., 2016).

The real fuel cell efficiency takes into account all the problems discussed above that impact its performance. Thus, to determine it, thermodynamic efficiency voltage efficiency and fuel efficiency should be taken into account, (O'hayre et al., 2016).

1. Thermodynamic efficiency, as stated above, reflects how not all the enthalpy contained in the hydrogen can be useful.
2. Voltage efficiency relates the ideal cell voltage ($E$) to the real operating cell voltage ($V$):

$$\mathcal{E}_{voltage} = \frac{V}{E}$$

3. Fuel efficiency, not discussed so far, accounts for the hydrogen provided to the fuel cell that does not participate in the electrochemical reaction. Some of the provided fuel may undergo side reactions or flow through the fuel cell without ever reacting. This efficiency is determined with the ratio of hydrogen used by the cell to generate electric current, and the total hydrogen provided to the fuel cell ($\upsilon_{fuel}$) specified in mol/s, but it is also possible to relate this factor to the stoichiometric value if the fuel cell control operates based on that parameter:

$$\mathcal{E}_{fuel} = \frac{\frac{\mathrm{I}}{n * F}}{\upsilon_{fuel}} = \frac{1}{\lambda}$$

The final fuel cell efficiency is described by the following equation that takes into account all the losses related to it:

$$\mathcal{E}_{real} = \mathcal{E}_{thermo} * \mathcal{E}_{voltage} * \mathcal{E}_{fuel}$$

One single unit of a fuel cell produces a maximum of 1.24V, as stated on the previous section. For vehicle and many other applications, a much higher voltage is required to achieve the desired power level for the application. To solve this problem multiple fuel cells units are stacked in series forming a fuel cell stack (O'hayre et al., 2016).

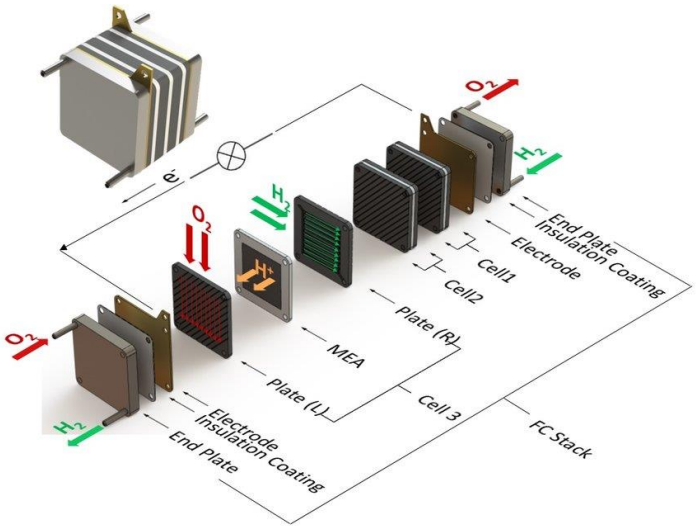


Figure 6 - Expanded view of a simple fuel cell unit in a fuel cell stack (Codina, 2017).

In Figure 6 a stack of 3 cells in series is described. In this case the flow of hydrogen is distributed horizontally through the plates that contain the gas diffusion layer and the catalytic material. Air or oxygen is distributed on the opposite direction, vertically. In cell number 3 is described how the Figure 4 is assembled on a stack, Plate L corresponds to the cathode side components, MEA to the membrane and Plate R to the anode side components. The flow of electrons is collected at the extremes of the stack (electrodes).

Physically all these parts are built together or independently depending on the manufacturing process and the materials used. To demonstrate the assembly of these components in a real application, private companies have benchmarked a fuel cell powered vehicle and dismantle it to give insights on how the fuel cell stack is assembled and how everything is manufactured.


Figure 7 - Expanded view of a physical unit cell (Maruo et al., 2017).

Figure 7 represents the actual fuel cell module that a specific vehicle uses. After the manufacturing process, using, in this case, for the semi bipolar plates - forming and titanium coating, for the membrane electrode assembly – platinum, cobalt and *Nafion* for the gas diffusion layer, micro porous layer (MPL) and membrane respectively, it is possible to have a complete unit in only 3 parts (membrane, gasket and bipolar plate).

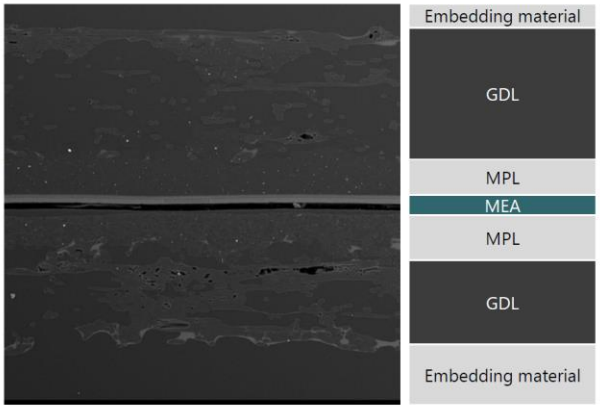


Figure 8 - Microscopical view of cross-section of the membrane electrode assembly (Maruo et al., 2017).

At a microscopic level, it is possible to understand how the membrane electrode assembly works, represented in Figure 8. It is a symmetrical sheet that has stacked all the necessary components for the anode and cathode side. It is also important to understand how air/oxygen and hydrogen reaches the gas diffusion layer.

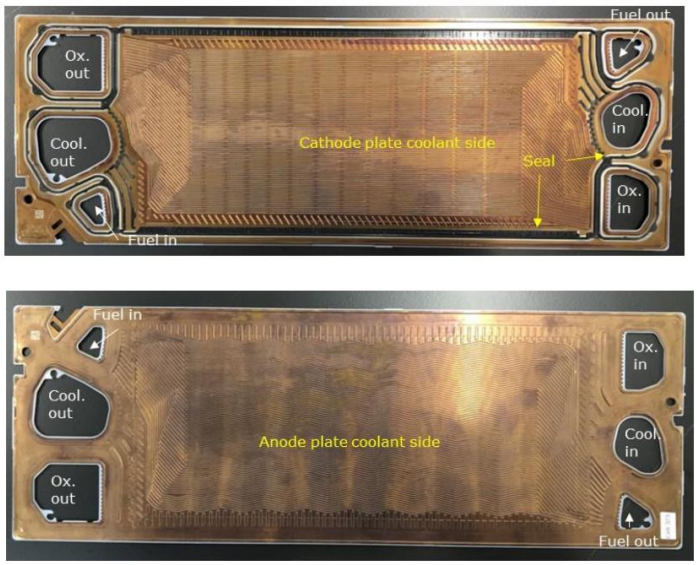


Figure 9 - Front (top) and rear (down) view of the bipolar plate (Maruo et al., 2017).

With a front and rear view of the bipolar plate (Figure 9) it is possible to understand how the air/oxygen and hydrogen are distributed by the gas diffusion layer. In the front view, the cathode side (in the upper left), at the oxygen out (in the bottom right), at the oxygen in passage there are thin guides that insert air/oxygen into the gas diffusion layer. In the rear view, the same design is applied to the fuel in and out passages. Note that the air/oxygen passage area is larger than the fuel passage and this is because of the higher flow required on the cathode side due to only 21% of air is oxygen. There are also coolant passages to remove heat from the bipolar plate generated in the membrane due to the chemical reaction.

In this way, fuel cells can have hundreds of volts. For example, the Toyota Mirai from year 2021 has a fuel cell of 330 units generating a nominal voltage of 330V resulting in a power output of 128kW.

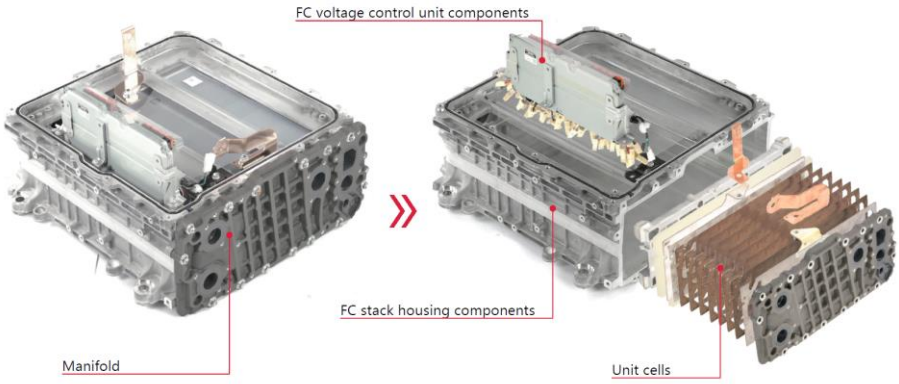


Figure 10 - Expanded view of fuel cell stack (Maruo et al., 2017).

Figure 10 represents all the fuel cell stack assembly, including the unit cells that are stacked in series, the housing that incorporates all the cells, at the end of the housing a manifold is bolted that will seal the

stack and guide all the essential fluids. At the top there is a voltage control unit that monitors the individual cell voltage for forward diagnostics and control of the fuel cell. In applications where more power is needed, for example in heavy duty vehicles, and it is not versatile continuing to make a series of unit cells due to fluid distribution issues, it is possible to place a parallel of multiple stacks or series and parallel to achieve the desired power output.

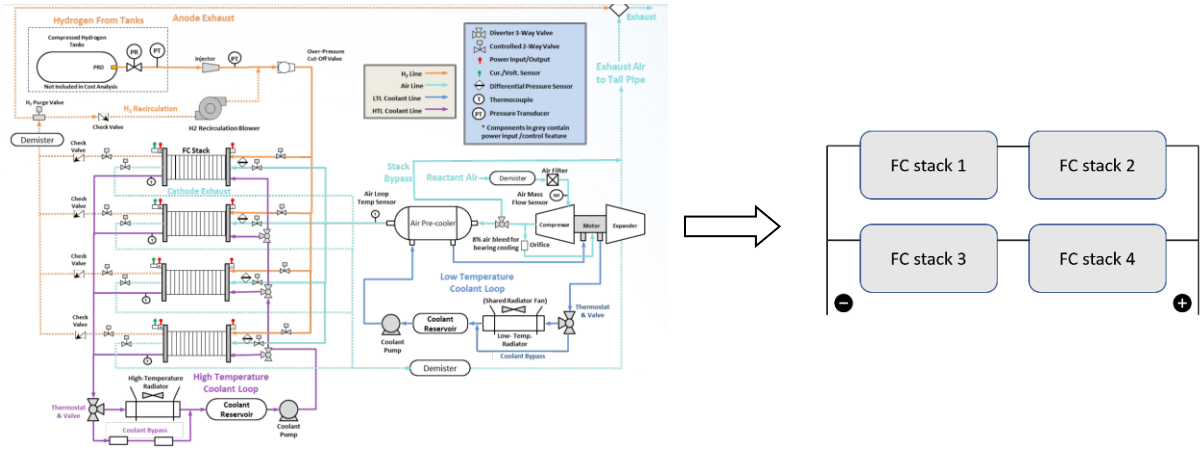


Figure 11 - Long-haul heavy duty vehicle fuel cell system (James et al., DOE Hydrogen and Fuel Cells - Fuel Cell System Analysis, 2021).

In the example of Figure 11 a complete fuel cell system is represented that has a parallel of 2 stacks in series resulting in a system output of 760V and 348kW of power. On the right side it is explained how the fuel cells are eletrically connected and on the left how the entire system interconnects with the multiple components (James et al., 2021).

### 2.3.2 External Fuel Cell System

Fuel cells require a complex system to operate at the most efficient point for different applied loads. This requires multiple components to supply the necessary hydrogen and air corresponding to the dimension and rate of the load.

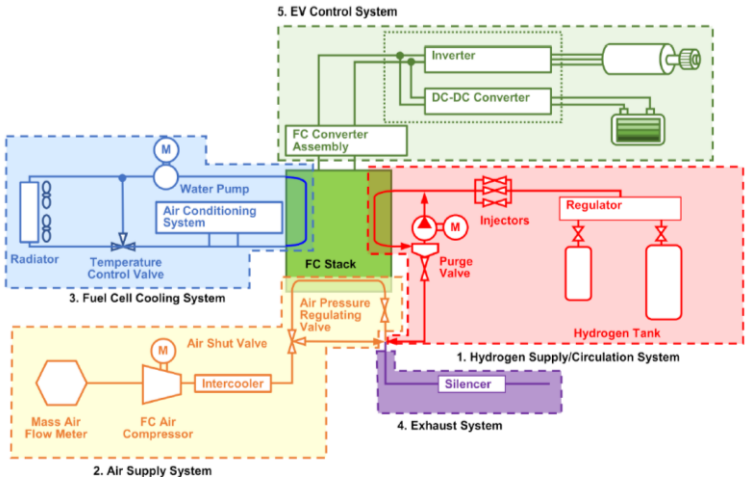


Figure 12 - Fuel Cell sub-systems (Maruo et al., 2017).

These components are organized into subsystems that have a specific function to control their individual components and are in sync with the other subsystems. In Figure 12 the fuel cell stack is at the center of the figure and the multiple subsystems around it controlling the specific components for cooling, air supply, hydrogen supply and energy control.

The EV control system contains all the components related to electrical energy conditioning and management. It is responsible for controlling all the parameters related to the battery, fuel cell and electrical motor status, such as voltage, available current, and demanded power, power split, signal conditioning, electrical frequency, and many others. Fuel cells produce electrical current at an unstable voltage. The voltage varies along with the requested power, from the energy management, and other physical inputs to the fuel cell (Zenith, 2007).

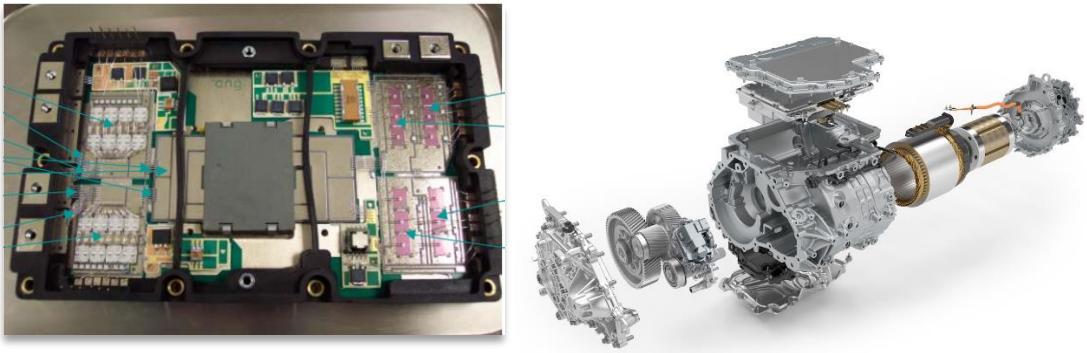

Figure 13 - DC/DC converter (left) and electric motor with DC/AC converter (Olszewski, 2007).

Many components of the vehicle and fuel cell system operate on direct current but with a stable voltage, while others work on alternating current, such as the motor. For each case, two different types of power conditioners are needed:

1. In the case of Direct Currents (DC), DC/DC converters are used to boost the fuel cell voltage to a stable voltage matching the voltage of the battery and other components (Figure 13 - left).
2. For Alternating Currents (AC), the inverter converts the DC current of the fuel cell to the desired current frequency and amplitude. This is necessary because electric motors operate under AC currents (Figure 13 - right).

These power conditioners processes entail a reduction in efficiency as well, ranging from 2% to 6% (Zenith, 2007).

The fuel cell needs pressurized air due to the mechanical properties of the membrane and to increase its power output. To achieve this, an electric compressor (Figure 14 - left) is used to raise the air intake pressure by up to 2-5 times the atmospheric pressure. The increase in pressure translates into an increase in temperature of the air due to thermodynamic properties. An intercooler is used to remove heat from the air, increasing the efficiency of the air supply system (O'hayre et al., 2016).

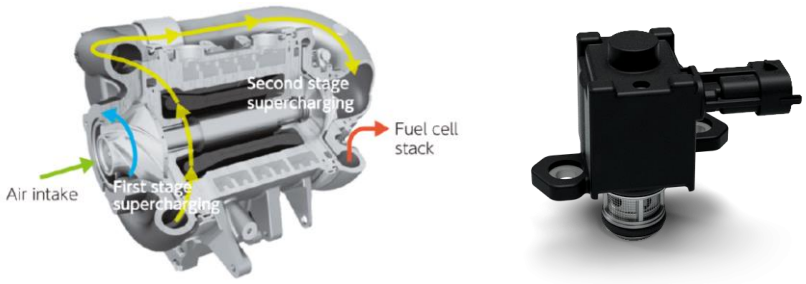


Figure 14 - Air compressor (left) (Kerviel et al., 2018) and hydrogen ejector (right) (Clark & Knight, 2005).

The hydrogen is stored in tanks with pressures of up to 700 bar in order to contain the maximum possible amount of hydrogen. To match the required pressure at the fuel cell intake a pressure regulating valve maintains a stable required pressure (1-4 bars) and the ejector (Figure 14 - right) feeds the intake with the required hydrogen flow. The hydrogen pump recirculates the unreacted hydrogen back to the intake, maximizing the hydrogen reaction (O'hayre et al., 2016).

As the fuel cell efficiency is not 100%, some produce energy is released in the form of heat. The cooling system has the function to maintain a stable operation temperature of the fuel cell, removing heat to the atmosphere (O'hayre et al., 2016).

All these subsystems need to be controlled in a synchronized environment and that is the task of the Fuel Cell Control Unit (FCCU). This component, also present in most of the actual vehicles that rely on combustion engines, has the job of generating electrical signals for the multiple actuators, receiving

signals from all the sensors and determining the optimal conditions for the current state of the fuel cell, preventing any damage operating point. Figure 15 presents an example of a FCCU, that consists of a board with multiple electrical components and a Micro Control Unit (MCU) that contains all the logic and programming of the control structure (Tanaka, 2020).

Figure 15 - FCCU based on Infineon MCU (Tanaka, 2020).

## 2.4 Powertrain architectures

At a higher level, the fuel cell system is just a part of the powertrain block. The powertrain is made up of all elements that convert, store and produce energy to move the vehicle. The layout of all components follows the technical requirements for the powertrain concept, for example: fuel consumption, drivability, homologation, performance, thermal, functional safety, costs, etc (Hick et al., 2020).

Some examples of the main powertrains applied to fuel cell vehicles are as follows:

1. Full fuel cell – these types of vehicles only use fuel cells to power the transmission system, being the simplest configuration composed of the fuel cell system, DC/DC converter, inverter, and the electric motor. This simplistic approach has the characteristics of being easy to control making it a good application in low-speed vehicles such as forklifts, small buses, and marine vehicles (Yu et al., 2022).

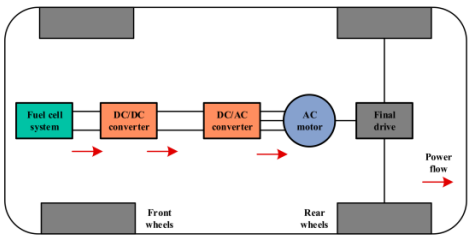


Figure 16 - Full fuel cell powertrain architecture (Yu et al., 2022).

2. Fuel cell + battery hybridization – the hybrid power system composed of fuel cell and batteries is the most common architecture used in vehicle applications. The use of batteries allows to have

a component with high energy density, which enables the possibility of energy regeneration under certain conditions. It can be organized into two architectures, the first is the battery connected directly to the DC bus and the other is the battery connected to the DC bus, but after the DC/DC converter as show in Figure 17 (Yu et al., 2022).

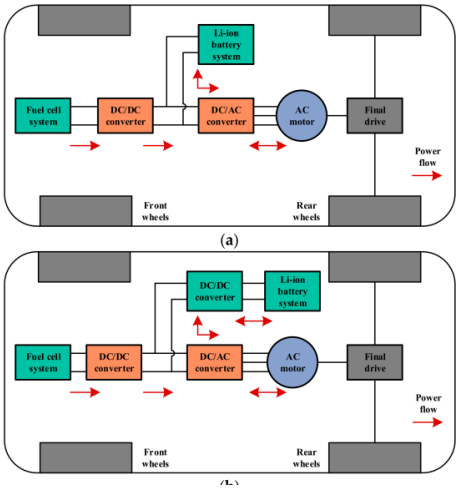


Figure 17 - Fuel cell + battery hybridization powertrain architecture (Yu et al., 2022).

3. Fuel cell + ultra-capacitor hybridization – Similar to the previous architecture, this setup uses an ultra-capacitor instead of a battery, having advantages in faster charge/discharge and longer life cycle. These advantages allow for a more efficient power recovery and better dynamic response to instantaneous high-power demand. The use of ultra-capacitators represents a high economic development cost, therefore this setup is only used for prototypes and racing applications (Yu et al., 2022).

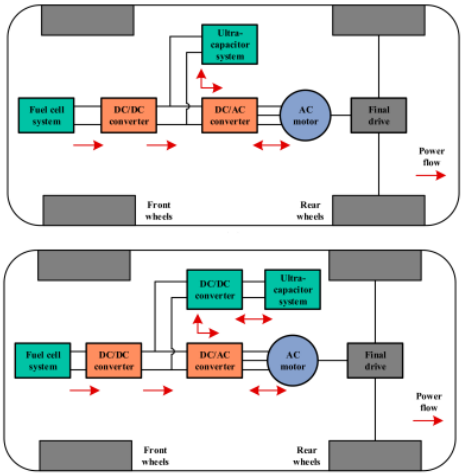


Figure 18 - Fuel cell + ultra-capacitator hybridization powertrain architecture (Yu et al., 2022).

## 2.5 Fuel Cell modelling and control strategies

Recently, considerable progress has been made in modelling and simulation of FC, reflecting the importance of having accurate models to understand the behaviour of FC under different operating points and also, assess potential improvements of the different components and design control solutions. In the following, a literature review on how to model the FC and the control strategies of FC will be addressed.

### 2.5.1 Fuel Cell modelling

The internal behaviour of a FC is very complex due to the different and tightly coupled phenomena that occur simultaneously within a cell: fluid-dynamics phenomena, electrochemical reactions, proton transport through proton-conductive polymer membrane, electron conduction though electrically conductive cell components, water transport and heat transfer.

Modelling is necessary to describe these fundamental phenomena in each subsystem of the FC System to evaluate steady-state and dynamic responses. All these complicated processes that take place within the FC System make the modelling task particularly challenging. Several articles on the literature can be found on ways to model complete FC Systems or individual models for each subsystem.

These models are then used to predict FC performance under different operating conditions, optimize and design control strategies, and also to evaluate improvements in particular components (Nehrir & Wang, 2009).

There are several types of FC models that, depending on the purpose, serve to evaluate different parameters and development topics.

A first type of models is focused on a specific part of the FC, for example membrane, gas diffusion channels, catalyst layer and helps study in depth the working conditions of that particular component. The second type of model includes a complete working unit cell that can be explored to study phenomena such as the electrochemical reaction, water transport, heat dissipation and other topics.

A more complex model of this type is a FC stack model, which considers the arrangement of more than one cell to supply the required power demand. At a higher level are system level models that include the complete FC stack and all the auxiliary components that make up the FC system. These higher-level models may use empirical functions that describe the behaviour of a component and avoid including the full specification of the component, which will have a lot of computational power impact when simulating (Yao et al., 2004).

As the focus of this dissertation is to study system level modelling of the FC system, only literature describing system level modelling techniques will be addressed.

Typically, system level models are combined parameter models used to evaluate FC behaviour under different operating conditions and to design controllers. A system model is one in which the dependent variables of interest are a function of time. This translates into solving a set of ordinary differential equations (ODE). Pukrushpan et al. (2004) developed a system level model that includes the fuel cell stack, hydrogen supply, air supply, cooling, and humidification systems. All of the system equations are based on physical, chemical and thermodynamic equations (equations similar to those described on previous subsections) that represent the nine states of the system at the current simulation time but only obtaining theoretical results (Pukrushpan et al., 2004).

A few years later, a more complex and accurate model (Figure 19) was developed by Bao et al. (2006), where a complete FC System could represent 9 states out of 10 very accurately compared to data obtained from a prototype FC System (Bao et al., 2006).

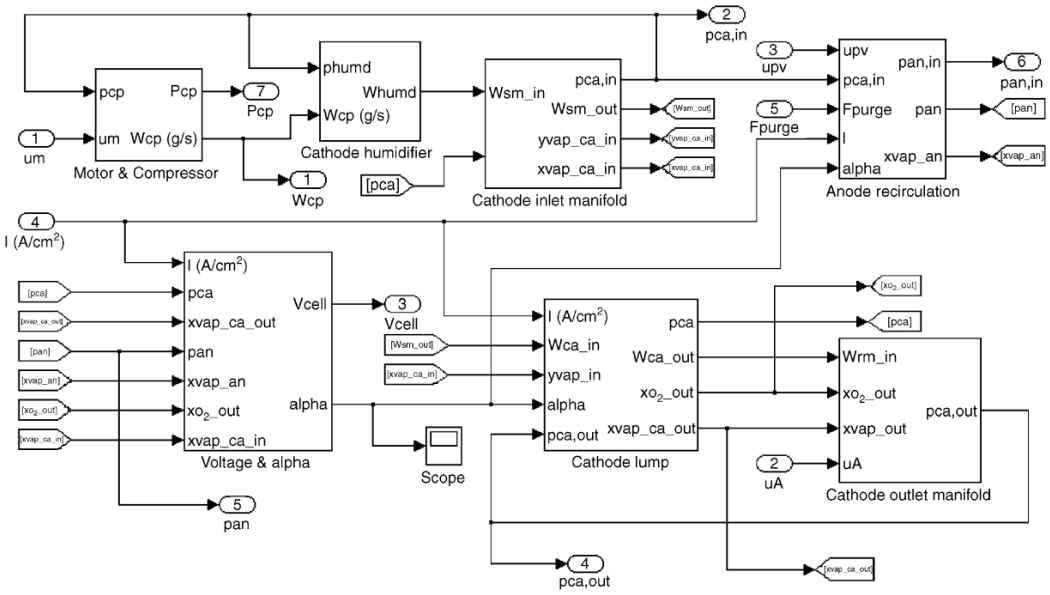


Figure 19 - Dynamical model of FC System implemented on MATLAB/Simulink (Bao et al., 2006).

The development of this type of mathematical based models is time consuming and requires many technical details about each component that can only be obtained when the physical characteristics are known.

In recent years, other types of modelling strategies have emerged. One of them is the use of dedicated software that has the capability to design an FC System based on pre-defined components and dynamics, which, through parameters, can be adjusted to behave as expected. This type of software allows a deeper

development and study of the overall system without specifying equations for all the necessary components. Wang and Xu (2019) have used GT-Suite software, a licensed product of Gamma Technologies, to model a complete FC System that can be integrated into a powertrain model (Figure 20). This powertrain model simulates all the dynamics of the vehicle in real cenarios, allowing to simulate homologation drive cycles, such as the Worldwide Harmonised Light-Duty Vehicles Test Procedure (WLTP), and evalute overall performance factors (Wang & Xu, 2019).

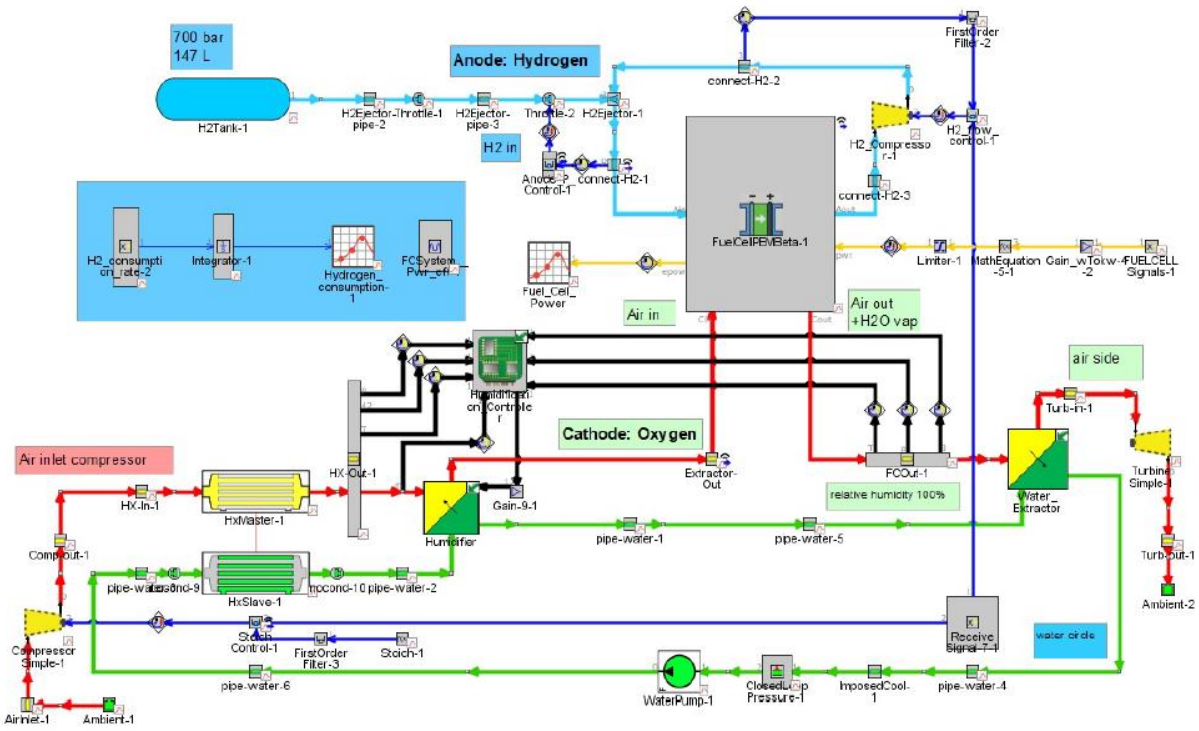


Figure 20 - FC System model in GT-Suite software (Wang & Xu, 2019).

The work presented by Wang and Xu (2019) evaluates the hydrogen consumption of two different powertrain architectures, with different control strategies, under various driving cycles and scenarios concluding that a plug-in fuel cell vehicle has lower hydrogen consumption and overall better performance when compared to the same powertrain architecture without plug-in capability. The use of dedicated software is a powerful tool to simulate and optimize complete vehicles under real driving scenarios (Wang & Xu, 2019).

Other approaches, as the one developed by Lu (2013), uses a hybrid model. Part of the model is the mathematical model developed by Pukrushpan et al. (2004) and an empirical model. These empirical model use Support Vector Machine (SVM) to determine empirical values (seven values) that correct the output of the mathematical model and approximate its behaviour according to real bench test dataset, taken from a prototype FC System developed by Ford Engineering (Lu, 2013).

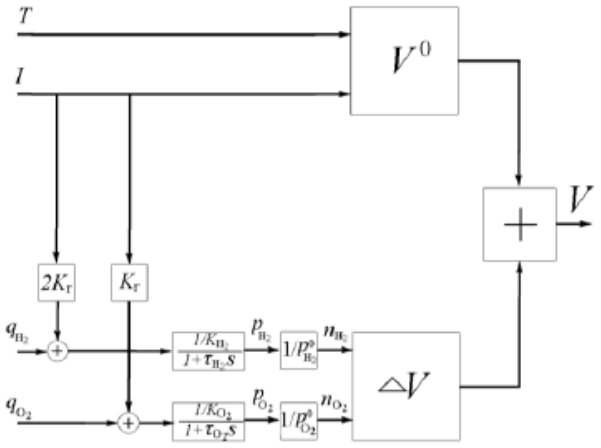


Figure 21 - Schematic of the FC System hybrid modelling model (Lu, 2013).

The mathematical model, developed by Pukrushpan et al. (2004) is inside the box $\triangle V$ and the empirical model inside the box $V^0$ (Figure 21). Both models work together to determine the fuel cell voltage, with the empirical model correcting the error of the mathematical model. The result of the overall model shows a 99% accuracy of the output signal, compared to the bench test dataset of the FC System (Lu, 2013). This strategy shows a quick way to develop models that can be representative of multiple FC System after being calibrated, speeding up the development process.

Another successful strategy using MATLAB and Simulink is presented by Surya et al. (2021) that applies Machine Learning (ML) techniques to estimate cell parameters based on a NASA dataset (Surya et al., 2021).

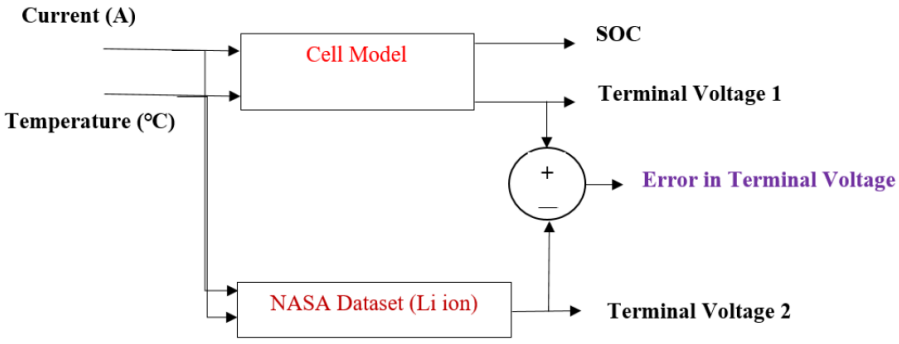


Figure 22 - Model structure to estimate cell parameters (Surya et al., 2021).

The available NASA dataset provides information on voltage response to load and temperature variation. A cell model was developed containing a standard electronic circuit of a cell. The model parameters were calibrated, using various algorithms (Artificial Neural Networks (ANN), SVM, linear regression), to match the voltage of the dataset, reducing the error (Surya et al., 2021).

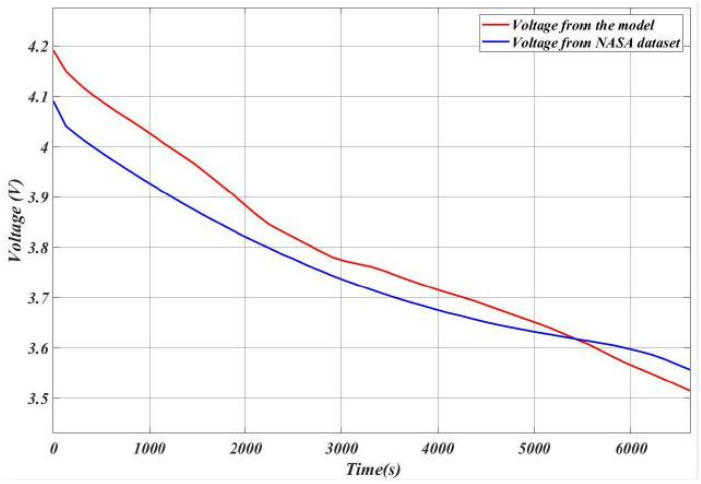


Figure 23 - Voltage comparison of the model developed by (Surya et al., 2021).

The result of this strategy is shown in Figure 23, achieving the desired error of less than 0.2V difference between the model and the dataset (Surya et al., 2021).

All the presented modelling strategies are considered to be a different possible approach to develop the FC System model that will be the base for the control strategy development and study.

### 2.5.2 Control strategies

The control of the FC System can be divided into two categories:

- The control algorithm that determines the target values for the actual state of the FC System, such as target pressure and flows of the respective reactants.
- The control logic that converts that target value into physical movement of the actuators (valves, compressor speeds, injectors, etc).

For the first topic, essentially there are two types of control algorithm: the classical mathematical algorithm and the application of ML techniques. For the second topic several options can be found from the classical Proportional Integrative Derivative (PID) control to Model Predictive Control (MPC) and ANN. The overall control of the FC System is composed by these two control types that are programmed into the FCCU (Figure 15) presented in the previous section.

Related to the first topic, a well established and studied algorithm published by Naganuma et al. (2012) represents the classical mathematical control. This algorithm was developed and tested in prototypes, built by Toyota, that use a FC System. The diagram of the Figure 24 shows how the optimal air quantities are calculated, based on measured FC System status, such as FC temperature, and request power (FC power demand) (Naganuma et al., 2012).

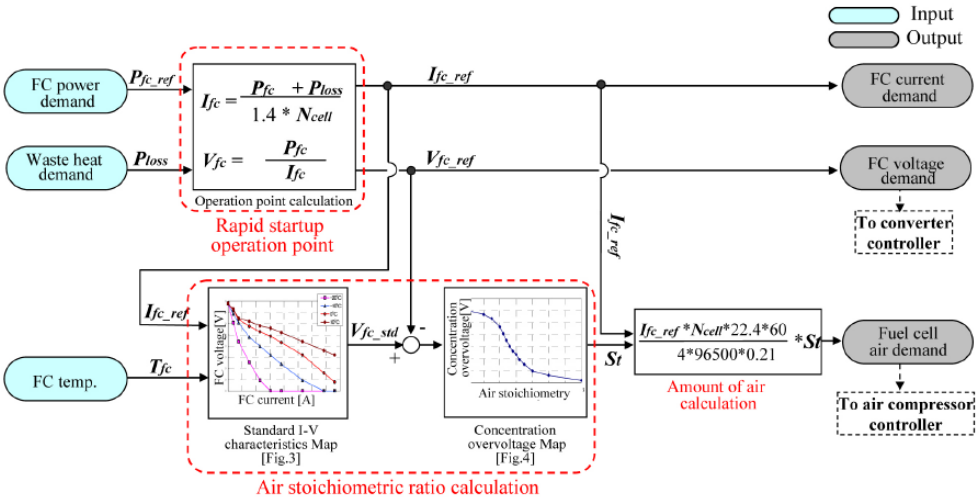


Figure 24 - Algorithm of the control logic implemented on a Toyota FC vehicle prototype (Naganuma et al., 2012).

Similar algorithms are presented for other physical quantities, such as hydrogen flow and pressure (Naganuma et al., 2012). Other articles have studies of the same type of algorithms, such as Qi et al. (2019) who implemented mathematical equations to develop the control algorithm achieving surprising results suing only simulation strategies based on specification parameters of an FC System. These classic mathematical control algorithms are well known for being implemented in Engine Control Units (ECU) that control ICEs (Qi et al., 2019).

Other strategies such as ANN have been studied, as the presented by Hatti and Tioursib (2009), that evaluates the use of a dynamic ANN, a neural network that accepts perpetual novelty (data that is always changing), and never finishes learning.

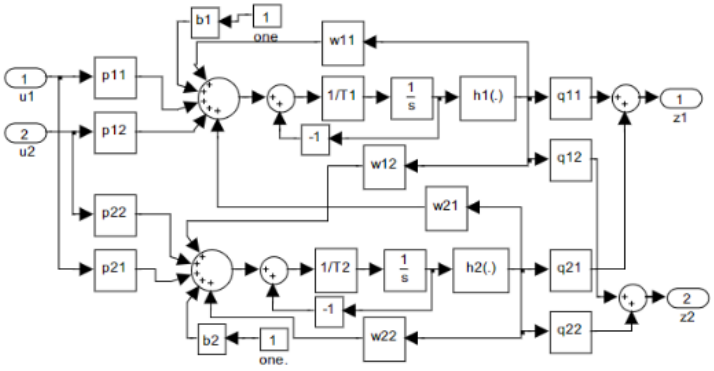


Figure 25 - Part of the dynamic ANN with two neuros and two inputs/outputs (Hatti & Tioursib, 2009).

The algorithm strategy presented in Figure 25 is based on supervised training and achieves a very good controller response with low error. Note that this model is tested in simulation environments only (Hatti & Tioursib, 2009).

For the second topic, control logic, many articles can be found in the literature because they are related to the general control theory applied on the vast majority of the electronic topics.

Combining control logic and FC System can be found in an article developed by Daud et al. (2017) which summarizes most of the literature that combines these two topics. Daud et al. (2017) evaluates multiple control logics, developed by other authors, applied to a particular sub-system of the FC System or to all of the FC System. This study evaluates the application of the major control logics: classical PID, ANN and MPC, having in consideration limiting conditions of the FC such as reactant starvation and flooding (Daud et al., 2017).

Classical control with PID has two types of implementations and is the most common type of control logic used to obtain better fuel cell performance. In feedback control, the control variable is measured (through sensors in the FC System) and compared with its desired value or set point (value generated by the control algorithm) and the error is fed back into the system via the action of the manipulated variable (acting directly on the actuators of the FC System), which is proportional to the error (proportional, P), the sum of recent errors (integral, I) and the rate of change of the error (derivative, D). In feed-forward control, the error is fed via a manipulated variable that is also an upstream variable so that anticipated disturbance of the upstream variable to the system is compensated beforehand. The two options are presented in Figure 26 where the block "Process" corresponds to a Plant, being in this case a specific actuator of the FC System (Daud et al., 2017).

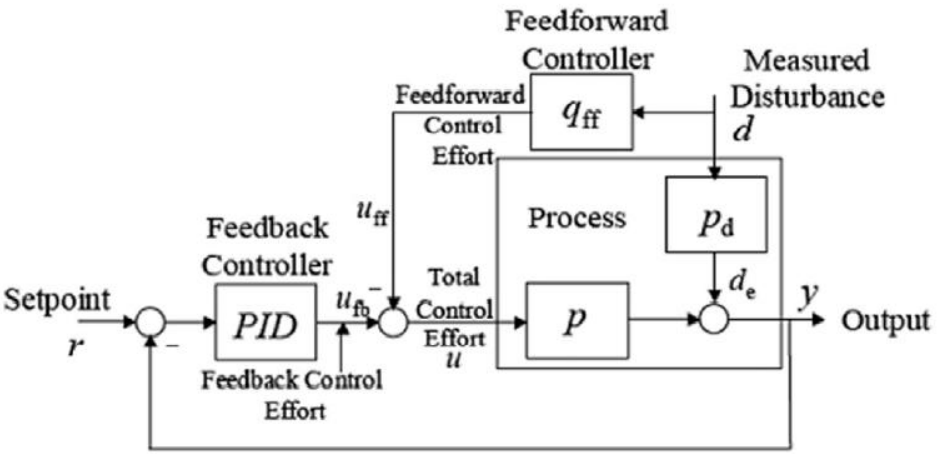


Figure 26 - Architecture of a feedback and feedforward control (Daud et al., 2017)

The use of this type of control logic proves to be a good and fast response control logic for multiple control variables of the FC System. A good calibration of the control parameters is crucial for its performance, representing an effective solution for simulating and early phases of prototyping (Daud et al., 2017).

Other control logic that can be used is ANN control, where the neural network is trained by input (value determined by the control algorithm) and output data (corresponding value that goes for the actuator) (Daud et al., 2017). Neural networks are known to have a fast response, an overall very good performance when well trained and can be implemented in a short time for testing (Krizhevsky et al., 2017).

Daud et al. (2017) evaluated multiple articles that implemented ANN in FC Systems and concluded that it shows a better performance compared to the classical PID control logic, but only if there is data available for training. Training an ANN in this configuration requires that all the control logic equations have been developed or any other control logic is implemented to capture the required data (Daud et al., 2017).

A more advance type of control logic is the MPC controller. This controller requires to develop a model of the FC System so that it can make predictions of how the FC System reacts to a change in the actuators, solving an optimization problem, based on a cost function while running. Several implementations of this controller have been made, representing the most effective control logic, but it requires considerable computational resources (Daud et al., 2017).

The authors Gómez et al. (2021) developed a model consisting of two MPC controllers (Figure 28) that control an FC System (Figure 27) and is tested under the New European Driving Cycle (NEDC) driving cycle.

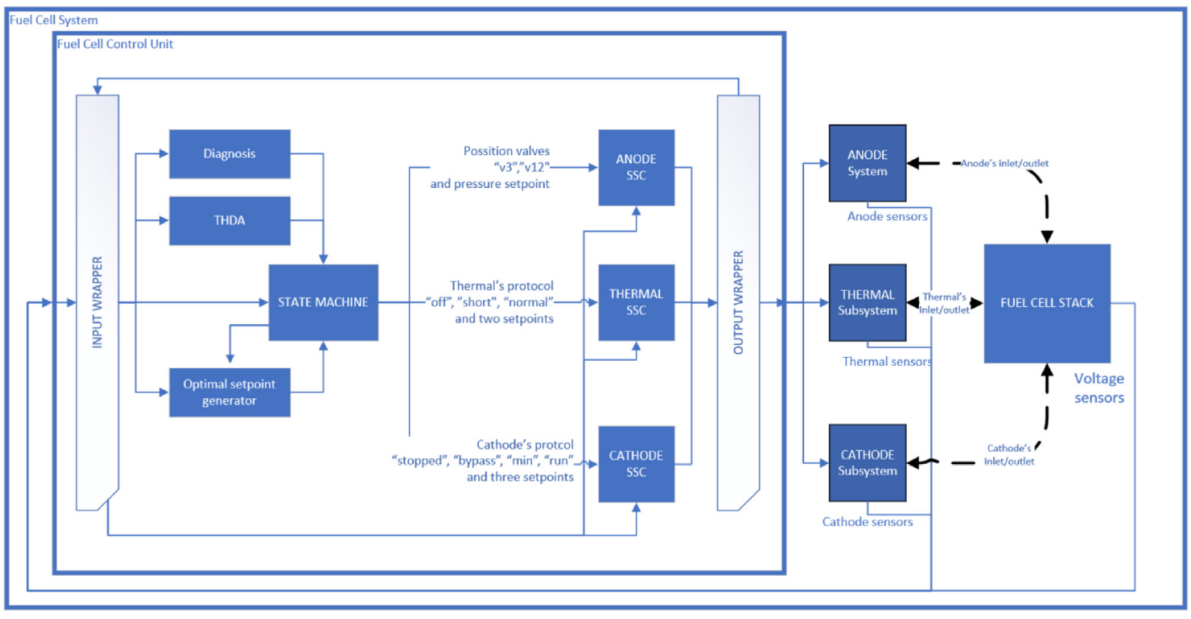


Figure 27 - FC System and control logic developed by Gómez et al. (2021).

The block "Optimal setpoint generator" is where all the control algorithms are located, based on look-up tables to reduce the computation time (Gómez et al., 2021).

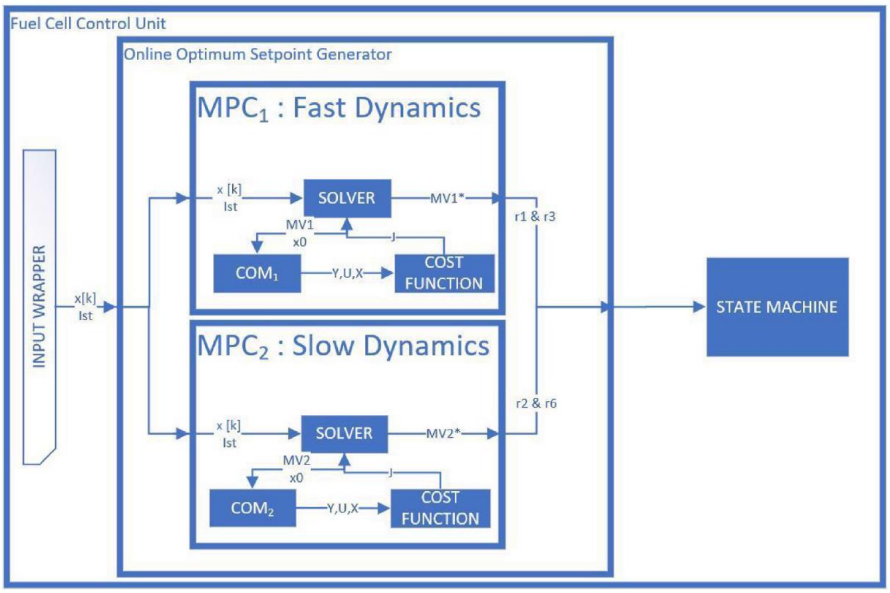


Figure 28 - Fast and slow dynamics applied to different controllers (Gómez et al., 2021).

Fast dynamics correspond to variables that change physical state very quickly, such as pressure and flow of reactants, which must be controlled very precisely to prevent starvation and flooding phenomena.

The slow dynamics represents the inverse, it controls variables such as fluid temperature and air humidity (Gómez et al., 2021).

Both MPC controllers have an objective function that maximizes the system efficiency. The MPC predicts the impact of a shift on a manipulated variable (an actuator) based on a representative model of the FC System that is developed specifically for the MPC. The solver chooses the best solution corresponding to the cost function, also respecting constrains of the optimization problem (Gómez et al., 2021).

This controller significantly reduces hydrogen consumption, increasing the FC System efficiency as expected, but due to its complexity and computational time required to solve the optimization problems while controlling the FC System, it shows a 30% delay in the response to a power request (Gómez et al., 2021).

# 3 FUEL CELL SYSTEM MODELLING

In this chapter the model of the FC System is developed using a base model that represents the theoretical operation of the FC System. In addition, available information about an FC System from a vehicle that is in the production phase will be used, as well as a dataset collected by Argonne National Laboratory that tested the vehicle on a dynamometer, measuring all variables related to the powertrain, performance evaluation in driving cycles and efficiency metrics. This information and dataset will be used to model the real behaviour of the FC System in the base model, implementing essential modifications and optimizing the system.

## 3.1 Production vehicle and dataset introduction

Argonne National Laboratory, based in Chicago, USA is an entity that focuses on research in engineering and science fields of multiple topics. The "Transportation and Power Systems Division" department carried out a research work on the Toyota Mirai 2016 with the aim of studying its powertrain behaviour under multiple conditions and driving cycles (Lohse-Busch et al., 2018).

The Toyota Mirai is a dominant fuel cell hybrid electric vehicle, following a powertrain architecture shown in Figure 17 and its relevant specifications in Table 3 (Lohse-Busch et al., 2018).

Table 3 - Main parameters of the test vehicle (Toyota Mirai) (Lohse-Busch et al., 2018).

| Vehicle specification | |
|---|---|
| Vehicle type | Fuel Cell with battery hybrid |
| Brand / Model / Start production date | Toyota / Mirai / 2016 |
| Battery capacity / type / voltage | 1.6kWh / Nickel-metal hydride / 244.8V |
| Fuel Cell power / number of cells / voltage | 113kW / 370 cells / 248V |
| Hydrogen storage pressure / weight | 700bar / 5kg |
| Maximum range | 502km |
| Hydrogen consumption | 0.8kg/100km |
| Weight | 1850 kg |

The WLTP driving cycles are chassis dynamometer tests to determine emission and fuel consumption for light-duty vehicles, divided by power-to-mass ratios, as shown in Table 4 (Tutuianu et al., 2013).

Table 4 - WLTP driving cycles (Tutuianu et al., 2013).

| Category | Power-to-Mass Ratio (PMR) (W/kg) | Maximum speed (km/h) |
|---|---|---|
| Class 3B | PMR > 34 | V_max ≥ 120 |
| Class 3A | - | V_max ≤ 120 |
| Class 2 | 34 ≥ PMR > 22 | - |
| Class 1 | PMR ≤ 22 | - |

As the Toyota Mirai is a class 3 vehicle (PMR = 62.8), the test data respects the profile in Figure 29, representative of real driving conditions such as urban, suburban, main road and highway (Tutuianu et al., 2013).

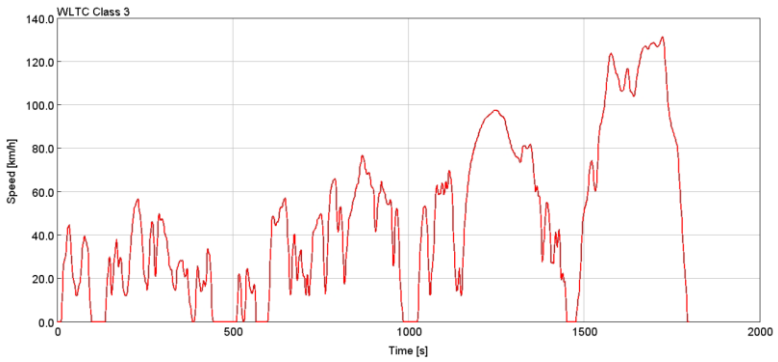


Figure 29 - WLTP class 3 cycle (Tutuianu et al., 2013)

The test procedure consists of placing the vehicle on the chassis dynamometer (Figure 30) and following the target speed of the graph, simulating multiple accelerations and decelerations. The data is collected with multiple sensors, mainly: speed, pressure, flow, temperature, current and voltage sensors, with more than 400 attributes (measured at the points in Figure 31) describing the behaviour of the entire powertrain, in which the relevant aspects related to the FC System are described at Appendix 1 – Measured attributes related to the FC System and exemplified in Figure 32 (Lohse-Busch et al., 2018).

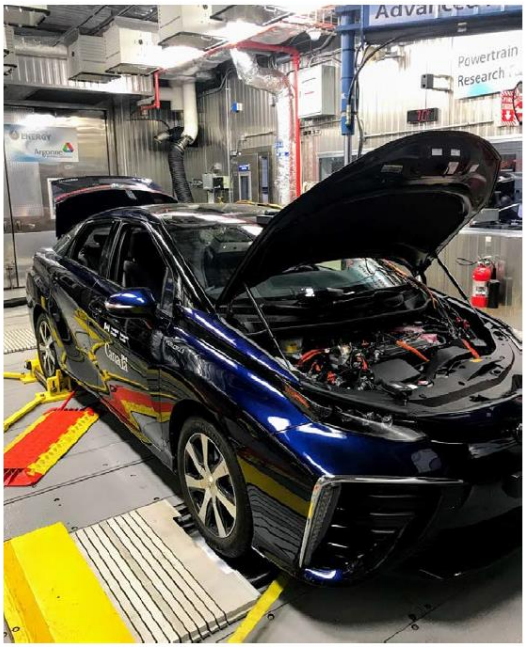


Figure 30 - The test vehicle in Argonne National Laboratory (Lohse-Busch et al., 2018).

The FC System peak efficiency is 63.7%, meaning that 63.7% of the consumed hydrogen generates electric power and the rest is lost through heat release. After an analysis of the test report done by Argonne, the following conclusions can be taken during the WLTP driving cycle test:

- No power comes from the fuel cell stack while the vehicle is stopped.
- Battery power is used for electric launch.
- The fuel cell stack provides most of the power during acceleration. For example, during one acceleration, 15 kW of power comes from the fuel cell stack and 5 kW of power comes from the battery. Another case is that 20 kW power comes from the fuel cell stack and 10 kW power comes from the battery.
- The fuel cell will recharge the battery when the traction power required is low.
- When traction power is low, the vehicle will operate as a battery electric vehicle.
- The fuel cell stack provides the power to cruise at steady state speed and the battery is inactive.
- The fuel cell stack will shut down when there is too much regenerative braking power. However, when regenerative braking power is low, the fuel cell stack still provides some power to charge the battery.

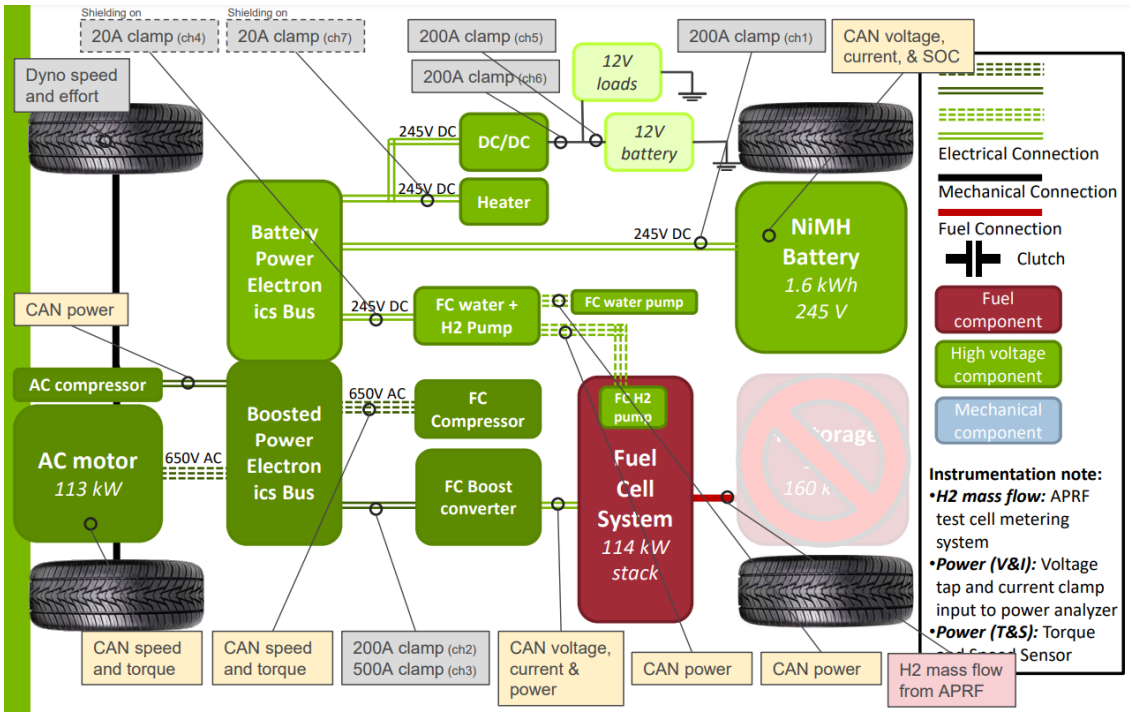


Figure 31 - Powertrain architecture and measurements (Lohse-Busch et al., 2018).

| Possible Vehicle Communication Signal | Value | Unit |
|---|---|---|
| FC Voltage before Boosting | 239.1 | V |
| FC Voltage after Boosting | 345.5 | V |
| FC Current | 2.9 | A |
| Target FC Output Power | 4.7 | kW |
| FC output Power | 0.94 | KW |
| FC Stack Air Temperature (FC Stack Inlet) | 38 | C |
| FC Stack. Air Pressure (FC Stack Inlet) | -0.91 | kPa(gauge) |
| Intake Air Temperature | 26 | C |
| Mass Air Flow Value | 300.9 | NL/min |
| Air Compressor Revolution | 639.5 | rpm |
| Air Compressor Consumption Power | 0 | W |
| FC Stack Coolant Temperature (Radiator Outlet) | 29 | C |
| FC Stack Coolant Temperature (FC Stack Outlet) | 45 | C |
| FC Water Pump Revolution | 735.25 | rpm |
| FC Water Pump Consumption Power | 19 | V |

Figure 32 - Test data example (Lohse-Busch et al., 2018).

To model this FC System, it is important to gather knowledge about its components and specifications. Thus, similar to the structure and components presented in Section 2.2.2, the FC System present in the Toyota Mirai is represented in Figure 33.

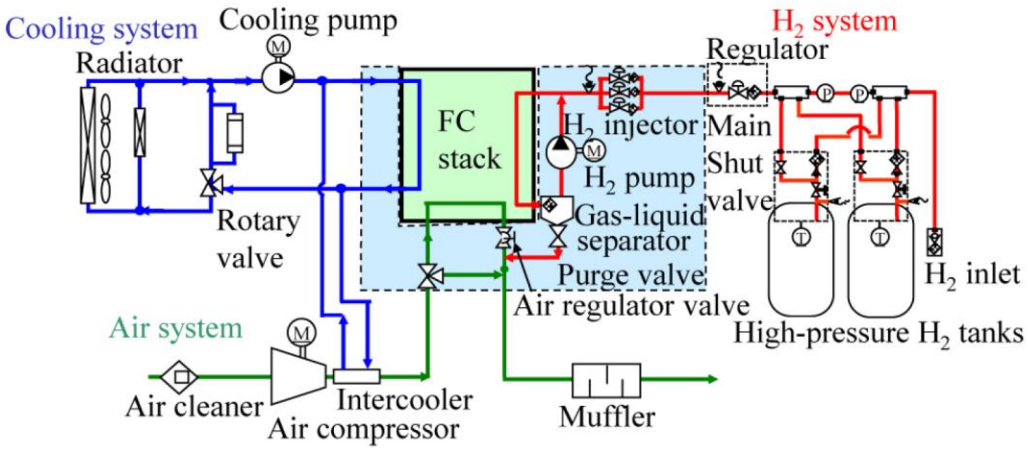


Figure 33 - Configuration of FC system in Toyota Mirai (Maruo T. et al., 2017).

This FC System does not require humidifiers (a component that adds humidity to the reactants to manage the water content within the stack) for the cathode and anode sides of the stack due to its water management strategy and gas diffusion layer properties.

The water generated, due to the chemical reaction, is stored downstream of the cathode and returned upstream through an internal circulation inside the anode as exemplified in Figure 34. This is achieved by the fact that air and hydrogen flow are in opposite directions to facilitate the water circulation. The complex 3D mesh gas diffusion layer promotes the oxygen diffusion into the catalyst layer using turbulence (Figure 35).

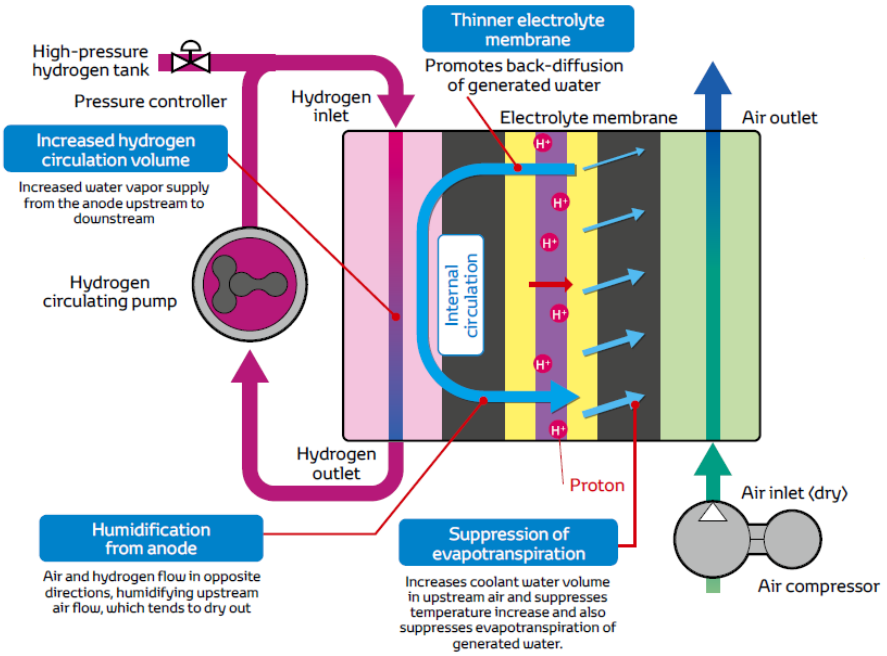


Figure 34 - Water recirculation in humidifier-less system (Nonobe, 2017).

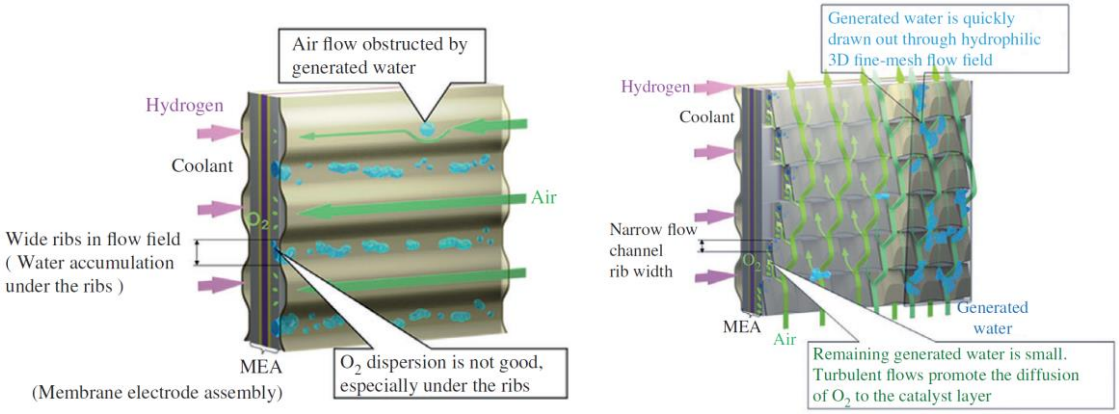


Figure 35 - Conventional flow field structure (left) / 3D Toyota flow field structure (right) (Nonobe, 2017).

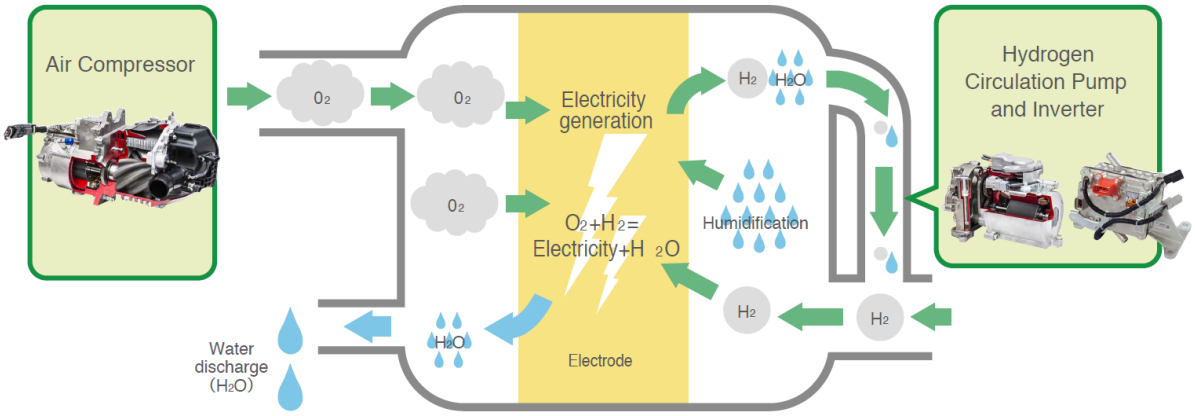


Figure 36 - Toyota FC System compressor (left) and recirculation pump (right) (Nonobe, 2017).

Two other important components to consider are the compressor on the cathode side and the recirculation pump, on the anode side. The compressor is a roots type with 6 helical lobes with a maximum speed of 12500rpm and 20kW of power output. The recirculation pump is also a roots type with 2 straight lobes with a maximum speed of 6200rpm and 420W of power output. Both compressor and pump are electrically powered with dedicated DC/AC inverter (Nonobe, 2017).

The membrane of the FC Stack is the crucial part of the FC System, which defines requirements for the FC System, such as in this case not using humidifiers. The specification of the membrane is important to determine the cell voltage, mainly its thickness, density and current density. The Toyota Mirai has a membrane co-developed in conjunction with GORE, a company that focuses on the development and production of fibres, medical, biopharmaceutical and electrochemical products. Zhao et al. (2007) in conjunction with GORE, have study the various types of membranes to date, exploring their specifications and applications. The GORE-Select membrane has multiple applications (being that a posssible derivation of this membrane is used in the Toyota Mirai FC Stack) with the following thickness ranges available:

- Membrane: 25 ≤ μm ≤ 250
- Gas diffusion layer: 210 ≤ μm ≤ 430

In addition, other important information about the FC Stack can be found in James et al. (2017), a report on the general development around the topic of fuel cells, setting out the following specification:

- Active area: 237$m^2$
- Maximum current density: 1.9$A/cm^2$
- Maximum power density: 1.295$mW/cm^2$
- Density: 2039$kg/m^3$.

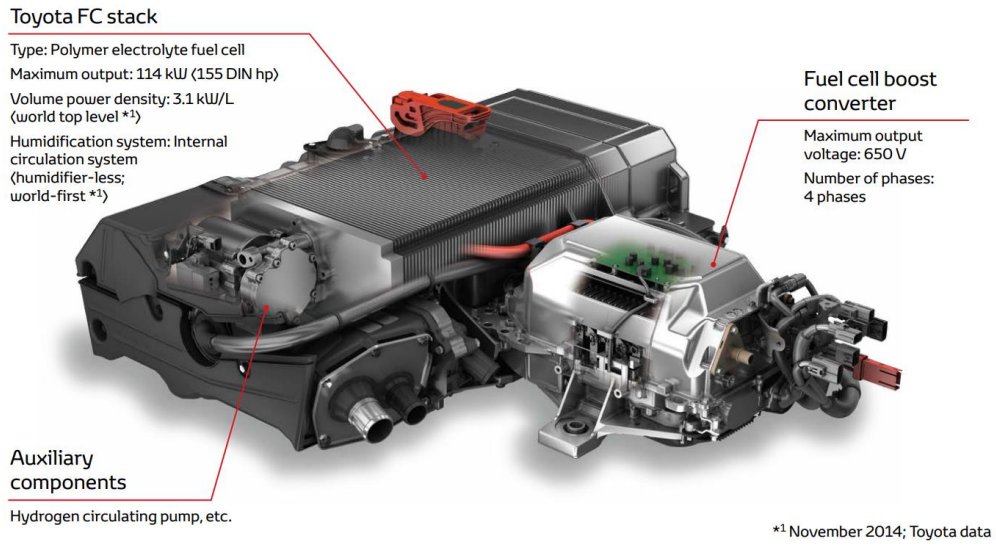


Figure 37 - Complete FC System of the Toyota Mirai (Nonobe, 2017).

The entire FC System is contained within a package to minimize space usage (see Figure 37), and a boost converter is used to raise the voltage off 247V to 650V.

After gathering all the necessary information and analysing the dataset, the next step is to implement all the necessary modifications to a theoretical model available on Simulink.

## 3.2 Model development

In this section, the model will be developed, which basically consists of converting an existing theoretical model to one that represents the real behaviour of a FC System (in this case, the one present in the Toyota Mirai). The development of the model will allow the study and development of advanced control

strategies and prediction models on the degradation of components, being essential to define requirements to validate the final model.

The requirements defined for the final model are the following:

- The FC System must have an architecture of a real FC System
- The FC Stack must have similar output voltage to the real FC System
- The FC Stack must have similar output resistance to the real FC System

Based on the literature review, a first diagram was made to understand the multiple pads in order to model the FC System. In Figure 38, three options are represented, where the first one consists of making a black box type model that, as inputs and outputs, uses Model Based Calibration toolbox from MATLAB or develops a neural network. This approach was discarded because in this type of models, the development might be accelerated in some cases, but in the end, there is no physical understanding of what is happening inside the black box. The third option was also discarded because developing a model from scratch, at a developer level, requires a good knowledge of this particular FC System, which is not possible. This type of model would be the best representation of the FC System, if direct contact with the developers were possible, ending with a well-defined model and accurate physical understanding of every component behaviour. The second option, the one that was chosen, represents a well studied option by Surya et al. (2021) and Lu (2013) that consists of starting from a known physical model and modify it as much as possible, parametrizing the components with the gathered information, and optimizing its behaviour via optimization of empirical values.

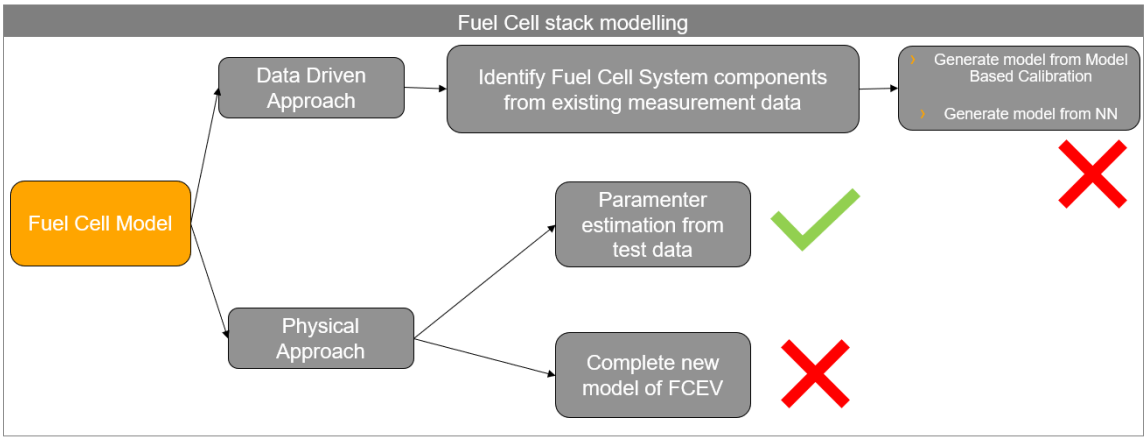


Figure 38 - FC System modelling options.

The initial model, represented at Figure 39, was obtained from a Simulink custom library available on CES private servers. The “Membrane Electrode Assembly” block represents the FC Stack, and the entire

model represents the FC System. This custom model represents a standard FC System that is different on many aspects from the one found on the Toyota Mirai.

The main differences are the following:

- FC Stack uses theoretical equations to determine cell voltage
- FC Stack has different specifications (number of cells, area, thickness of membrane, etc)
- Compressor, in the oxygen source block has completely different specifications
- Recirculation pump, in Recirculation block, has completely different specifications
- On both sides (anode and cathode) it uses humidifiers
- Membrane water management strategy requires expelling all the water produced by the chemical reaction, not taking advantage of it to humidify the membrane.

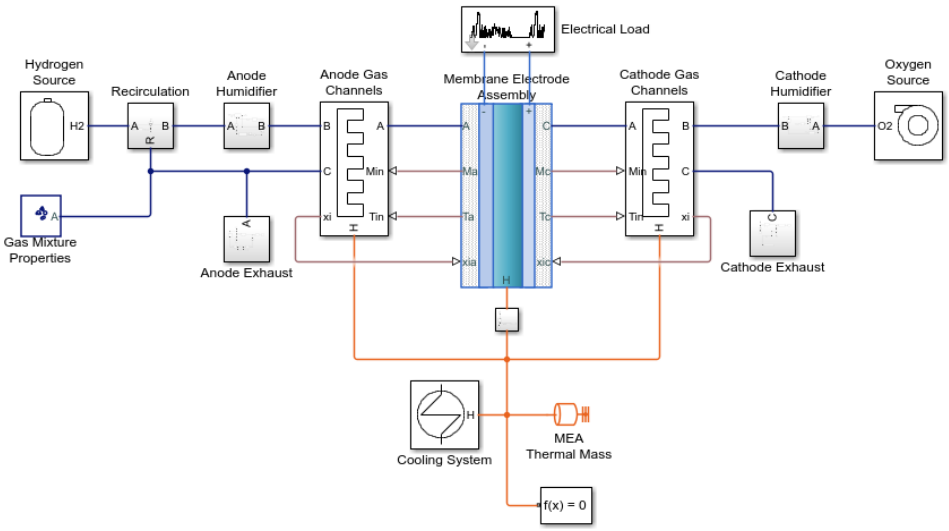


Figure 39 - Initial FC System model.

Other differences can be found such as pressures, flows, lambda factors, load application that depend on the used control strategy. In this case, each component is individually controlled through equations (Figure 40) similar to the ones described in Section 2.2.

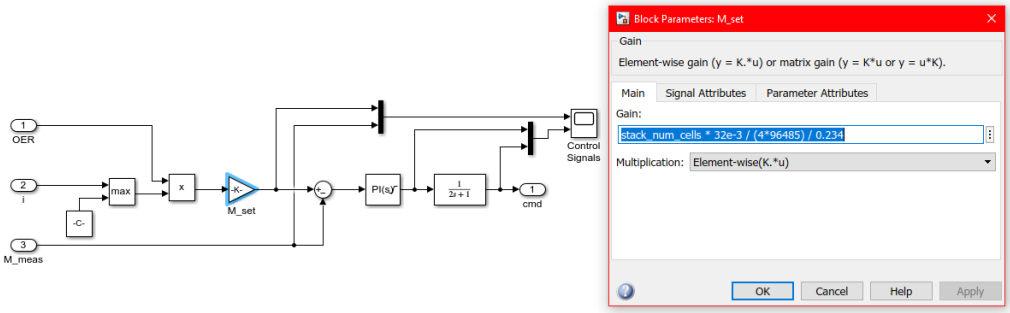


Figure 40 - Example of control equation to determine required air flow using fixed lambda factor.

The differences in control strategy have no impact on the modelling of the FC System, because it is possible to force the model to respect the data from the tests, putting apart the control strategy and focusing on the component parametrization and FC Stack calibration.

The first step to develop the model is to get the necessary data from the test and run the model on the Toyota Mirai under the same conditions as the FC System to check for differences related to the voltage and resistance values.

The plots in Figure 41 refer to relevant operating conditions in which the FC System of the vehicle was working under the WLPT driving cycle. This is the data that will be used to force the model to operate under the same conditions as the FC System vehicle.

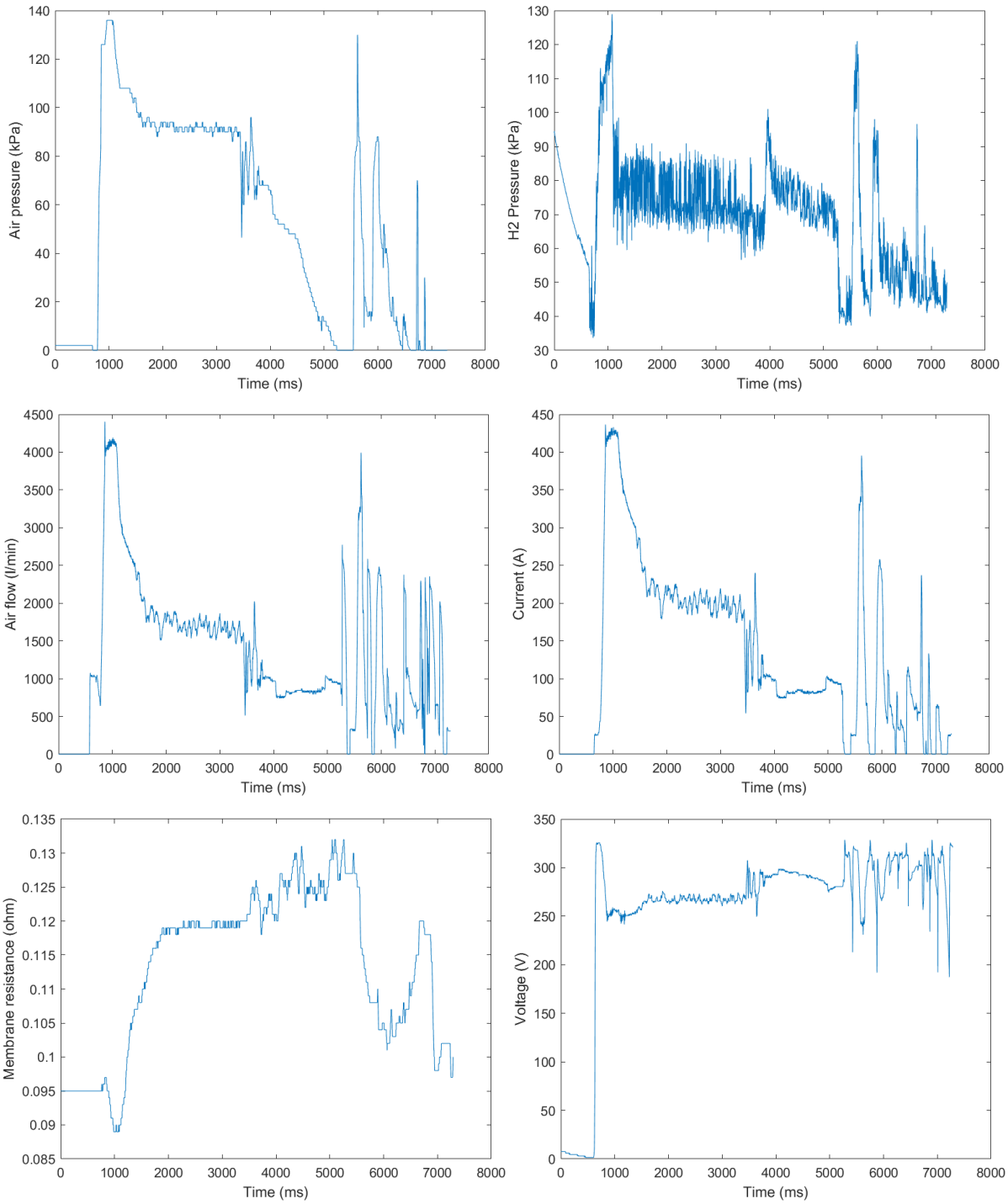


Figure 41 - Relevant operating conditions of the FC System on the Toyota Mirai.

In the case of the Toyota Mirai, the measured pressures for air and hydrogen are relative, meaning that it measures the pressure at a given location relative to the atmospheric pressure. Notice that the pressure and flow data are the main conditions to force the model to run on the same conditions as the FC System of the vehicle. For the required power of the FC Stack, that is done via current (also referred as load), multiplying this load by the corresponding voltage leads to an output power. These four important data (air pressure, hydrogen pressure, air flow, current) can guarantee that the FC System will operate under

the same conditions as found in the vehicle. The corresponding output as defined in the requirements can be seen in the membrane resistance and voltage plots of Figure 41. Thus, the main objective is to have a model whose output is as close as possible to these data points.

To develop the model using this data, it is possible to read a data point at a given time and force a component to have the same physical response. Figure 42 shows how the data is read from the Workspace and is applied directly to a component, forcing its physical state.

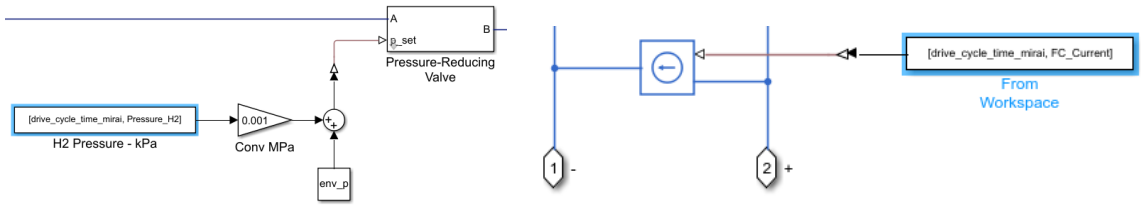


Figure 42 - Forcing hydrogen pressure (left) and load application (right).

Analysing the behaviour of the simulation running up to a time of 250 seconds, it is clear that the theoretical equations have very different representation for determination of voltage and resistance. This can be seen on Figure 43 where the voltage values and profile are very different from the expected, as well as for the resistance of the membrane (compare to membrane resistance and voltage plots of Figure 41).

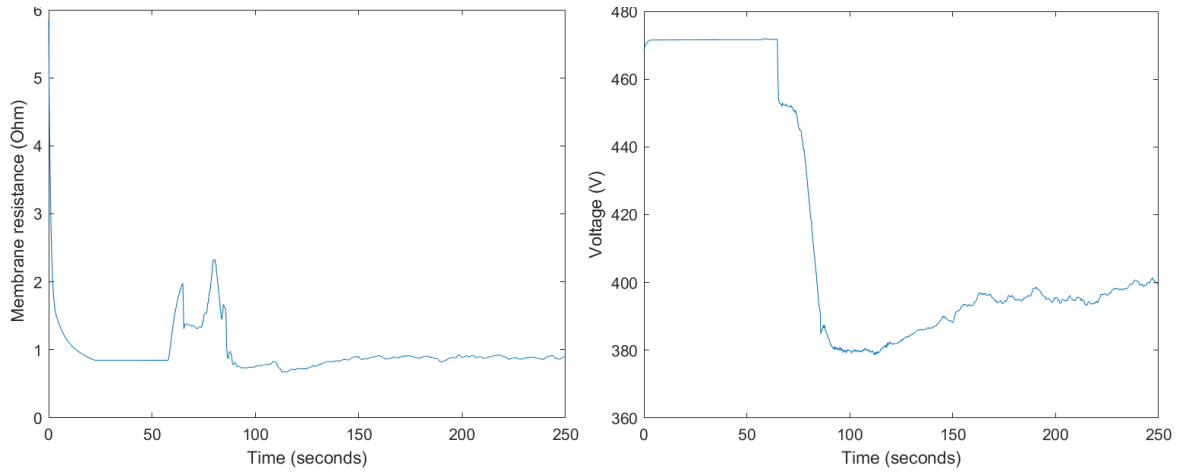


Figure 43 - Measured initial outputs from the model.

Before making any modification or optimization to the model, the I-V curve should be analysed. Figure 44 shows how this curve behaves, being a useful data for future comparison after all the necessary implementations have been made.

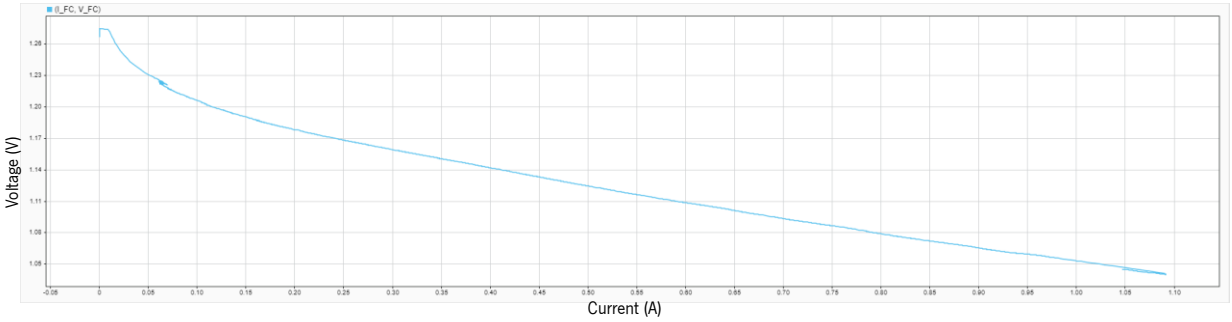


Figure 44 - Initial I-V curve of the model (X axis is FC current and Y axis is FC voltage).

At this stage, it is possible to conclude that under the same conditions of the FC System present on the Toyota Mirai, the FC System of the initial model has a completely different behaviour, showing a very high voltage and resistance. The next step is to evaluate the necessary modifications to components and FC Stack that do not match the information presented in Section 4.1, about the specifications of the FC System.

Maintaining the same approach of using data to impose a physical state allows to test modifications at the FC Stack and optimize its behaviour. After implementing all the necessary component parametrizations, such as: FC Stack configuration, water management strategy, humidifiers removal, compressor map estimation, recirculation pump configuration and general component specifications based on the information gathered and thermodynamic approaches (Figure 45), the strategy tested by Lu (2013) and Surya et al. (2021) can be applied, which consists of using empirical values to calibrate the FC Stack response.

Block Parameters: Simscape Component

Membrane Electrode Assembly

Auto Apply

Settings | Description

| NAME | VALUE | |
|---|---|---|
| **Parameters** | | |
| Number of cells | stack_num_cells | |
| Fuel cell area | stack_area | cm^2 |
| Membrane thickness | stack_t_membrane | um |
| Gas difusion layer thickness | stack_t_gdl | um |
| Ohmic conductivity model | Tabulated data - Conductivity vs. temperature and relative humidity | |
| Relative humidity vector, RH | [0, .1, .2, .3, .4, .5, .6, .7, .8, .9, 1] | |
| Temperature vector, T | [303.15, 353.15, 393.15] | K |
| Table of conductivity(T,RH) | [0, .0093, .019, .031, .045, .063, .086, .11, .15, .2, .25; 0, .0... | S/cm |
| Exchange current density | stack_io | A/cm^2 |
| Max (limiting) current density | stack_iL | A/cm^2 |
| Charge transfer coefficient | stack_alpha | |
| Concentracion losses altas | stack_alpha1 | |
| Concentracion losses baixas | stack_alpha2 | |
| Charge transfer coefficient | stack_alpha3 | |
| Concentracion losses altas | stack_alpha4 | |
| Concentracion losses baixas | stack_alpha5 | |
| Shift point of concentration losses equa... | stack_shift | |
| Density of dry membrane | stack_mea_rho | kg/m^3 |
| Equivalent weight of dry membrane | 0.7 | kg/mol |
| N2 diffusion coefficient | 1e-5 | cm^2/s |

Figure 45 - Custom FC Stack parametrization.

A set of six empirical values (alpha and alpha1 to apha5) was implemented in the equations (15) and (16) that determine the voltage losses for activation and concentration, similar to those implemented by Lu (2013). On Figure 46 it is represented the code in Matlab that allows to declare these losses equations, where can be seen the the theoretical equations (on the left) and the empirical equations (on the right).This six empirical values will allow to calibrate the FC Stack and match the voltage response of the FC Stack of the vehicle.

$$b = \begin{cases} \dfrac{-R_u * T_{stack}}{2 * alpha3 * F}, & icell > 0.38 * iL \\ \dfrac{-R_u * T_{stack}}{2 * alpha * F}, & icell \leq 0.38 * iL \end{cases} \quad (15)$$

$$Vconc = \begin{cases} \dfrac{-R_u * T_{stack}}{2 * alpha4 * F} * \left(\dfrac{icell}{iL}\right)^{alpha5}, & icell > 0.38 * iL \\ \dfrac{-R_u * T_{stack}}{2 * alpha1 * F} * \left(\dfrac{icell}{iL}\right)^{alpha2}, & icell \leq 0.38 * iL \end{cases} \quad (16)$$

```
% Nernst voltage
Vnernst = -G_H2O/(2*F)+ R_u*T_stack/(2*F)*log((pH2 * pO2^0.5)/pH2O);

% Activation losses from Tafel equation
b = R_u*T_stack/(2*0.5*F);
Vact = if ge(i_cell, io), b*log(i_cell/io) else 0 end;

% Gas transport voltage loss
Vconc= -R_u*T_stack/(2*F) * ...
    if le(i_cell, 0.999*iL), ...
        log(1 - i_cell/iL) ...
    else ...
        log(1 - 0.999) - (i_cell/iL - 0.999)/(1 - 0.999) ...
    end;
```

```
% Nernst voltage - correto
Vnernst = -G_H2O/(2*F)+ R_u*T_stack/(2*F)*log((pH2 * pO2^0.5)/pH2O);

% Activation losses from Tafel equation - correto
b = ...
    if ge(i_cell, 0.38*iL), ...
        -R_u*T_stack/(2*alpha3*F)...
    else...
        -R_u*T_stack/(2*alpha*F)...
    end;
Vact = if ge(i_cell, io), b*log(i_cell/io) else 0 end;

% Gas transport voltage loss - correto
Vconc = ...
    if ge(i_cell, 0.38*iL),...
        -R_u*T_stack/(2*alpha4*F) * ((i_cell/iL))^alpha5...
    else...
        -R_u*T_stack/(2*alpha1*F) * ((i_cell/iL))^alpha2...
    end;
```

Figure 46 – Theoretical equations (left) and empirical equations (right) for voltage losses equations.

For the membrane resistance it is important to know that it is calculated based on the thickness of the membrane and the thickness of the gas diffusion layer (attribute t_membrane and t_gdl in Figure 47). These two values must be optimized to match the resistance response of the FC Stack of the vehicle.

```
%Resistencia da membrana em ohm, segundo area transversal relativa ao fluxo de eletroes
Resis == Rohm/((t_membrane + (2 * t_gdl)) * (sqrt(area_cell)))
```

Figure 47 - Membrane resistance calculation.

The parametrized model is shown in Figure 48, including all the necessary changes to match the specifications of the FC System in the vehicle and a custom code was developed for the FC Stack, taking into account the water management strategy and the implementation of empirical values (block "MEA_Code").

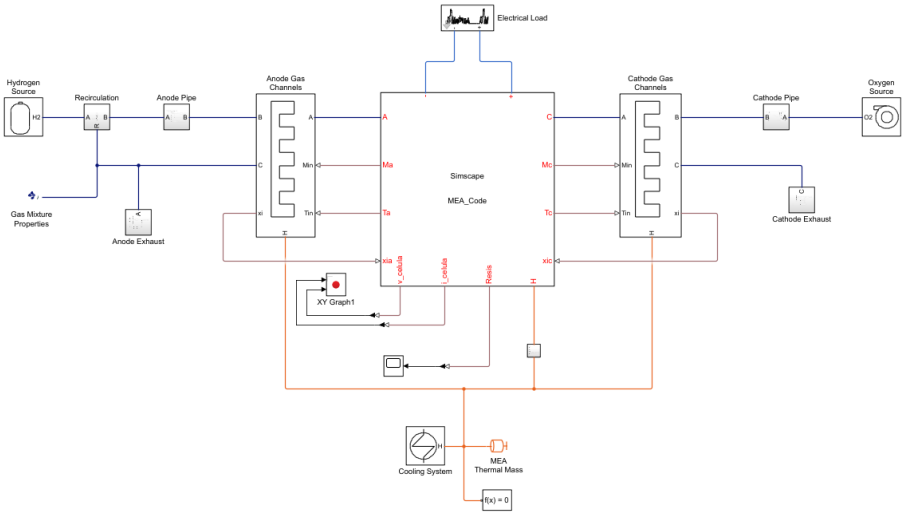


Figure 48 - Parametrized model.

Simulink has an app called "Parameter Estimation" (Figure 49) that allows to estimate values and approximate the model response to an expected response.

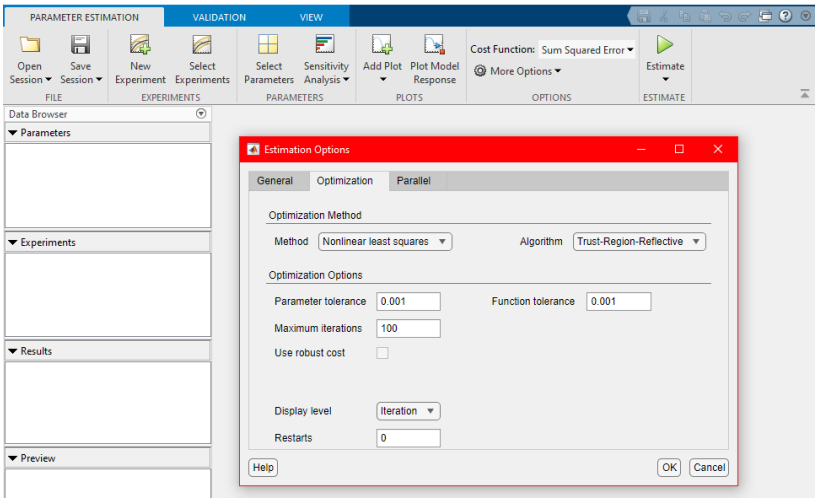


Figure 49 - Parameter estimator app.

The app has the option to select the parameters to be estimated, select where the signal will be measured in the model and for that signal the expected result – data points. To solve the optimization problem multiple methods are available and specific algorithms for each method. The following optimization methods are presented in the documentation of the app (Coleman et al., 2022):

- Nonlinear least squares - lsqnonlin
- Gradient descent - fmincon
- Pattern search - patternsearch
- Surrogate optimization - surrogateopt

- Simplex search - fminsearch

The choice of the optimization method should be in sync with the desired cost function to be minimized. In this case, it makes sense to choose the cost function – root mean squared error, to heavily penalize larger error residuals, because there is a large nominal voltage error between the model output and the data points. Thus, the most appropriate method is the Nonlinear least squares method, also recommended by Simulink documentation for this specific type of cost function, since it is an algorithm to determine the best fit to data. The Nonlinear least squares method implemented in Simulink has two algorithms available (Coleman et al., 2022):

- Trust Region Reflective (TRR)
- Levenberg Marquardt (LM)

It is advised in the documentation to test each algorithm and verify which gives the best result (Coleman et al., 2022).

First, the parameters must be specified in the parameter estimator app (Figure 50). The boundary equations for each of the 5 empirical parameters define that they must be positive and non-zero, with an approximation to the initial value of 1. The measured output signal must also be defined as the voltage signal, and at the same time the corresponding expected voltage signal. To run the optimization, the model must have the same run time as the expected voltage signal. For computation reasons it was decided to run only 450 seconds out of the 700 seconds to speed up the optimization process.

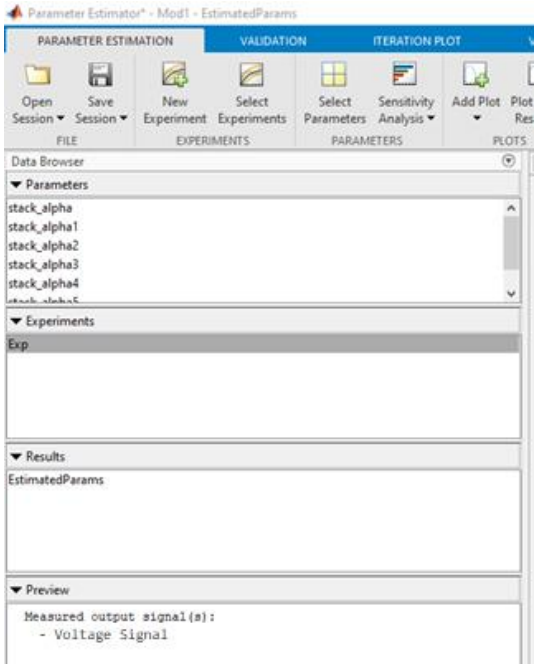


Figure 50 - Parameter estimator configuration.

Then, the app performs an initial check to evaluate the initial state of the optimization problem. Figure 51 shows the measured signal from the vehicle data (blue line) and the simulated signal from the model (red line). When comparing the initial state of the model, with that of Figure 43, it is clear the impact of the changes made in the components and in the FC Stack parametrization, verifying that the voltage signal at the beginning was very high and now is very low.

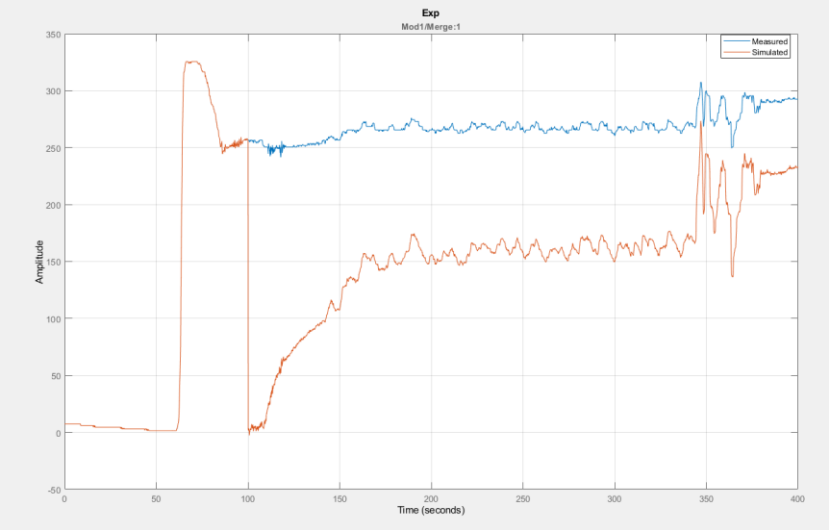


Figure 51 - Initial state of the optimization problem.

The first optimization attempt was made using the Trust Region Reflective algorithm, and an initial RMSE of 664.7 was determined for the first iteration. After 35 iterations and a run time of 63 hours, the results were acceptable, having an RMSE value of 1.25 and a wave form very similar to the vehicle FC System data. The results, presented in Figure 52, show the estimated curve after of the Trust region reflective optimization procedure. As can be seen, it seems to be a good fit of the data, obtaining a small value for the RMSE.

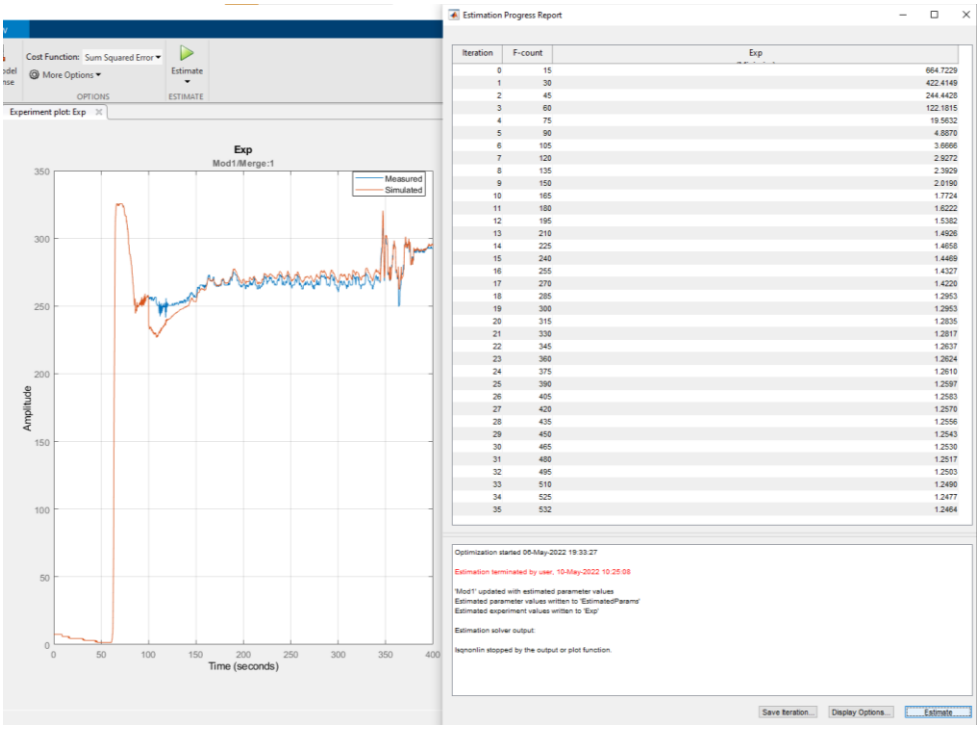


Figure 52 - Results using the Trust region reflective algorithm.

Running the optimization, under the same conditions as the previous one, but using the Levenberg Marquardt method, an initial value of 420.623 was obtained for RMSE in the first iteration.

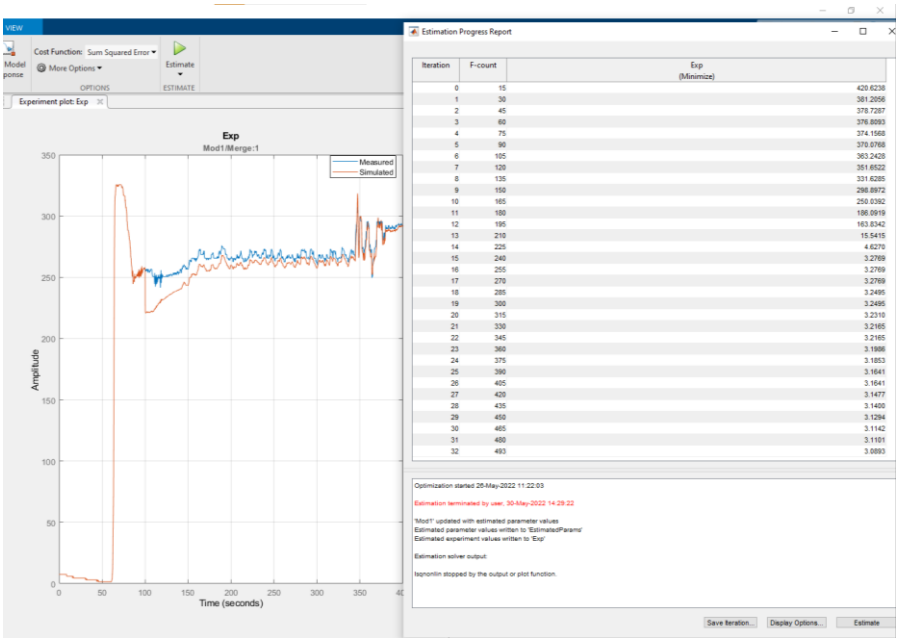


Figure 53 - Results for the Levenberg Marquardt algorithm.

In this case, after 32 iterations and a run time of 75 hours, the RMSE value converged to 3.09. This algorithm presented a longer computation time with a higher RMSE value. Despite these results being

satisfactory, the Trust Region Reflective algorithm managed to obtain better results (less error) with less computational time.

Table 5 - Results for the empirical values

| Empirical values | Initial value | Final value (TRR Algorithm) | Final value (LM Algorithm) |
|---|---|---|---|
| alpha | 1 | 0.1372 | 0.1342 |
| alpha1 | 1 | 0.0597 | 0.0003 |
| alpha2 | 1 | 41.206 | 9.5507 |
| alpha3 | 1 | 0.1454 | 0.1393 |
| alpha4 | 1 | 0.3261 | 1.7556 |
| alpha5 | 1 | 6.4216 | 0.4119 |

Table 5 shows the final values for each empirical value obtained in each optimization algorithm. Some values are similar but in the case of stack_alpha1, stack_alpha2 and stack_alpha5 very distinct values were found by the algorithms and this affects the behaviour of the FC System, having a more accurate output in the case of the values determined by Trust Region Reflective algorithm.

Table 6 - Results of each optimization algorithm

| Algorithm | Final RMSE | Total iterations | Total run time |
|---|---|---|---|
| TRR | 1.2464 | 35 | 63 hours |
| LM | 3.0893 | 32 | 75 hours |

When analysing the performance of the algorithms, Table 6 shows that Trust Region Reflective achieved more accurate results in less time. After these optimization results for the output voltage of the FC System, it was decided to use the empirical values determined by Trust Region Reflective algorithm.

The same strategy was used to reduce the error for the membrane resistance but using specific boundaries for each attribute.

In Figure 47 it is clear that the membrane thickness, gas diffusion layer thickness and area of the membrane are the attributes that have direct impact in the resistance calculation. Since the area and membrane thickness are constant, the only attribute that can be determined is the gas diffusion layer thickness. This attribute has known boundaries of 210 ≤ µm ≤ 430, and having the same approach as done for the voltage, it was possible to optimize the output of the resistance values as showed on Figure 54.

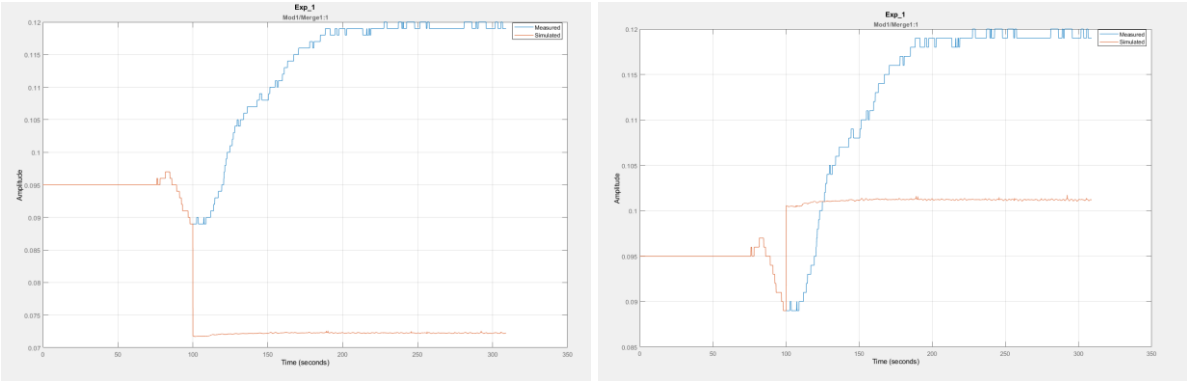


Figure 54 – Best results for resistance optimization – left before and right after optimization.

Using the Trust Region Reflective algorithm, the obtained RMSE value is 5.2 with a thickness of 219.642 µm. In the case of using the Levenberg Marquardt algorithm the obtained RMSE is 8.9 with a thickness of 243.729 µm. Again, in this case, the Trust Region Reflective algorithm provides better results.

Comparing the initial state, in Figure 43, it is clear how close the resistance is to the desired value. To better optimize the resistance calculation, several proprieties of the membrane must be known and how the vehicle control unit determines its value. Only in this case would be safe to develop a model and, if necessary, implement empirical values, doing the optimization process at the end. These results show a difference of less than 0.02 Ohm (as seen on Figure 54), an acceptable tolerance.

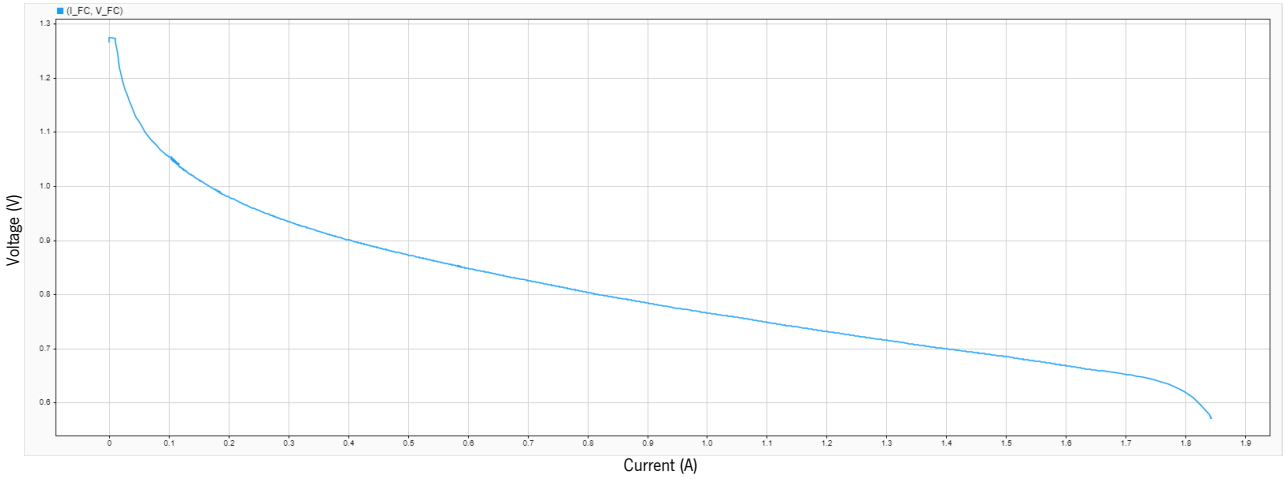


Figure 55 - Final I-V curve of the model (X axis is FC current and Y axis is FC voltage).

One of the main characterizations of the FC Stack is the I-V curve (Figure 55). When comparing this final I-V curve with the previous one (Figure 44), differences in the shape and voltage values can be seen within a more acceptable range as showed in Figure 5, with the three losses very well defined.

# 4 FUEL CELL CONTROL MODELLING

In this chapter it will be presented the development of the control unit that has two main parts: the control algorithm and the control logic, that work together to control the FC System model; and all the necessary components that are within it. An approach based on available data will be formulated to develop both control blocks allowing to test the response of it and compare it with the available data.

## 4.1 Introduction

After modelling the complete FC System, now it is possible to model and test control strategies. As stated on the Section 2.5.2, the control strategy is composed of two parts: the control algorithm and the control logic. The first step is to identify which are the control variables and sensors that quantify a physical state in the FC System. For this control development only the stated actuators and sensors in Table 7 will be considered, these being the most important control properties in the FC System.

The second step consists of building the control algorithm to determine the required physical state (set point) and then build the control logic, which will actuate the components to meet the determined set point.

Table 7 - Main actuators and sensors Identified in the FC System

| Side | Actuators | Sensors |
|---|---|---|
| Anode | • Pressure regulating valve<br>• Recirculation pump | • Pressure sensor<br>• Mass flow sensor |
| Cathode | • Air compressor<br>• Pressure relief valve | • Mass air flow sensor<br>• Pressure sensor |

Furthermore, it is important to understand the dynamics between the controller and the FC System. Figure 56 illustrates the overview of the complete model, where the current is the load required for the FC System and the FCCU receives a measurement signal of this current.

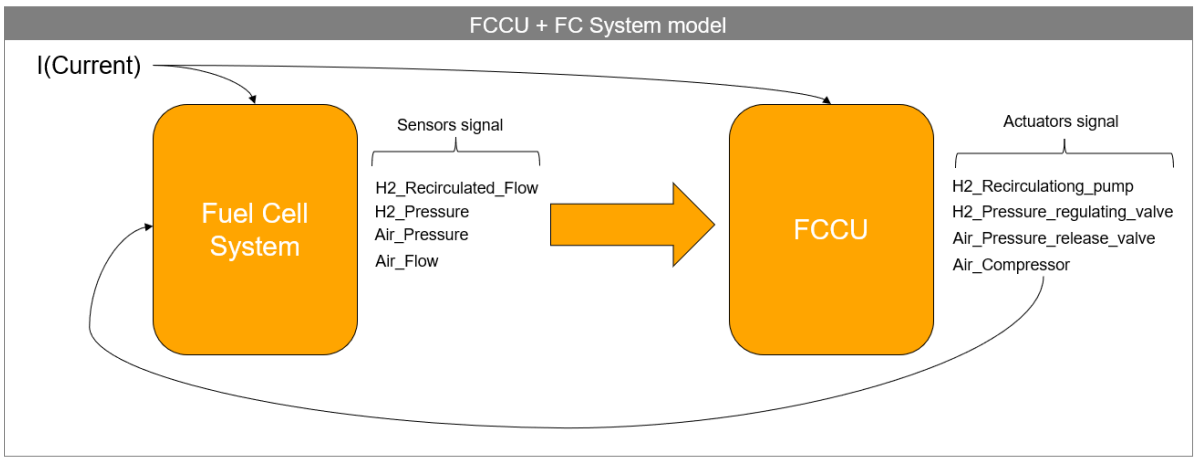


Figure 56 - Interaction between FC System model and FCCU.

In this step, the FCCU must calculate the ideal physical quantities of air and hydrogen required and convert them to the corresponding actuator signal, which is sent to the FC System model. The loop ends by feeding back to the FCCU the corresponding measured value of the physical quantity in the FC System.

The options presented for the control algorithm in the literature review, referring the mathematical control algorithm and the ANN option will be implemented and studied, the first option representing the classical methodology, and the ANN a new emerging approach in vehicle control algorithms.

For the control logic, three approaches were presented in the literature review and are summarized in Table 8.

Table 8 - Comparison between control logic options.

| Control logic | Advantages | Disadvantages |
|---|---|---|
| PID | • Simplistic and easy-to-interpret control<br>• Good response and accuracy when well tuned<br>• Rapid implementation and calibration of parameters for an initial testing phase<br>• Good for SISO systems | • MIMO systems only with multiple PID logic<br>• Does not directly respect constraints<br>• Does not work properly on non-linear systems<br>• Slow acting and not accurate when tuned incorrectly<br>• Difficulty in correctly tuning the parameters for high dynamic system |
| ANNC | • Fast response<br>• Low computational power<br>• Easy implementation | • Low precision and accuracy<br>• Data availability for training the neural network at every possible situation |

| | | |
|---|---|---|
| MPC | • Good for MIMO systems<br>• Respects constraints<br>• Works on non-linear models<br>• Easy implementation | • Requires a model to predict the future state<br>• Needs a lot of computational power |

The ANNC and MPC options were discarded due to, in the first case, there is no data available about the signal that goes to the actuators, and for the second option, due to its complexity to develop the prediction model of the FC System. In an initial phase of development, an MPC controller was tested, controlling hydrogen and air pressure, but it was abandoned because it took a long time to simulate, due to the FC System model using SimScape components, and requiring a continuous type of simulation, forcing the MPC working in a continuous mode. For these reasons, PID control logic is the one that best fits due to its effective and simple implementation, speeding up the development and testing of the model.

## 4.2 Classical control algorithm development

Usually, for most production vehicles, the control algorithms are derived from equations and calibrated with dedicated tools. Such example is shown in Figure 24 as a set of equations and calibrated look up tables (via for example Model Based Calibration Toolbox from MATLAB).

The development of this type of control algorithm starts with the definition of a structure with equations and calibrated look up tables. As reviewed in the literature, the study by Naganuma et al. (2012) represents a control algorithm that was developed during the development of a prototype vehicle. This control algorithm uses the standard theoretical equations that are forward calibrated with look up tables, and the look up tables are calibrated by exprimentation.

Thus, to develop this control algorithm, the first step was to identify the main equations that determine the required air and hydrogen pressures and flows. With these equations based on theoretical behaviour, a structure was developed respecting a flow of calculus that corrects the response of these equations. Figure 57 presents this structure, taking as inputs the power demand and fuel cell temperature (yellow circles at the top left).

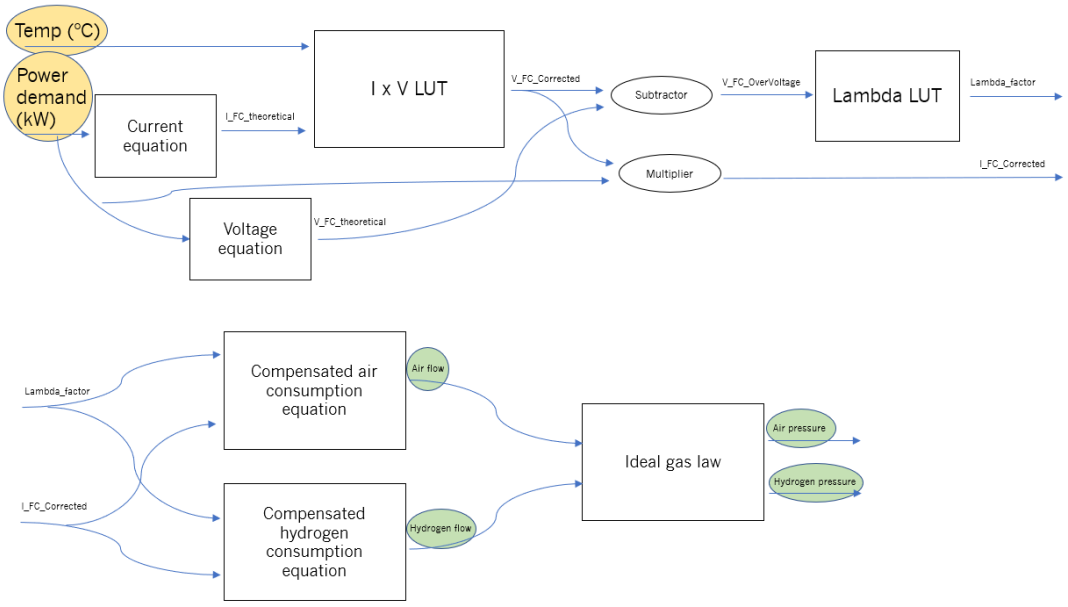


Figure 57 - Classical control algorithm structure.

Each block represents a set of equations or 3D look up tables, and the main parameters to offset the theoretical behaviour of the equations to the real behaviour are the “V_FC_Overvoltage” (Figure 58) and “Lambda_factor” (Figure 59).

The outputs represented with green circles, in Figure 57, are the main outputs to determine the actuators effort (managed by the control logic), respecting the architecture of Figure 56. The algorithm was then implemented in Simulink (Figure 60) that interacts in series with the control logic, controlling the FC System model.

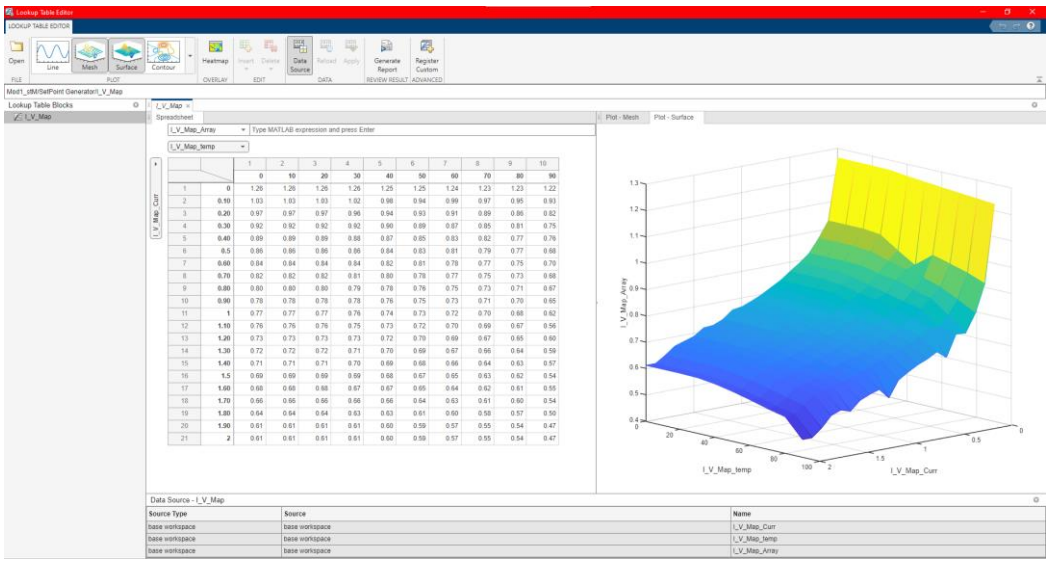

Figure 58 - 3D look up table for determining "V_FC_Overvoltage".

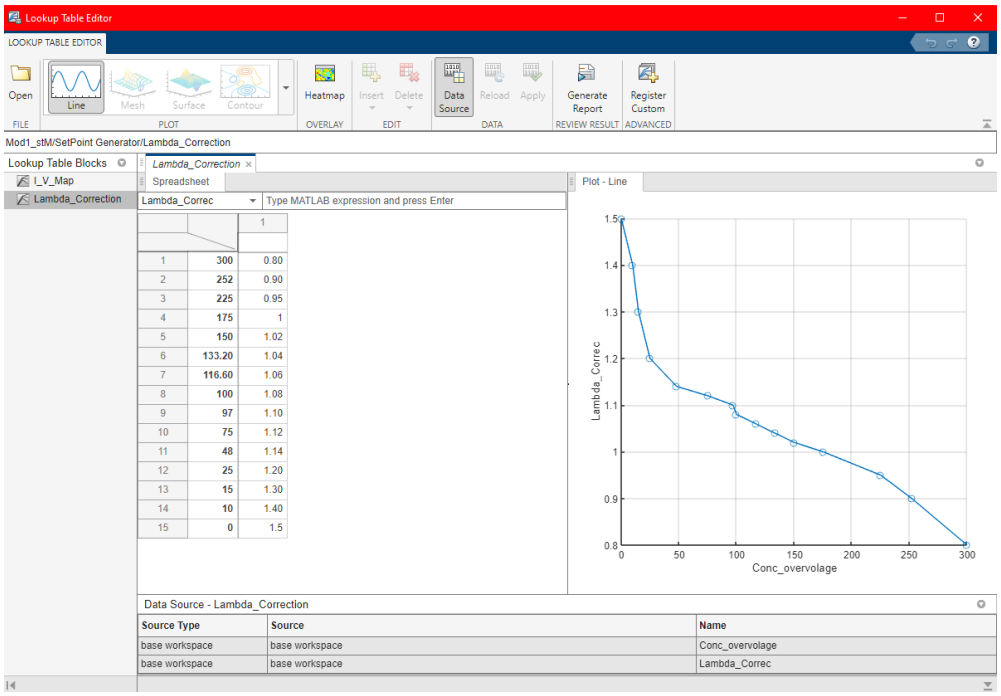


Figure 59 - 2D look up table for determining "Lamda_factor".

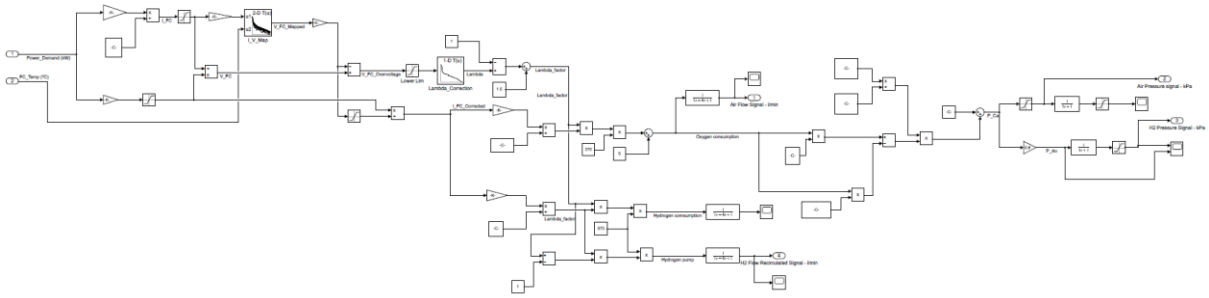

Figure 60 - Classical control algorithm developed in Simulink.

## 4.3 Neural Network control algorithm development

To develop a control algorithm using neural networks it was decided to use an ANN for each physical state. So, on this case, four ANN are needed to be trained and tested in order to evaluate the best configuration for the final control algorithm. Using power as an input, the same input as the classical control algorithm, each ANN would determine the corresponding quantity of each reactant (Figure 61).

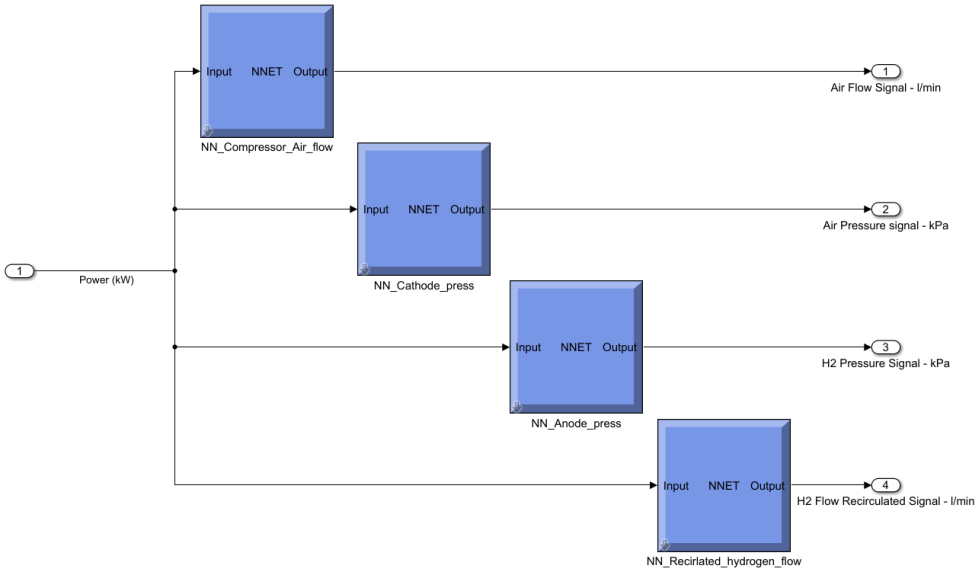


Figure 61 – Artificial neural network control algorithm developed in Simulink.

The "Deep Learning Toolbox" from MATLAB allows to train ANN with different learning algorithms and layer sizes. To understand which the best configuration for each ANN is, a training structure was defined to select the lowest RMSE option.

There are three learning algorithms available:

- Levenberg-Marquardt backpropagation
- Bayesian Regularization backpropagation
- Scaled conjugate gradient backpropagation

These algorithms were tested with different layer sizes, ranging from 2 to 30 layers. To evaluate the randomness of the seed (initial random values of the weights that are established at the beginning of the training session), each combination of algorithm and layer size was tested three times and the average of the RMSE was considered as the final result. Through this strategy, each ANN was trained 36 times, with a limit of 1000 epochs, to evaluate the configuration that presents lowest RMSE.

Figure 62 shows the toolbox used, exemplifying a train session using "Levenberg-Marquardt backpropagation" algorithm and 20 hidden layers. The ANN structure is presented in Figure 63 and has the corresponding number of layers on the hidden layer.

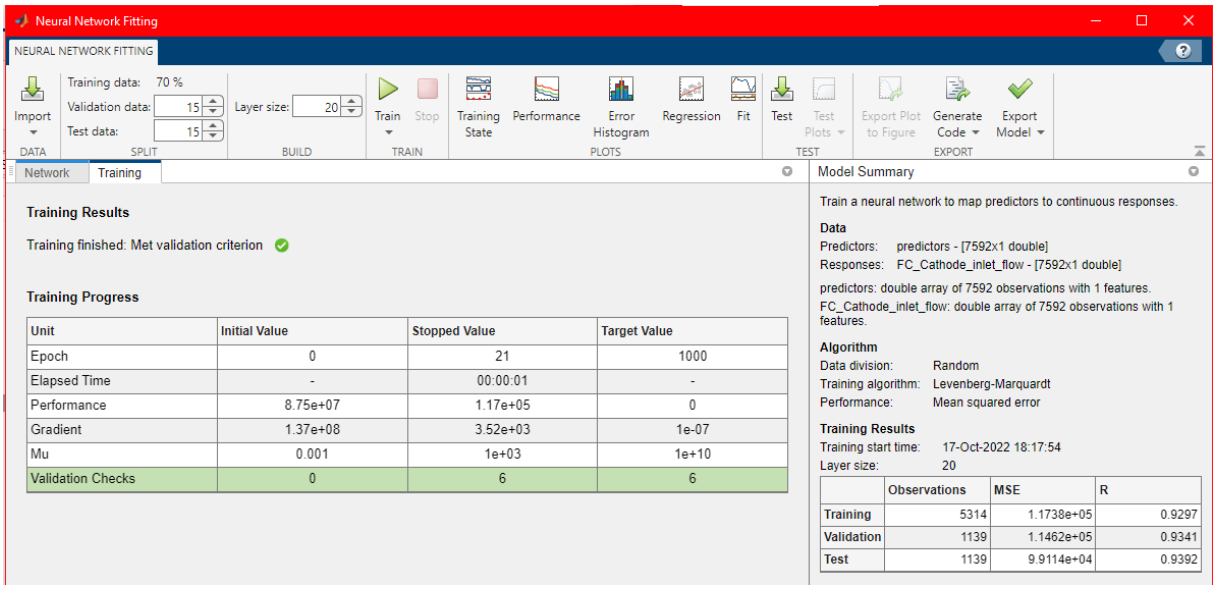


Figure 62 – Artificial neural network training using Deep Learning Toolbox in MATLAB.

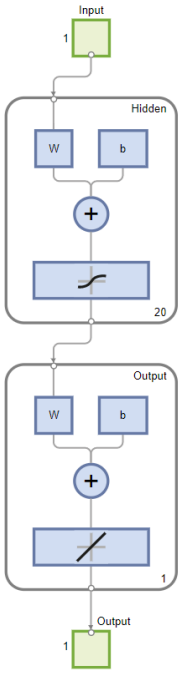


Figure 63 - Neural network structure for training in MATLAB.

Following the structure of Figure 61, the input data is the power demand in kW and the output is the corresponding physical state. Since this data are a quantity measured by sensors and do not follow any particular statistical distribution, it is necessary to smooth the frequency of oscillation of each physical state measured.

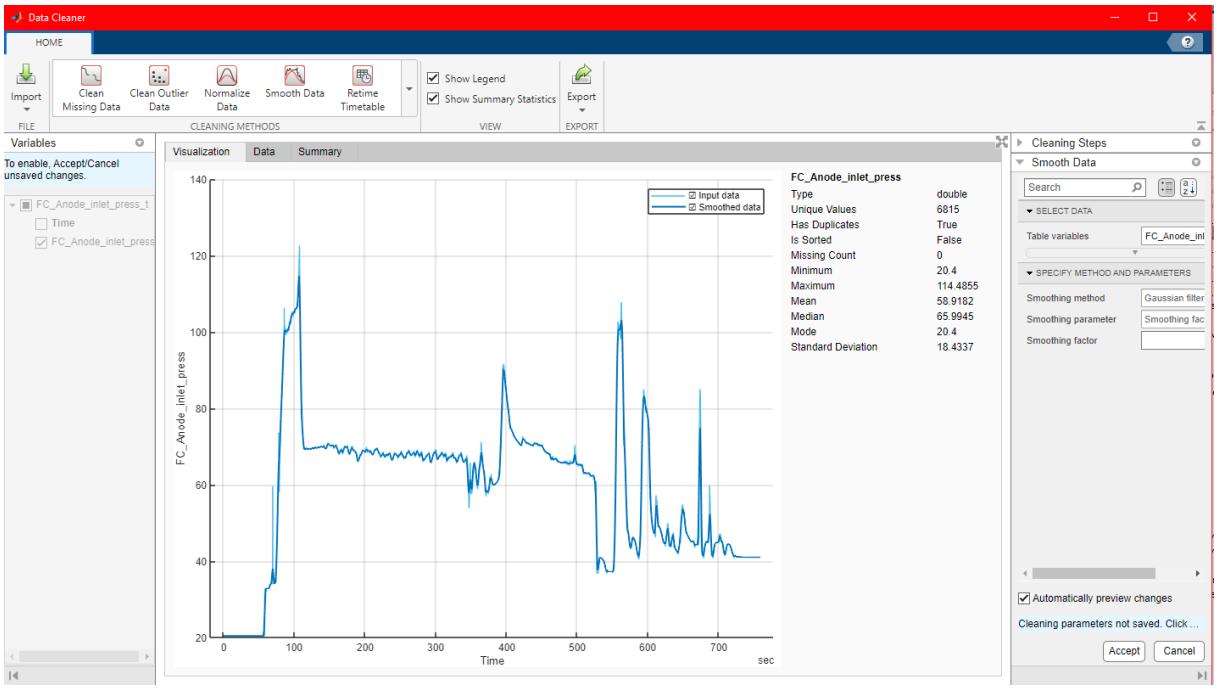


Figure 64 - Sensor signal filtering using "Data Cleaner toolbox".

In the case of the anode inlet pressure, corresponding to the hydrogen pressure, Figure 64 shows how these oscillations are smoothed after applying a Gaussian filter with a smoothing factor of 0.02. The same procedure was done to the remaining attributes – Air pressure, air flow, hydrogen recirculated flow, applying the best fit to smooth out high oscillations and not lose information.

Since all the attributes were treated, the next step would be to train each NN individually and collect the results, which are exposed from Table 9 to Table 12, with the ANN names corresponding to the corresponding Simulink block in Figure 61. In each table, the best result is marked with a green colour.

Table 9 - Training results for the neural artificial network of hydrogen/anode pressure.

| NN_Anode_press | | | |
|---|---|---|---|
| Layer size | Levenberg-Marquardt backpropagation | Bayesian Regularization backpropagation | Scaled conjugate gradient backpropagation |
| 2 | 6.757 | NAN | 7.946 |
| 10 | 6.436 | | 6.74 |
| 20 | 7.058 | | 6.477 |
| 30 | 6.753 | | 7.93 |

Table 10 - Training results for the artificial neural network of air/cathode flow.

| NN_Compressor_Air_Flow | | | |
|---|---|---|---|
| Layer size | Levenberg-Marquardt backpropagation | Bayesian Regularization backpropagation | Scaled conjugate gradient backpropagation |
| 2 | 11998.333 | NAN | 12328.554 |
| 10 | 38089.667 | | 12743.333 |
| 20 | 10294.667 | | 10551.333 |
| 30 | 8502.864 | | 9832.333 |

Table 11 - Training results for the artificial neural network of air/cathode pressure.

| NN_Cathode_press | | | |
|---|---|---|---|
| Layer size | Levenberg-Marquardt backpropagation | Bayesian Regularization backpropagation | Scaled conjugate gradient backpropagation |
| 2 | 259.75 | NAN | 268.797 |
| 10 | 194.583 | | 240.93 |
| 20 | 205.257 | | 212.05 |
| 30 | 194.41 | | 212.1 |

Table 12 - Training results for the artificial neural network of hydrogen recirculated flow.

| NN_Recirculated_Hydrogen_Flow | | | |
|---|---|---|---|
| Layer size | Levenberg-Marquardt backpropagation | Bayesian Regularization backpropagation | Scaled conjugate gradient backpropagation |
| 2 | 4520.267 | NAN | 13966,211 |
| 10 | 4399.389 | | 4672.556 |

| | | | |
|---|---|---|---|
| | 20 | 3774.711 | 3605.189 |
| | 30 | 3868.822 | 3117.4 |

In the case of using the "Bayesian Regularization backpropagation" algorithm, the toolbox was not able to train the ANN in a range of 1000 epochs (marked in the table with NAN) and the option of training with longer epochs was abandoned. The other algorithms presented acceptable results for this stage of development.

## 4.4 Control logic development

After the development of the control algorithm, the control logic is the module that will connect the control algorithm with the developed FC System model. The control logic approach decided is using PID to control each actuator of the FC System.

PID, as stated on the literature review, are the most known control logic used due to its simplicity and effectiveness. In MATLAB, the implementation of PID control logic can further simplified with auto tuning calibration options. The PID control acts on the error, which is the difference between the request or setpoint and the measured process variable. The difference between these two values gives an error and the PID will increase or decrease its effort on the output signal based on the dimension of this error.

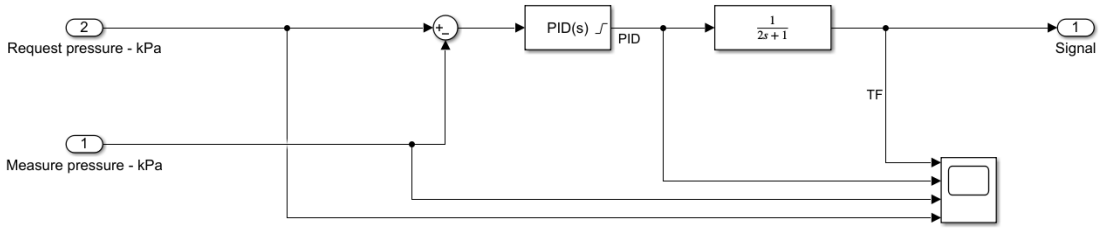


Figure 65 - PID control logic structure implemented on Simulink.

The example in Figure 65 calculates this error on the block behind the PID block. In the PID block, the proportional, integrative, and derivative coefficients are requested to determine the behaviour of the effort in the output signal (Figure 66).

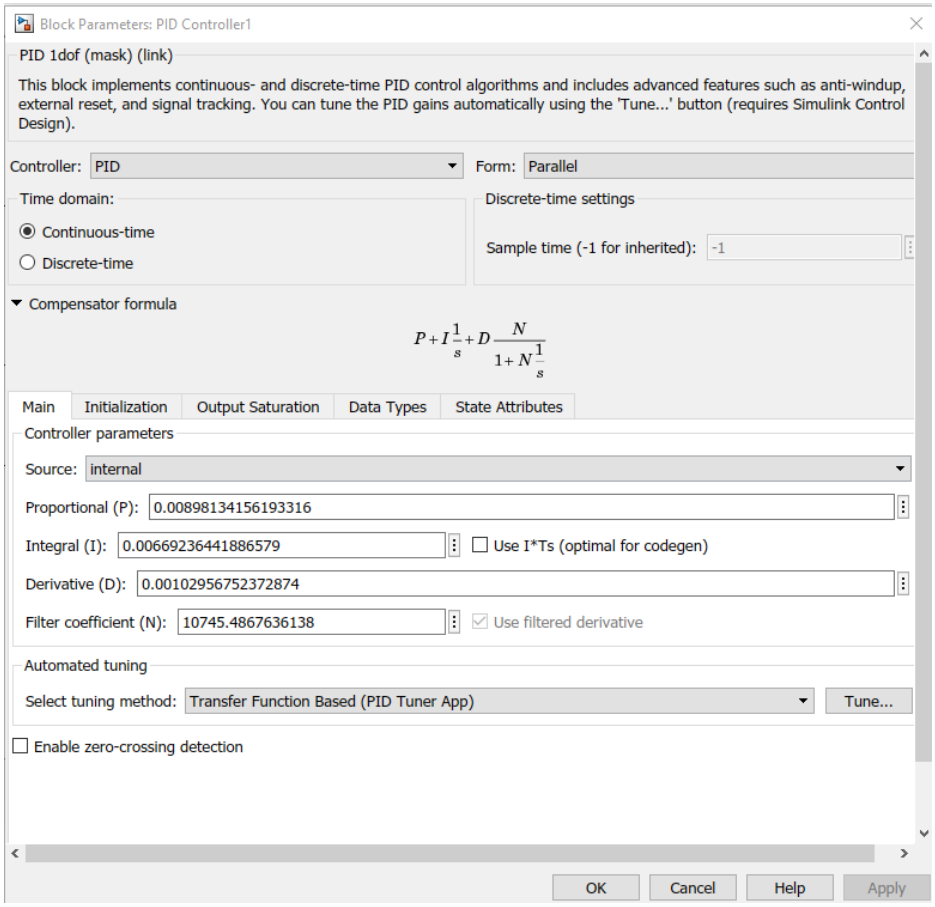


Figure 66 - PID configuration window.

The option to tune this parameter avoids long calculation times and trial and error to determine the coefficients. Using the "PID Tuner" app, the initial behaviour of the PID is shown in Figure 67, presenting overshoot and long time to react.

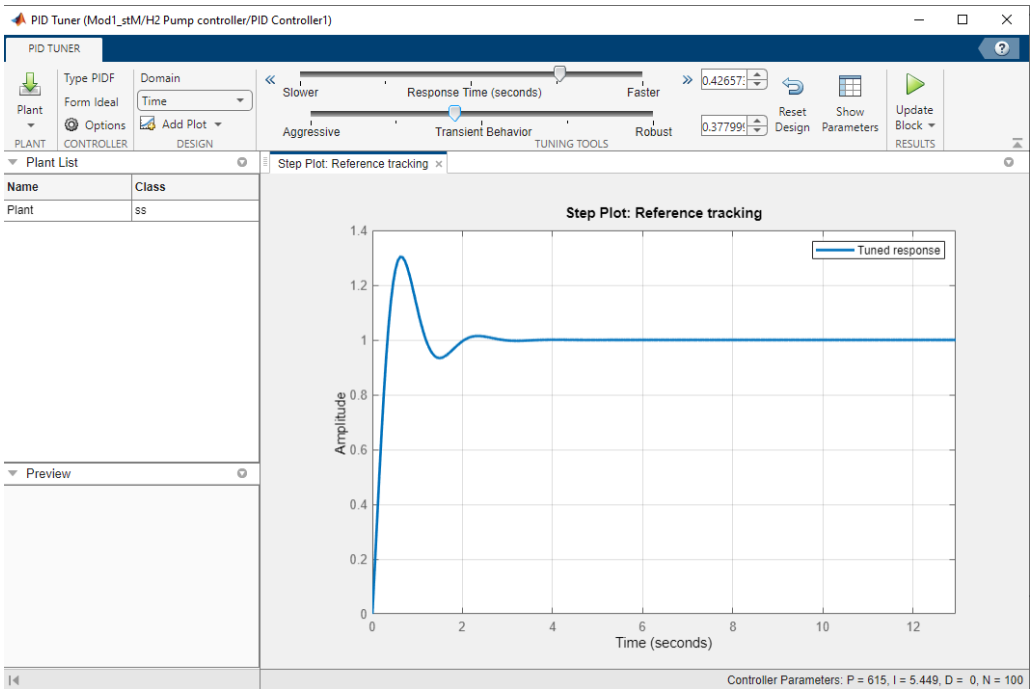


Figure 67 - PID Tuner app and signal with overshoot and delay.

By adjusting the response time and the transient behaviour it is possible to obtain a more stable and faster response signal as shown in Figure 68.

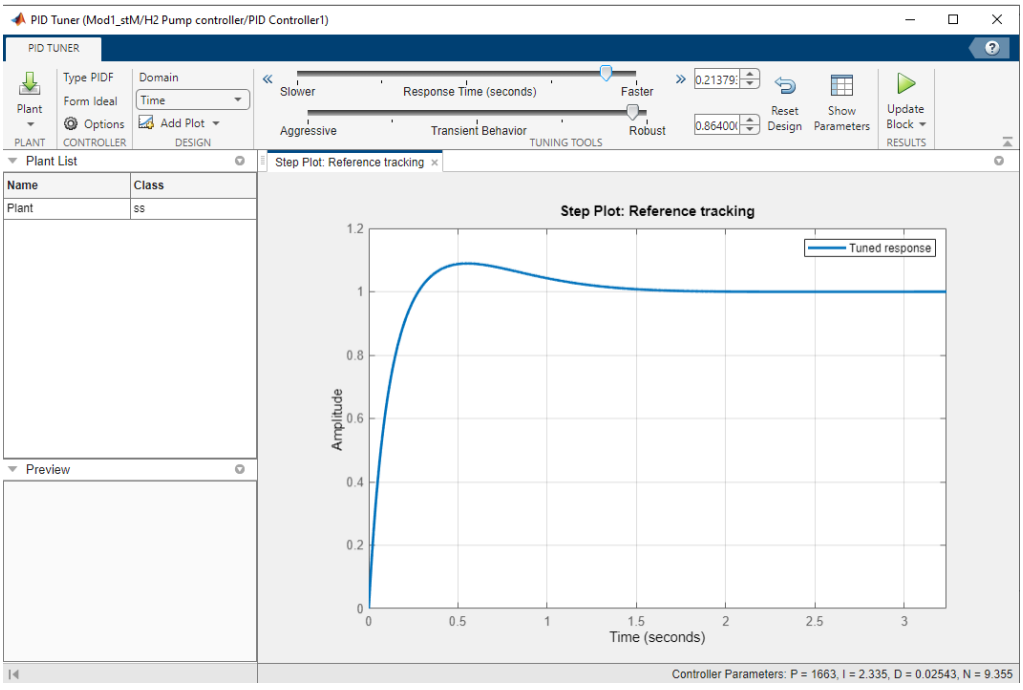


Figure 68 - PID Tuner app and signal smoothed and faster response.

This procedure of coefficient calibration was performed for each actuator, in a total of 4 implementations of PID control logic for each version of the FCCU (the classical control algorithm and the ANN control algorithm).

The final model is presented in Figure 69, where the FCCU (composed by the control algorithm and control logic, including the capability to switch between the two versions of the control algorithm) and the FC System model developed in the previous chapter are identified.

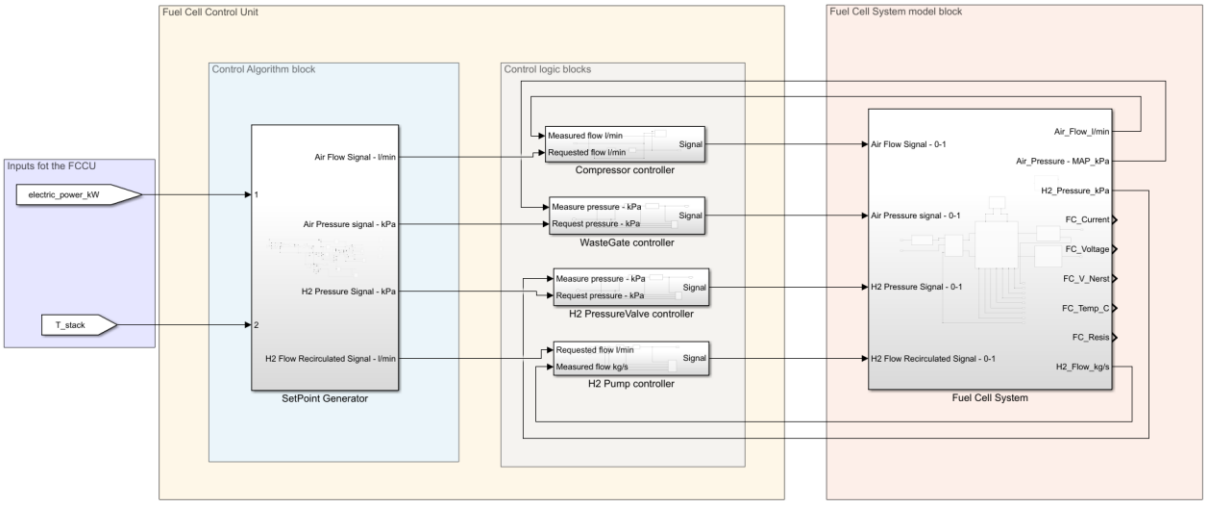


Figure 69 - Complete model developed in Simulink.

## 4.5 FCCU testing

To test the FCCU and the FC System, it needs to be stimulated with a current demand. For this, a test cycle of 400 seconds was selected as shown in Figure 70.

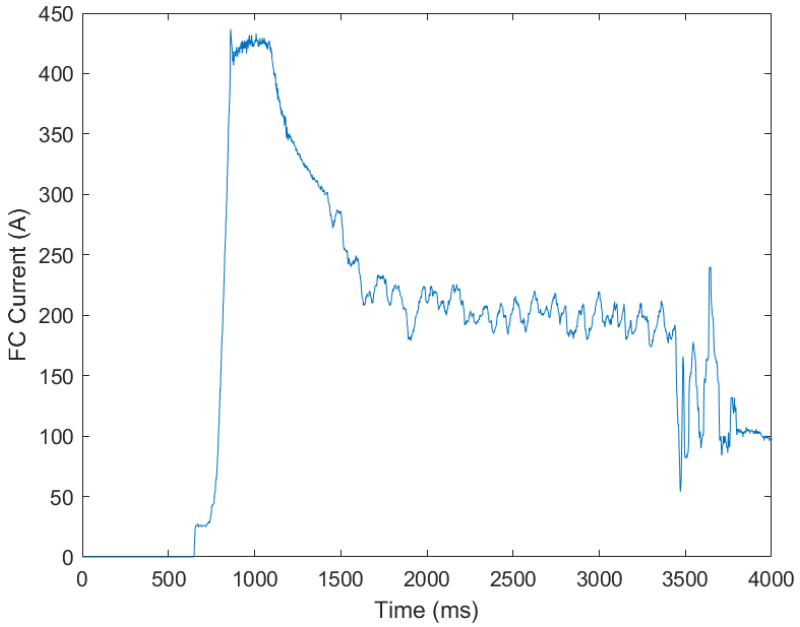


Figure 70 - Fuel Cell current demand for testing.

With the selected model input, the simulations were executed for both versions of the FCCU. The results evaluated were the outputs from the control algorithm and control logic, also taking into account the FC System model response.

The first test intends to evaluate the control algorithm strategies by comparing the output with the corresponding available data. For this, the simulation was carried out and the comparison of the results obtained is presented in the graphs (Figure 71 to Figure 74). For each graph, the yellow line represents the data measured from the sensor on the vehicle, the blue line the output from the classical control algorithm and the red line the output of each ANN control algorithm.

In addition, the error between the control algorithm and the data, the RMSE value, was determined as shown in Table 13.

Table 13 - RMSE values between control algorithms and data.

| Attribute | RMSE (ANN vs Data) | RMSE (Classical control vs Data) |
|---|---|---|
| Air flow | 66.386 | 318.254 |
| Air pressure | 6.978 | 1.511 |
| Hydrogen pressure | 11.942 | 27.842 |
| Recirculated hydrogen | 14.403 | 264.532 |

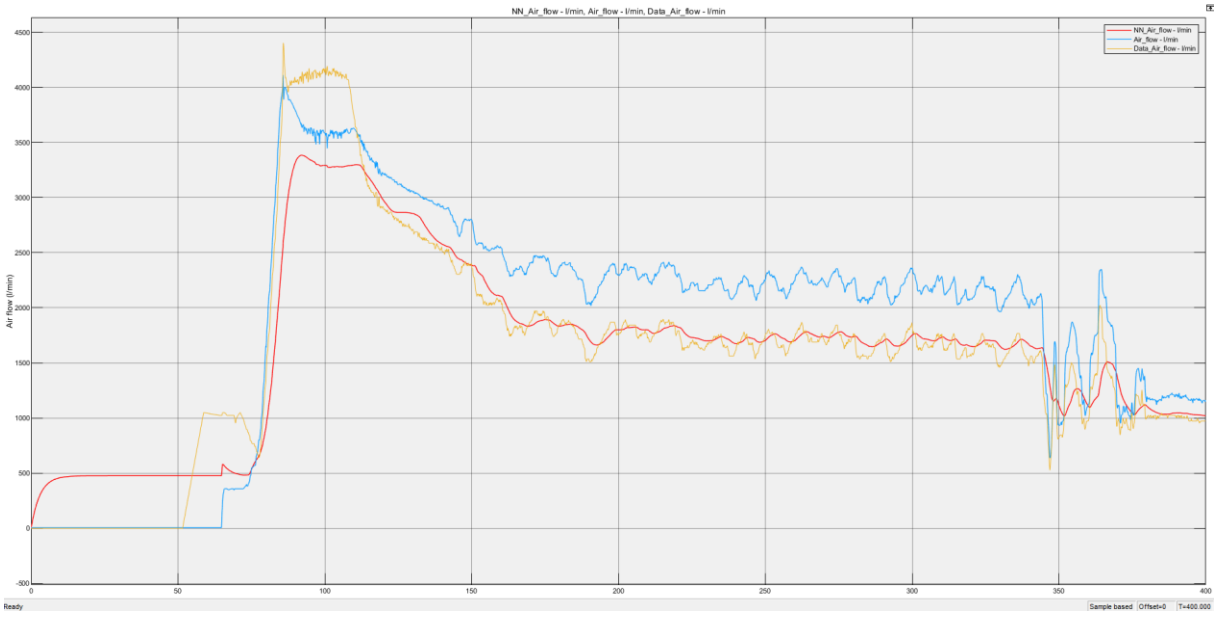


Figure 71 - Control algorithms response and corresponding data for air flow.

For the air flow in Figure 71, the classical control shows a wave form very similar to the data curve, with slightly higher values throughout the test. The ANN shows an opposite response, having very similar values to the data, but with a smoother wave form. Both algorithms show output values very close to the measured data, although the ANN shows a lower RMSE value (66.386) when compared to the classical control.

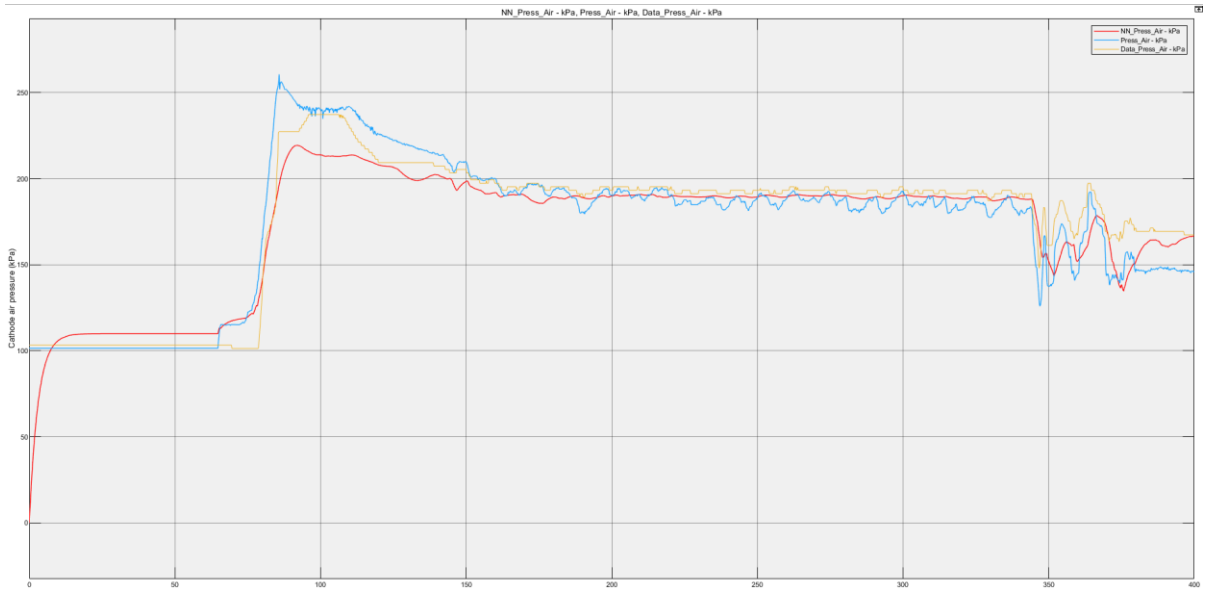


Figure 72 - Control algorithms response and corresponding data for air pressure.

The air pressure (in Figure 72) shows the same behaviour, but the data obtained from the vehicle has a step type of wave form, suspecting that it could be obtained from a communication port. The important thing is that both algorithms show close relation between them and are in sync with the data values having both low RMSE values, with classical control indicating the lowest.

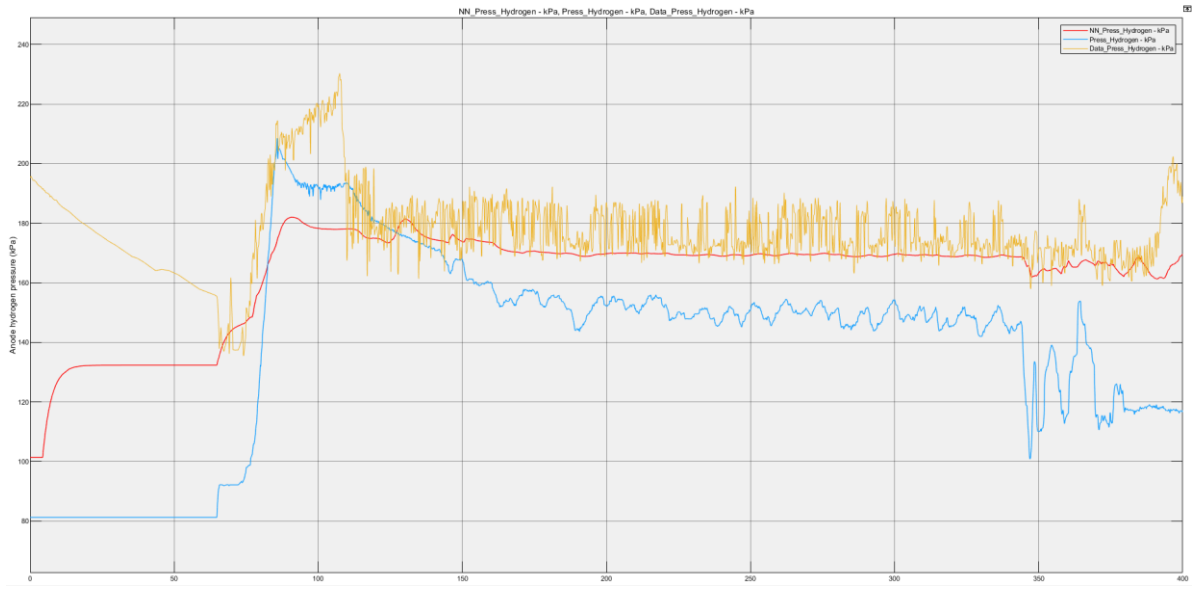


Figure 73 - Control algorithms response and corresponding data for hydrogen pressure.

For the hydrogen pressure (Figure 73) the data shows a very oscillating behaviour (due, for example, to a very sensitive sensor) and none of the algorithms were able to replicate this behaviour. The closer response is from the ANN with an RMSE of 11.942.

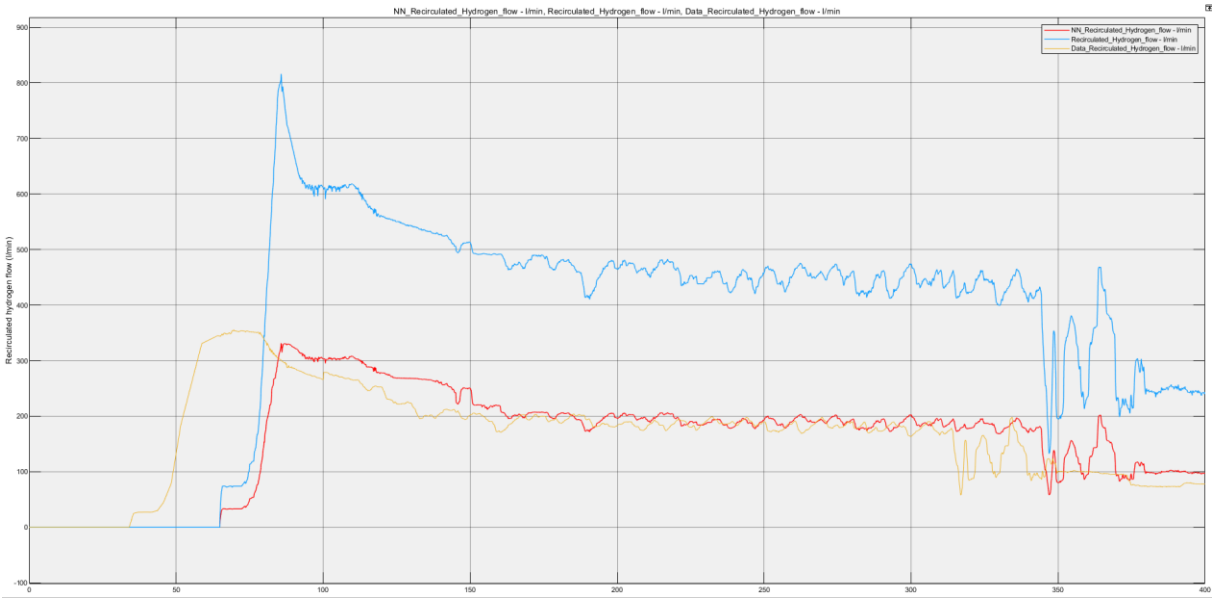


Figure 74 - Control algorithms response and corresponding data for recirculated hydrogen flow.

Comparing the curves for the recirculated hydrogen flow (Figure 74) a notable difference between the classical control algorithm and the ANN control algorithm is verified. The closest behaviour to the data is

the ANN control algorithm and shows a wave form similar to the classical control algorithm, but with lower values. In this case, clearly the ANN has the best result.

In addition, it is important to evaluate the model response and the control logic response against the data. For that, a set of graphs was made, for each version of the FCCU, showing the control algorithm response, control logic response, model response and the corresponding data attribute.

Figure 75 to Figure 78 show the control algorithm version for each version of the FCCU. Each graph has four plotted lines, the black line (signal) represents the output of the PID control logic that goes directly to the component (air compressor, pressure valves or pump). The red line represents the measured data from the vehicle, the green line represents the requested quantity, which is the output of the control algorithm, and the blue line the output of the FC System model.

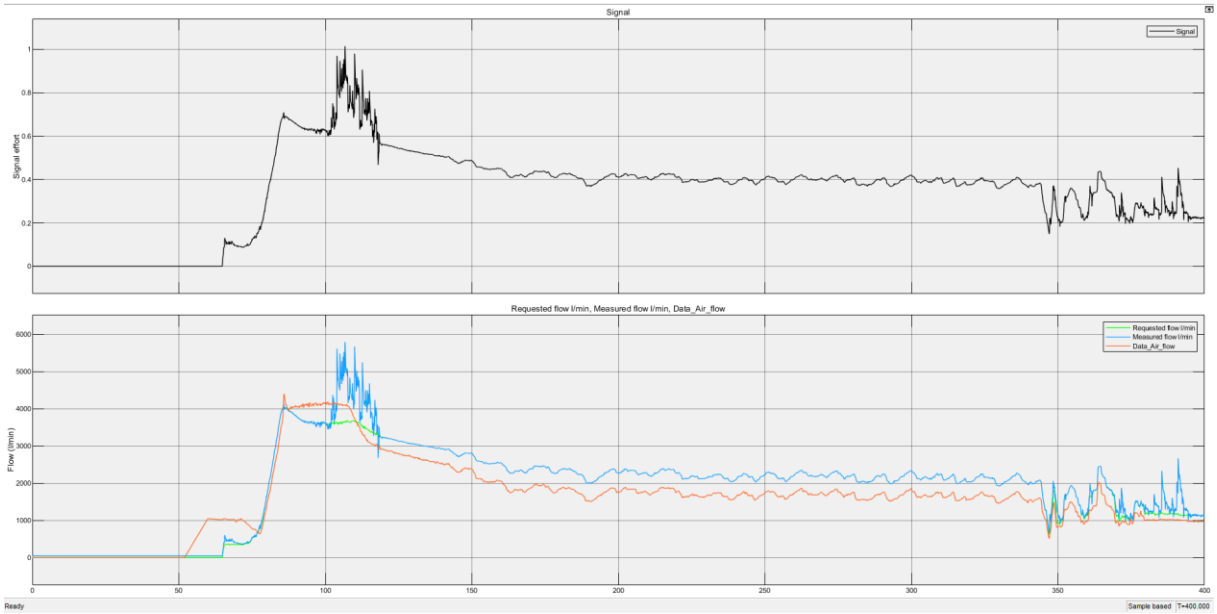


Figure 75 – FCCU response (classical control algorithm) and model response for the Air flow.

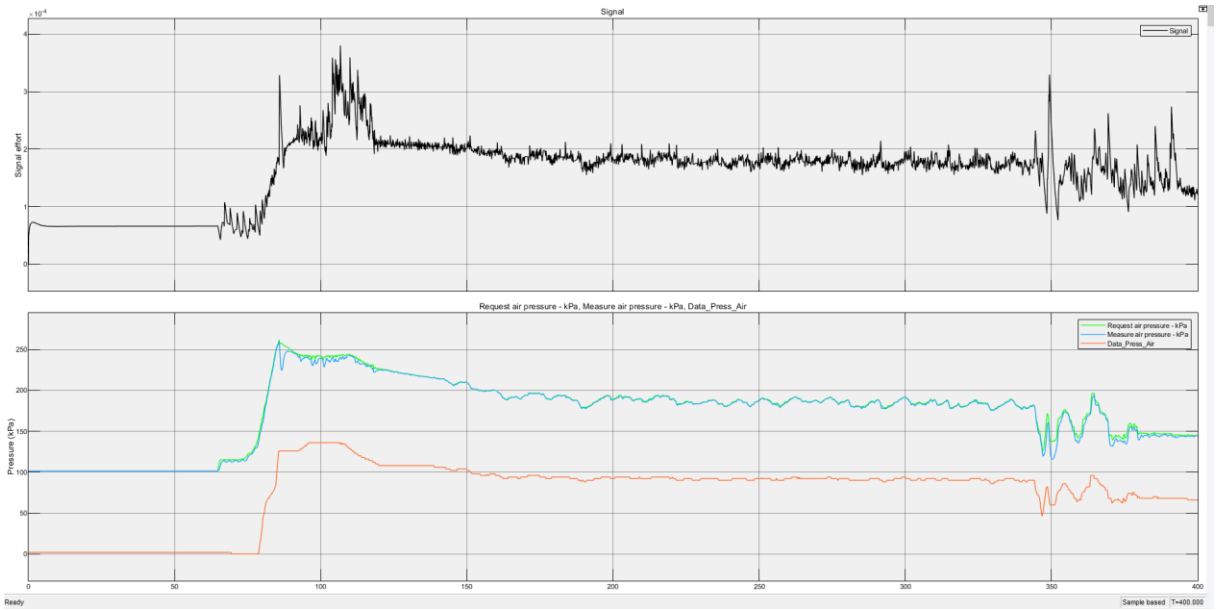


Figure 76 - FCCU response (classical control algorithm) and model response for the Air pressure.

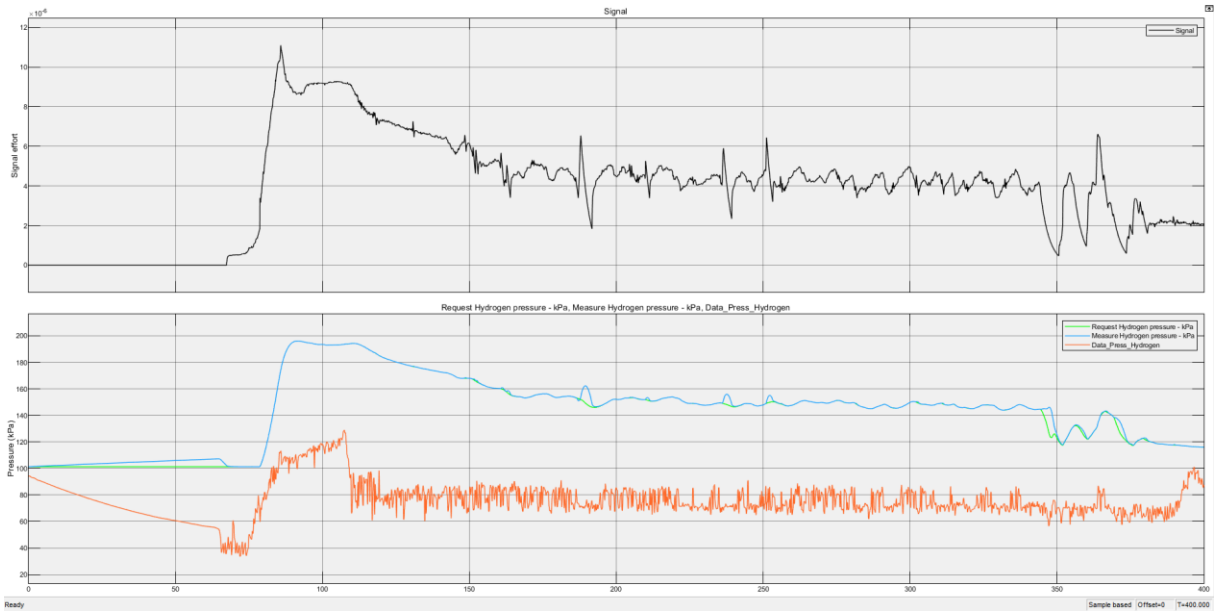


Figure 77 - FCCU response (classical control algorithm) and model response for the Hydrogen pressure.

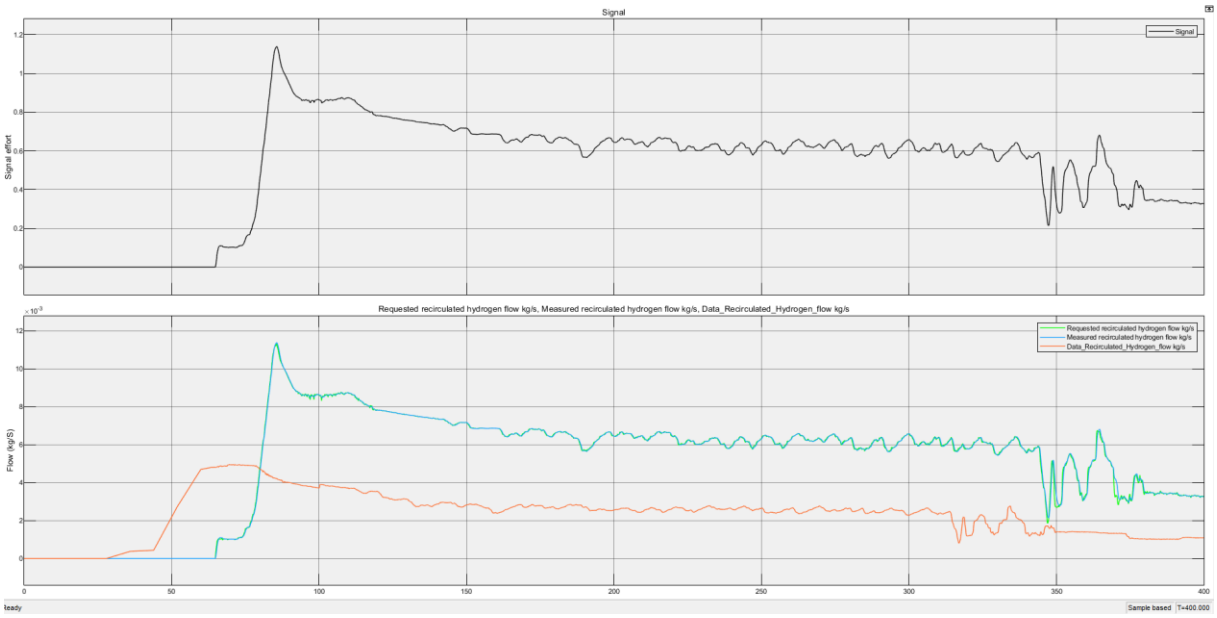


Figure 78 - FCCU response (classical control algorithm) and model response for the recirculated hydrogen.

The same procedure was carried out for the ANN version of the FCCU, and the next four pictures (Figure 79 to Figure 82) were obtained.

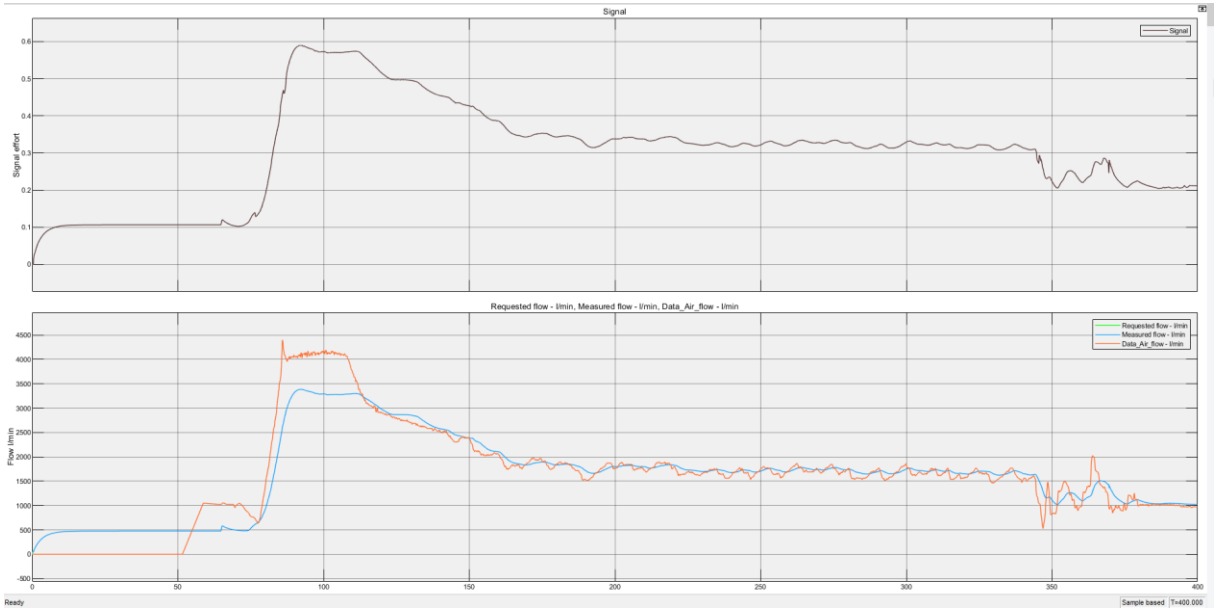


Figure 79 - FCCU response (ANN control algorithm) and model response for the Air flow.

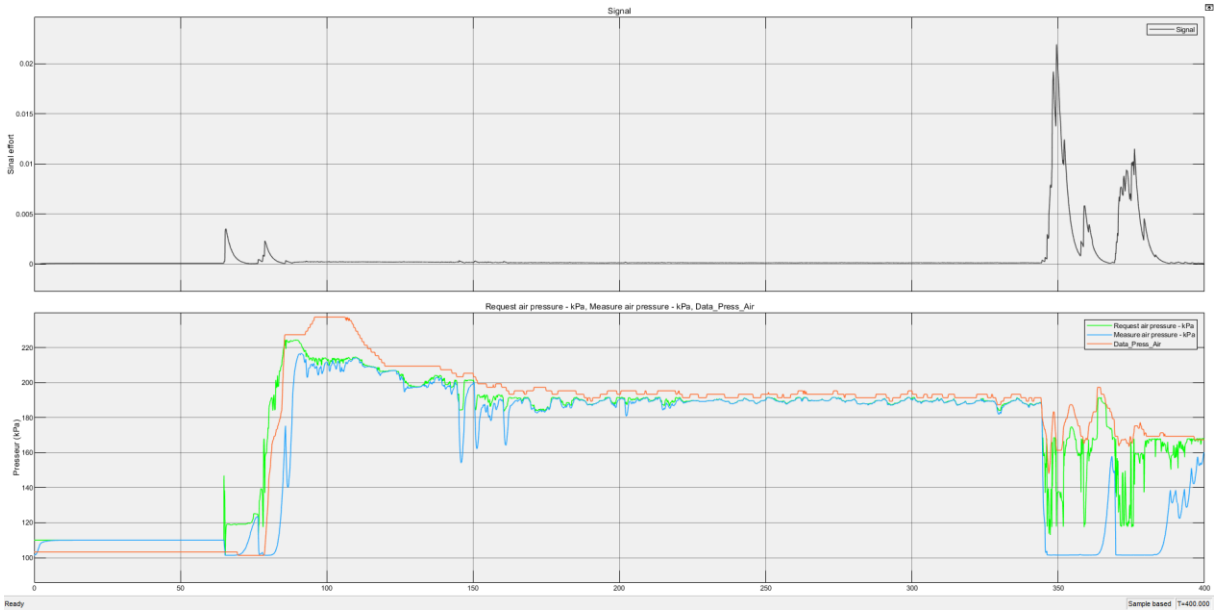


Figure 80 - FCCU response (ANN control algorithm) and model response for the Air pressure.

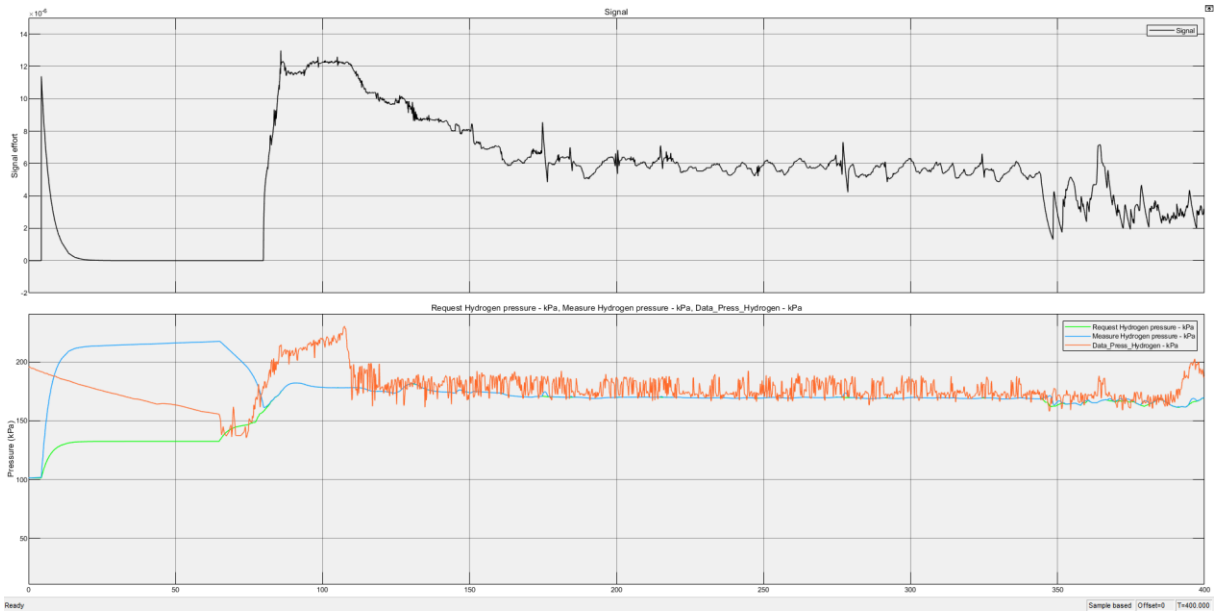


Figure 81- FCCU response (ANN control algorithm) and model response for the Hydrogen pressure.

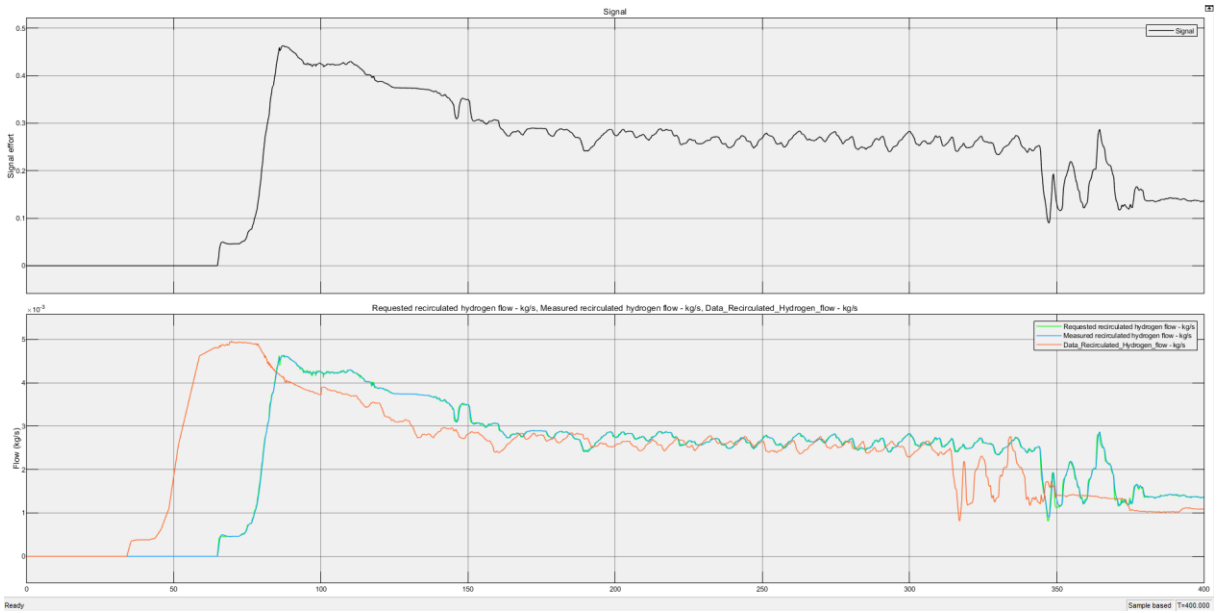


Figure 82 - FCCU response (ANN control algorithm) and model response for the recirculated hydrogen.

The RMSE values were calculated for each version of the FCCU and presented in Table 14.

Table 14 - RMSE values between FCCU version and data.

| Attribute | RMSE (ANN PID vs Data) | RMSE (Classical control PID vs Data) |
|---|---|---|
| Air flow | 66.385 | 192.865 |
| Air pressure | 15.422 | 98.382 |
| Hydrogen pressure | 10.383 | 67.044 |
| Recirculated hydrogen | 0.000202 | 0.003 |

The green line on each graph represents the requested physical quantity of air or hydrogen, this corresponds to the control algorithm response. The signal of the control logic is the black line and cannot be directly compared to any of the available data. On this case, the correct comparison to do is between the FC System response (blue line corresponding to the measured value of sensors on the FC System model) and the data. Also, in this case the RMSE values were calculated to have a clear understanding of the best FCCU versions.

Discussing the results of Figure 75 and Figure 79, the air flow plots, the control logic signal (black line) is more stable in the ANN version, resulting in a very stable FC System model response (blue line). For the classical control algorithm version, the very oscillation behaviour could be a not well calibrated PID, meaning that it must be forward calibrated. Having a look at the RMSE values, also the ANN version has smallest error, almost 7 times less.

For the air pressure (Figure 76 and Figure 80) the same oscillation behaviour is verified for the control logic response in the classical control algorithm. The ANN has a stable and accurate signal with an RMSE value of 10.383.

For the hydrogen pressure (Figure 77 and Figure 81) the ANN version also has the lowest RMSE value showing a notable bias on the initial seconds, due to an unexpected behaviour of the control logic that could be solved with advanced calibration of the PID.

The last attribute, recirculated hydrogen presented in Figure 78 and Figure 82 shows a similar trend. In this attribute, the classical control algorithm version of the FCCU performs worse than the ANN version. In both cases, the control logic (PID) shows an exceptional tracking of the requested value. It is safe to assume that the control logic in this case, for both versions, is well calibrated and the verified error comes from the control algorithms with the ANN showing the lowest RMSE.

# 5 CONCLUSIONS

This dissertation aims to develop of a model that includes the FC System and the FCCU models that can be used for by CES in forward testing and development of functions needed for future projects. The initial established goals were all fulfilled during the development of the project.

The development of the FC System model involved the use of optimization techniques that allowed meeting the initial requirements for the model, the main one being the replication of results.

The optimization of the FC System model uses the available data of air and hydrogen flow and pressure with the corresponding current and resistance values. In order to the estimation of empirical values, the Simulink design optimization using the TRR and LM algorithms was used. The lowest error was achieved with the TRR algorithm for both cases of voltage (RMSE value of 1.2464) and resistance (RMSE value of 5.2).

The model can successfully replicate the voltage but for the optimization results for the membrane resistance should be taken in account, since the results achieved can satisfy the initial requirements of the experimentation.

Respecting the FCCU model two versions were developed, one with the classical control algorithm and PID control logic, and other with ANN control algorithm and PID control logic. The interaction between the two models (FC System and FCCU) was a success, allowing to test both models solely with load application from the data. The model has four outputs (air and hydrogen flow and pressure) and for each output the RMSE values were determined, with the ANN version revealing 66.385 for air flow, 15.422 for air pressure, 10.383 for hydrogen pressure and 0.000202 for recirculated hydrogen. On every output the RMSE values of the ANN were significantly lower than the classical control algorithm version.

Clearly the version with ANN control algorithm shows a better performance both in accuracy and simulation performance, due to the fact that was trained with the data from the vehicle. The classical control algorithm shows inferior results mainly because the structure of equations may not match the exact one programmed on the vehicle FCCU (information that could not be obtained) and the look up tables could be forward calibrated to match the expected behaviour.

Forward development could be made if time and computational power was not a constraint, allowing to do tasks such as:

- Development of membrane resistance prevision code

- Better calibration of look up tables for classical control algorithm
- Better calibration of PIDs for control logic
- Continue to develop of the MPC controller

Overall, the project was successfully developed, now assisting on the study of powertrain models and functions that are needed to develop FC Systems, FCCU, diagnostic functions, testing, DC/DC converters and powertrain architectures.

## BIBLIOGRAPHY


Alanne, K. a. (2019). An overview of the concept and technology of ubiquitous energy. *Applied energy*, pp. 238-302.

Bao, C., Ouyang, M., & Yi, B. (2006). Modeling and control of air stream and hydrogen flow with recirculation in a PEM fuel cell system. *International journal of hydrogen energy, 31*(13), 1879-1895. https://doi.org/doi:10.1016/j.ijhydene.2006.02.031

Choudhury, A., Chandra, H., & Arora, A. (2013). Application of solid oxide fuel cell technology for power generation—A review. *Renewable and Sustainable Energy Reviews, 20*, 430-442.

Clark, T., & Knight, B. (2005). Development of Sensors for Automotive Fuel Cell Systems. *DOE Hydrogen Program*, 1005-1011.

Codina, A. C. (2017). *System Level modelling of fuel (Master's thesis).* Chalmers University of Technology.

Cohn, E. M. (1965, January 1). NASA's fuel cell program. *Advances in Chemestry*, pp. 1-8.

Coleman, T., Branch, M. A., & Grace, A. (2022). *Optimization toolbox. For use with MATLAB. User's guide for MATLAB.* The MathWorks, Inc.

Costamagna, P. S. (2001). Quantum jumps in the PEMFC science and technology from the 1960s to the year 2000: Part II. Engineering, technology development and application aspects. *Journal of power sources, 102*(1), 253-269.

Daud, W., Rosli, R., Majlan, E., Hamid, S., Mohamed, R., & Husaini, T. (2017). PEM fuel cell system control: A review. *Renewable Energy, 113*, 620-638. https://doi.org/http://dx.doi.org/10.1016/j.renene.2017.06.027

EG & G Services, Ralph M. Parsons Company, & Science Applications International Corporation. (2000). Fuel Cell Handbook. DIANE Publishing.

European Commission. (2012). Energy: roadmap 2050. *Directorate-General for Energy.* https://doi.org/https://doi.org/10.2833/10759

Gelmanova, Z. S., Zhabalova, G. G., Sivyakova, A., G., Lelikova, N., O., . . . Kamarova, S. N. (2018). Electric cars. Advantages and disadvantages. *In Journal of Physics: Conference Series, 1015*(5).

Gómez, J. C., Serra, M., & Husar, A. (2021). Controller design for polymer electrolyte membrane fuel cell systems for automotive applications. *International journal of hydrogen energy, 46*(45), 23263-23278. https://doi.org/https://doi.org/10.1016/j.ijhydene.2021.04.136

Grove, W. (1839). On voltaic series and the combination of gases by platinum. *The London, Edinburgh, and Dublin Philosophical Magazine and Journal of Science, 14*, 127-130.

Hartmann, N., & Özdemir E., D. (2011). Impact of different utilization scenarios of electric vehicles on the German grid in 2030. *Journal of power sources, 196*(4), 2311-2318.

Hatti, M., & Tioursib, M. (2009). Dynamic neural network controller model of PEM fuel cell system. *International Journal of Hydrogen Energy, 34*(11), 5015-5021. https://doi.org/https://doi.org/10.1016/j.ijhydene.2008.12.094

Hertzberg, M., Siddons, A., & Schreuder, H. (2017). Role of greenhouse gases in climate change. *Energy & Environment, 28(4)*, 530-539.

Hick, H., Küpper, K., & Sorger, H. (2020). *Systems Engineering for Automotive Powertrain Development.* Cham, Switzerland: Springer International Publishing. https://doi.org/https://doi.org/10.1007/978-3-319-99629-5

Ibrahim, I. A., Ötvös, T., Gilmanova, A., Rocca, E., Ghanem, C., & Wanat, M. (2021). *Global Energy Review.* Kluwer Law International BV.

James, B. D., Huya-Kouadio, J. M., & Houchins, C. (2017). *DOE Hydrogen and Fuel Cells Program Review.* Fuel Cell Systems Analysis.

James, B. D., Huya-Kouadio, J. M., & Houchins, C. (2021). *DOE Hydrogen and Fuel Cells - Fuel Cell System Analysis.* Strategic Analysis Inc.

Kabza, A. (2016, November 9). *Fuel cell formulary.* Retrieved from kabza: http://www.kabza.de/

Kerviel, A., Pesyridis, A., Mohammed, A., & Chalet, D. (2018). An Evaluation of Turbocharging and Supercharging Options for High-Efficiency Fuel Cell Electric Vehicles. *MDPI Applied Sciences*. https://doi.org/10.3390/app8122474

Krizhevsky, A., Sutskever, I., & Hinton, G. E. (2017). Imagenet classification with deep convolutional neural networks. *Communications of the ACM, 60*(6), 84-90.

Lohse-Busch, H., Stutenberg, K., Duoba, M., & Iliev, S. (2018). *Technology assessment of a fuel cell vehicle: 2017 Toyota Mirai (No. ANL/ESD-18/12).* Argonne National Lab, (ANL), Argonne, IL (United States).

Lu, J. (2013). Modelling and Control of Proton Exchange Membrane Fuel Cell. *Doctoral dissertation.* James Cook University.

Martinez, L. H. (2005). Post industrial revolution human activity and climate change: Why The United States must implement mandatory limits on industrial greenhouse gas emmissions. *Journal of Land Use & Environmental Law*, 403-421.

Maruo, T., Toida, M., & Ogawa, T. (2017). Development of Fuel Cell System Control for Sub-Zero. *SAE International*.

Maruo, T., Toida, M., Ogawa, T., Ishikawa, Y., Imanishi, H., & Mitsuhiro, N. I. (2017). Development of fuel cell system control for sub-zero ambient conditions. *SAE Technical Paper., 1*(1189). https://doi.org/doi:10.4271/2017-01-1189.

Naganuma, Y., Manabe, K., Imanishi, H., & Nonobe, Y. (2012). Development of system control for rapid warm-up operation of fuel cell. *SAE International Journal of Alternative Powertrains, 1*(1), 365-373. https://doi.org/doi:10.4271/2012-01-1230.

Namar, M. M., Jahanian, O., Shafaghat, R., & Nikzadfar, K. (2021). Engine Downsizing; Global Approach to Reduce Emissions: A World-Wide Review. *HighTech and Innovation Journal, 2*(4), 384-399.

Nehrir, M. H., & Wang, C. (2009). *Modeling and control of fuel cells: distributed generation applications.* John Wiley & Sons.

Nonobe, Y. (2017). Development of the Fuel Cell Vehicle Mirai. *IEEJ TRANSACTIONS ON ELECTRICAL AND ELECTRONIC ENGINEERING, 12*(1), 5-9. https://doi.org/DOI:10.1002/tee.22328

O'hayre, R., Cha, S. W., Colella, W., & Prinz, F. B. (2016). *Fuel cell fundamentals.* John Wiley & Sons.

Olszewski, M. (2007). *DC-DC Converter for fuel cell and hybrid vehicles.* U.S. Department of Energy.

Pollet, B. G., Kocha, S. S., & Staffell, I. (2019). Current status of automotive fuel cells for sustainable transport. *Current opinion in Electrochemistry, 16*, 90-95.

Pukrushpan, J. T., Peng, H., & Stefanopoulou, A. G. (2004, March). Control-oriented modeling and analysis for automotive fuel cell systems. *Journal of Dynamic Systems, Measurment and Control, 126*(1), 14-25. https://doi.org/https://doi.org/10.1115/1.1648308

Qi, Y., Espinoza-Andaluz, M., Thern, M., Li, T., & Andersson, M. (2019). Dynamic modelling and controlling strategy of polymer electrolyte fuel cells. *International Journal of Hydrogen Energy, 45*(54), 29718-29729. https://doi.org/https://doi.org/10.1016/j.ijhydene.2019.09.178

Radcliffe, J. C. (2018). The water energy nexus in Australia–the outcome of two crises. . *Water-Energy Nexus, 1(1)*, 66-85.

Scott, D., & Gössling, S. (2021). Destination net-zero: what does the international energy agency roadmap mean for tourism? *Journal of Sustainable Tourism, 30*(1), 14-31.

Staffell, I., Scamman, D., Abad, A. V., Balcombe, P., Dodds, P. E., Ekins, P., & Ward, K. R. (2019). The role of hydrogen and fuel cells in the global energy system. *Energy & Environmental Science, 12*(2), 463-491.

Surya, S., Saldanha, C. C., & Williamson, S. (2021). Novel Technique for Estimation of Cell Parameters Using MATLAB/Simulink. *Electronics, 11*(1), 117-119. https://doi.org/https://doi.org/10.3390/electronics11010117

Tanaka, S. N. (2020). Fuel cell system for Honda CLARITY fuel cell. *ETransportation, 3*(100046).

Thomas, C. S. (2009). Transportation options in a carbon-constrained world: Hybrids, plug-in hybrids, biofuels, fuel cell electric vehicles, and battery electric vehicles. *International Journal of hydrogen energy, 34*(23), 9279-9296.

Tutuianu, M., Marotta, A., Steven, H., Ericsson, E., Haniu, T., Ichikawa, N., & Ishii, H. (2013). *Development of a World-wide Worldwide harmonized Light duty driving Test Cycle (WLTC).* WLTP DHC.

Vishnyakov, V. M. (2006). Proton exchange membrane fuel cells. *Vacuum, 80*(10), 1053-1065.

Wang, S., & Xu, Y. (2019). Battery Electric Vehicle with a Fuel Cell - A System Study of Propulsion Concepts and Scenarios. *Masters Thesis.* Chalmers University of Technology.

Wang, Y., Biswas, A., Rodriguez, R., Keshavarz-Motamed, Z., & Emadi, A. (2022). Hybrid electric vehicle specific engines: State-of-the-art review. *Energy Reports, 8*, 832-851.

Yao, K. Z., Karan, K., McAuley, K. B., Oosthuizen, P., Peppley, B., & Xie, T. (2004). *A review of mathematical models for hydrogen and direct methanol polymer electrolyte membrane fuel cells.* John Wiley. https://doi.org/https://doi.org/10.1002/fuce.200300004

Yoshida, T., & Kojima, K. (2015). Toyota MIRAI fuel cell vehicle and progress toward a future hydrogen society. *The Electrochemical Society Interface, 24*(2), 45.

Yu, P., Li, M., Wang, Y., & Chen, Z. (2022). Fuel Cell Hybrid Electric Vehicles: A Review of Topologies and Energy Management Strategies. *World Electric Vehicle Journal, 13*(9), 172. https://doi.org/https://doi.org/10.3390/

Zenith, F. (2007). Control of fuel cells. *Doctoral dissertation.* Norwegian University of Science and Technology.

Zhao, T., Kreuer, K. D., & Van Van Nguyen, T. (2007). *Advances in Fuel Cell.* Elsevier.

## APPENDIX 1 – MEASURED ATTRIBUTES RELATED TO THE FC SYSTEM

| ID | Name | Units |
|---|---|---|
| 6 | Cell_Temp_C | °C |
| 7 | Cell_RH_per | % |
| 8 | Cell_Press_inHg | inHg |
| 10 | GaseousFuel_VehDelivery_Press__psi | Psi |
| 11 | GaseousFuel_Low_Flow__gps | g/s |
| 13 | GaseousFuel_High_Flow__gps | g/s |
| 15 | Exhaust_Bag | Boolean |
| 25 | FC_Out_Curr_Hioki_analog10hz__I2__A | A |
| 26 | FC_Out_Volt_Hioki_analog10hz__U2__V | V |
| 27 | FC_Out_Power_Hioki_analog10hz__P2__kW | kW |
| 28 | Pumps_H2_Water_Curr_Hioki_analog10hz__I4__A | A |
| 29 | Pumps_H2_Water_Power_Hioki_analog10hz__P4__W | W |
| 38 | FC_Out_Hioki_IH2__Ah | Ah |
| 39 | FC_Out_Hioki_WP2__Wh | Wh |
| 40 | Pumps_H2_Water_Hioki_U4__V | V |
| 41 | Pumps_H2_Water_Hioki_IH4__Ah | Ah |
| 42 | Pumps_H2_Water_Hioki_WP4__Wh | Wh |
| 51 | FC_converter_input_voltage_EV__V | V |

| | | |
|---|---|---|
| 52 | FC_converter_output_voltage_EV__V | V |
| 53 | FC_air_compressor_motor_torque_EV__Nm | Nm |
| 85 | FC_smoothed_value_of_barometric_pressure_FC__kPa | kPa |
| 86 | FC_stack_internal_resistance_FC__ohm | Ohm |
| 87 | FC_exhaust_drainage_valve_driving_request_FC | Booelan |
| 88 | FC_hydrogen_injector1_injection_request_FC | Booelan |
| 89 | FC_hydrogen_injector2_injection_request_FC | Booelan |
| 90 | FC_hydrogen_injector3_injection_request_FC | Booelan |
| 91 | FC_high_range_hydrogen_pressure_FC__MPa | MPa |
| 92 | FC_low_range_hydrogen_pressure_FC__kPa | kPa |
| 93 | FC_medium_range_hydrogen_pressure_FC__MPa | MPa |
| 94 | FC_smoothed_value_of_hydrogen_pump_motor_temp_FC__C | °C |
| 95 | FC_smoothed_value_of_medium_range_hydrogen_pressure_FC__kPa | kPa |
| 96 | FC_target_low_range_hydrogen_pressure_FC__kPa | kPa |
| 117 | Pedal_accel_position_vsCAN2__per | % |
| 119 | FC_current_vsCAN3__A | A |
| 120 | FC_smoothed_value_of_fc_voltage_vsCAN3__V | V |
| 121 | FC_hydrogen_pump_revolution_vsCAN3__rpm | Rot/min |
| 122 | FC_target_low_range_hydrogen_pressure_vsCAN3__kPa | kPa |
| 123 | FC_smoothed_value_of_low_range_hydrogen_pressure_vsCAN3__kPa | kPa |

| | | |
|---|---|---|
| 124 | FC_hydrogen_pump_consumption_power_vsCAN3__W | W |
| 125 | FC_mass_airflow_value_target_vsCAN3__NLpm | l/min |
| 126 | FC_air_compressor_revolution_vsCAN3__rpm | Rot/min |
| 127 | FC_smoothed_value_of_fc_stack_air_pressure_at_fc_stack_intlet_v | kPa |
| 128 | FC_smoothed_value_of_fc_stack_air_temperature_at_fc_stack_intle | °C |
| 129 | FC_smoothed_value_of_intake_air_temperature_vsCAN3__C | °C |
| 130 | FC_target_fc_stack_air_pressure_at_fc_stack_inlet_vsCAN3__kPa | kPa |
| 131 | FC_smoothed_value_of_fc_stack_coolant_temp_at_radiator_outlet_v | °C |
| 133 | FC_water_pump_consumption_power_vsCAN3__W | W |
| 133 | FC_water_pump_revolution_vsCAN3__rpm | Rot/min |
| 136 | FC_voltage_before_boosting_vsCAN3__V | V |